The development of a vertical axis tidal current turbine

Daniel Brinck

Nicklas Jeremejeff

Master of Science Thesis EGI 2013:090		
	The development of a vertical axis tidal current turbine	
	Daniel Brinck	
	Nicklas Jeremejeff	
Approved	Examiner	Supervisor
	Joachim Claesson	Peter Kjaerboe
	Commissioner	Contact person
	Subsea Technology Scandinavia AB	Peter Lindberg

Abstract

Globally the amount of electricity produced each year is increasing significantly. Between 1980 and 2010 the average increase was 407 billion kWh per year. To be able to meet this increasing electricity demand, without burdening the environment in a too large extent, the research and development of renewable energy production techniques is of great importance. In the light of this we wanted to dedicate our master thesis to help Subsea Technology Scandinavia AB with the development of a vertical axis tidal current turbine.

The project set out to do the initial design proposal of a 2 x 4 meter H-shaped Darrieus turbine by applying the Double Multiple Streamtube model. The optimization process was performed with the aid of MATLAB for four different foils. The study included two symmetrical foils; NACA 0012 and S-1046 together with two asymmetrical foils; S-1210 and E216. The parameters studied were the number of blades, chord length, tip speed ratio, fixed pitch and the operational range. In the project, effects such as blade to wake interaction, torque fluctuations etc. were also considered.

From the simulations the two bladed turbine fitted with the S-1046 hydrofoil showed the highest performance but was struggling with an unfavorable oscillating torque. In the light of this the three bladed turbine fitted with the S-1046 hydrofoil with a chord of 0.13 m and an optimal tip speed ratio of 3.2 was determined. From the simulations the power coefficient reached 53.47 % for this case. This configuration also showed good performance in a relatively wide range of both tip speed ratios and free stream velocities.

The model does not include several effects causing losses and the power coefficients calculated in this model are to be used as a comparison between the different turbine configurations and not as absolute values of performance.

The simulations showed good potential for the use of asymmetrical foils in vertical axis turbines. The performance was evaluated for the upstream half of the turbine where the E216 foil exceeded the symmetrical foils in the range of ten percentage points.

Acknowledgements

First of all we would like to extend our thanks to our supervisor Peter Kjaerboe for all the guidance and reassuring meetings during the full five months of this project.

We would also like to thank Peter Lindberg, Pontus Runesson and Floris Marselje at Subsea Technology Scandinavia AB for believing in us and providing us with this project.

Table of Contents

List of figures

List of tables

Nomenclature

A	Projected frontal area
a	Induction factor (upstream)
á	Induction factor (downstream)
BBL	Bottom boundary layer
BEM	Blade element momentum model
BET	Blade element theory
c	Chord
C_D	Drag force coefficient
C_L	Lift force coefficient
C_n	Normal force coefficient
C_P	Power coefficient
C_Q	Torque coefficient
C_T	Thrust coefficient
C_t	Tangential force coefficient
CFD	Computational fluid dynamics
DMST	Double multiple streamtube
d	Diameter
E	Energy
H	Height
HAWT	Horizontal axis wind turbine
L	Lift force
l	Length
MST	Multiple streamtube
m	Mass
N	Number of blades
N_Θ	Number of streamtubes
P	Power

p	pressure
Q	Torque
R	Resulting force
r	Radius
Re	Reynolds number
T	Thrust
TSR	Tip speed ratio
u	Velocity (fluid)
v	Blade periphery velocity
VAWT	Vertical axis wind turbine
w	Relative velocity
č	Time averaged chord length
θ	Azimuth angle
α	Angle of attack
$\mathfrak{D}$	Drag force
ϱ	Density
Ω / ω	Angular velocity
μ	Dynamic viscosity
τ_w	Wall shear stress

SI units are used throughout this report.

List of indexes

avg	Average
d	Downstream
e	Equator
f	Full scale
i	Instantaneous
K	Kinetic
M	Model
m	Mean
o	Ambient
R	Rotor
u	Upstream
w	Wake
∞	Free stream

1 Background

Globally the amount of electricity produced each year is increasing significantly. Between 1980 and 2010 the average increase was 407 billion kWh per year (EIA). To be able to meet this increasing electricity demand, without burdening the environment in a too large extent, the research and development of renewable energy production techniques has been extensive during the last decades. An increased awareness of CO_2-emissions, the greenhouse effect and the issues regarding storage of various waste products has also contributed to this development. The result has been an extremely rapid development of especially wind and solar power production, but now also sea-based techniques. For both the wind and solar techniques the electricity production is very dependent on the weather which leads to large production variations both in the short term (during a day) and in the long term (during the yearly seasons). In Europe this problem is solved by investing in more flexible and global electricity grids between the countries so that a larger area is interconnected and electricity can be produced with the renewable techniques somewhere at any given time. However, this approach also has its obvious disadvantages and it will be difficult to replace a to large amount of the traditional base load production techniques why it is the authors of this reports belief that more stable electricity producing renewable base load techniques will become more sought after.

The company "Subtech" (Subsea Technology Scandinavia AB) is a company working with professional diving work and subsea solutions contacted us for help with the development of their latest product. The product is an underwater electricity generation device for ocean- and tidal currents. The techniques involving these energy sources are, relative to other renewable energy techniques, undeveloped and provide a very stable and reliable energy production from a huge energy source without any CO_2 emissions or visual pollution. This work is therefore about the first phase of work in the development of a product that produces electricity from tidal currents and that require little maintenance. The strength of this specific project is the combination of both practical and theoretical knowledge from the beginning. This master thesis will then hopefully serve as a good basis for Subtech to apply for investments in order to further develop this product with the hope of making it commercial.

1.1 Objectives

The objectives of this master thesis are to first write a literature study that explains the theory behind:

- The energy and power in flowing water.
- Boundary layer, viscous effects and similar necessary flowing mechanical properties.
- The occurrence of tidal and ocean currents.
- Drag force and lift force solutions, some basic knowledge about the ingoing parts and theory.

The literature study will also include existing solutions, simulation methods and environmental impacts.

Based on the acquired knowledge from the literature study the choice of basic design will be made and the development of the initial design for the turbine will commence. This thesis will provide the initial design proposal as well as theoretical and practical improvement advices for both groups of energy conversion techniques.

1.2 Case

Subtech wishes to develop a turbine that is a bit smaller than most competing turbines because of their experience of the difficulties and costs of managing large equipment at sea. Then several turbines can be assembled on a common foundation or be used individually with a smaller generator. Because of this reasoning the maximum dimensions for this vertical axis turbine is 2 meters in diameter and 4 meters high. The following are also agreed together with Subtech and our supervisor for this master thesis:

- The turbine should contain few moving parts and demand as little maintenance as possible since its final placement can be difficult to access. Simple mechanics and control systems are therefore desired.
- The key figure "kW/tonnes" should be taken into consideration throughout the work, meaning that both efficiency as well as simplicity/weight will be of importance.
- The work will focus on optimizing the turbine itself for electricity production (maximize power coefficient) but it is beyond the scope of this thesis to include the development of gearboxes, generators, dimensioning of axes etc. or similar mechanical engineering work.
- Examine the effect on the power coefficient of using asymmetric hydrofoils.*

*This requirement was added after the decision to apply the turbine designed to utilize the lift force created by the mounted foils.

2 Literature study

This chapter will give an insight of the different parts involved in the project. The fundamentals and some theory regarding the ingoing parts will be presented and explained.

2.1 Tidal currents - Gravitational forces from the moon/sun

Tidal currents are the effect of the longest oceanic waves which are characterized by the rhythmic rise (**flood**) and fall (**ebb**) of the sea level during a period of time of half a day or a day. This effect can be seen in Figure 2.1 where a 30-day tidal record from Tay estuary, Scotland shows the vertical movement of the sea level in approximately 12.5 hour periods (Evelyn Brown, 2005). The rise and fall of the sea level is caused by the resulting gravitational force of mainly the moon, but also the sun, acting on the oceans. The tidal currents are the horizontal water movements corresponding to the rise and fall in sea level. This is most obvious along the coast lines where the water is "coming in" or "going out" since the height difference often move the shoreline when it is covering larger or smaller areas of land with water. However, this is only the effect of the whole oceans water level rising/falling (Evelyn Brown, 2005).
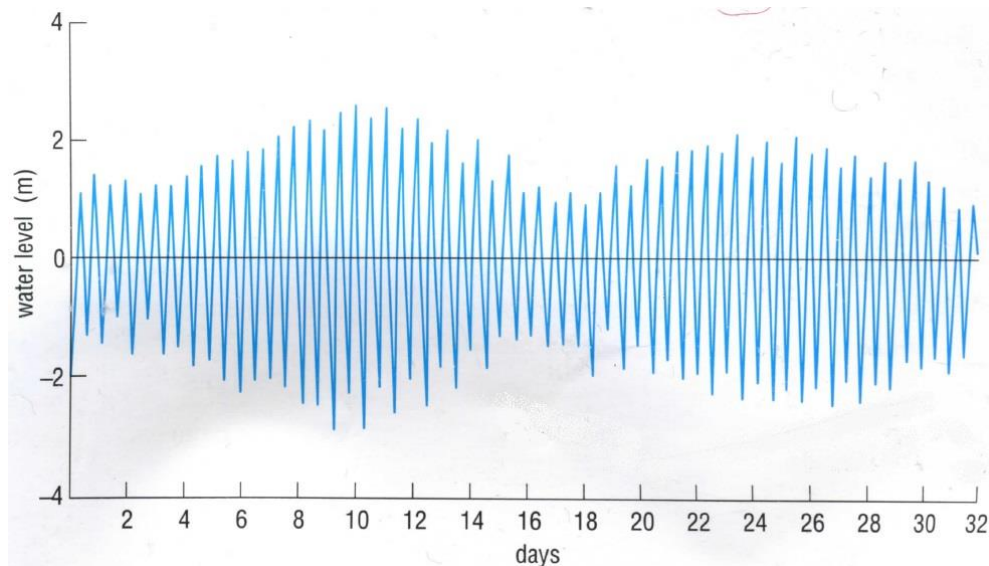
Figure 2.1. Flood and Ebb over a period of one month

Figure 2.1 clearly shows the daily oscillations and also that the days are different in another rhythmic pattern. The periods with higher sea levels around day 9 and 24 are called spring tides and have an amplitude of, relative to the mean level, nearly 3 meters with a range of nearly 6 meters. The lowest amplitude sections are called neap tides and in this case have a range of a little more than 2 meters (Evelyn Brown, 2005). These effects are very predictable and depend on the combination of the earth-moon (lunar tide) and earth-sun (solar tide) systems. Without being to theoretical Figure 2.2 shows the reason for these effects if one consider that the forces must be added up to a resultant acting force (Evelyn Brown, 2005).
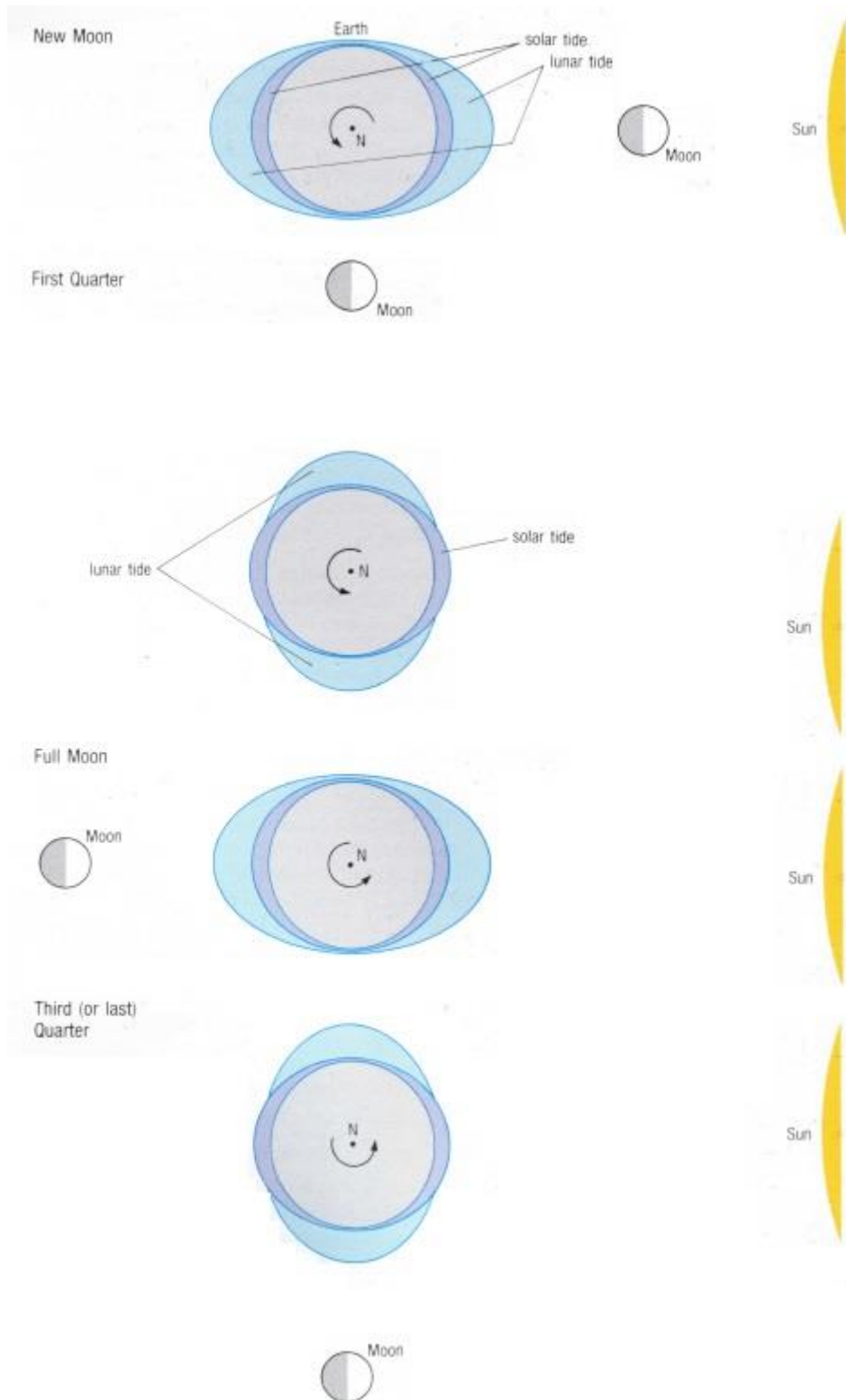
Figure 2.2. The interaction of the lunar and solar tides

The tidal current velocity is crucial to decide if an area is suitable for electricity production and to optimize the turbine that should operate in that specific area. In Figure 2.3 below one can see a mapping of the flow velocities along Ireland's coasts.
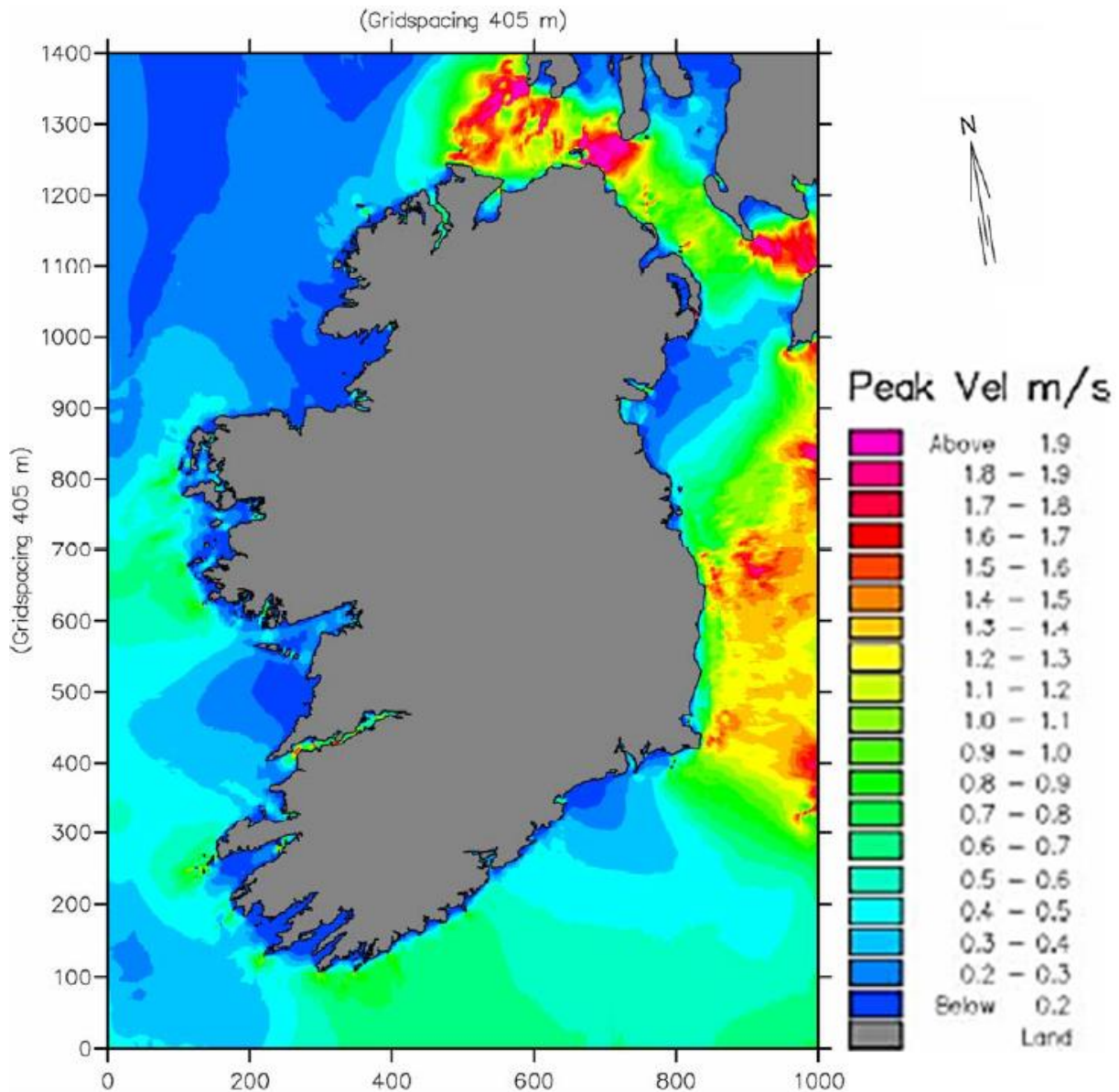
Figure 2.3. Example of tidal current velocities in Ireland

Bild från: PDF som heter irland

A tidal current power plant was tested in 2001 outside Messina by the Sicilian coast where the tidal current velocities was measured to between 1.5-2 m/s with peaks above 3 m/s (INSEAN, 2007). It is however an extensive task to measure the precise velocities in large areas and it is difficult to find good specific information in all parts of the world. However, to get an understanding of the global resources one can see in Figure 2.4 (a study that was carried out to identify suitable locations for tidal barrages) the mean range of the tidal water in one of the columns. In areas where the mean range is high there should be a good possibility that there are locations with high tidal current velocities too. Figure 2.4 is also very interesting in order to get an idea of the potential in tidal power production.

Location	Mean range (m)	Basin area (km²)	Potential mean power (MW)	Potential annual production (GW h/year)
North America				
Passamaquoddy	5.5	262	1800	15,800
Cobscook	5.5	106	722	6330
Bay of Fundy	6.4	83	765	6710
Minas-Cobequid	10.7	777	19,900	175,000
Amherst Point	10.7	10	256	2250
Shepody	9.8	117	520	22,100
Cumberland	10.1	73	1680	14,700
Petitcodiac	10.7	31	794	6960
Memramcook	10.7	23	590	5170
South America				
San Jose, Argentina	5.9	750	5870	51,500
United Kingdom				
Severn	9.8	70	1680	15,000
Mersey	6.5	7	130	1300
Solway Firth	5.5	60	1200	10,000
Thames	4.2	40	230	1400
France				
Aber-Benoit	5.2	2.9	18	158
Aber-Wrac'h	5	1.1	6	53
Arguenon	8.4	28	446	3910
Frenaye	7.4	12	148	1300
La Rance	8.4	22	349	3060
Rotheneuf	8	1.1	16	140
Mont St Michel	8.4	610	9700	85,100
Somme	6.5	49	466	4090
Ireland				
Strangford Lough	3.6	125	350	3070
Russia				
Kislaya	2.4	2	2	22
Lumbouskii Bay	4.2	70	277	2430
White Sea	5.65	2000	14,400	126,000
Mezen Estuary	6.6	140	370	12,000
Australia				
Kimberley	6.4	600	630	5600
China				
Baishakou	2.4	No data	No data	No data
Jiangxia	7.1	2	No data	No data
Xinfuyang	4.5	No data	No data	No data

Figure 2.4. Major world tidal barrage sites

2.1.1 Boundary layer

To understand what a boundary layer is one has to understand that the viscosity of a fluid is. Simply explained this is a measurement of the fluids resistance to deform. For example, syrup moves a lot slower than water because it has a higher viscosity. These effects combined with the friction between a surface and a moving fluid creates a boundary layer where the velocity closest to the surface is zero and then increases with the distance to the surface until it reaches the free streams velocity as in Figure 2.5. This is called the boundary layer and as seen in the figure its properties are also dependent on the properties of the flow, for example the boundary layer is thicker if the flow is turbulent.
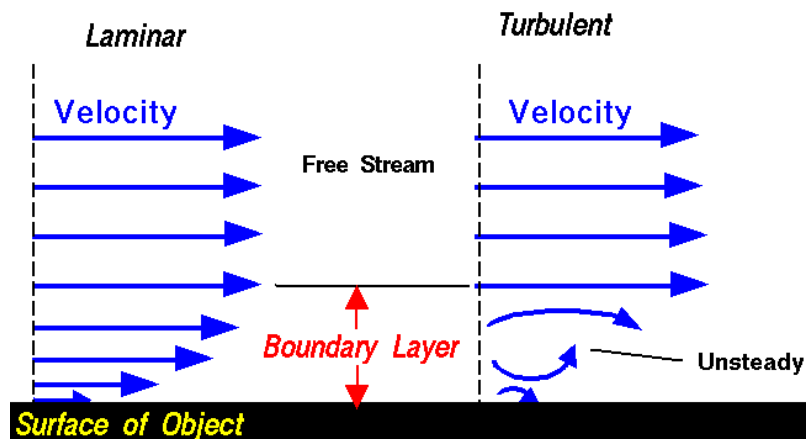
Figure 2.5. Boundry layer visualization

On the deep ocean floor (depths up to 4000 meters) the bottom boundary layer (BBL) is of the order of 10 meters, however with high velocity currents the BBL thickness may reach 40 meters and the whole

boundary layer may involve the whole water column in more shallow water areas (S Salon, 2008). That means that if one is to place a turbine for electricity generation it is better to have it just below the surface than at the bottom where the current velocities are lower.

2.2 Existing tidal energy extraction techniques

There are mainly two techniques to extract energy from tidal currents:

Tidal impoundment. A volume of water is impounded in order to create a height (head) difference when the sea level is rising/lowering. Then low-head hydro turbines are used when the water is released to flow through the outlets to generate electricity. This can be done using either barrages or lagoons. Figure 2.6 illustrates the different technologies.
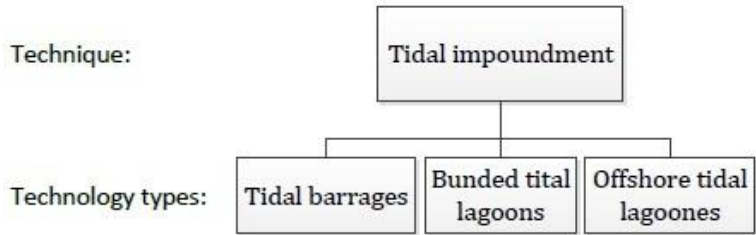
Figure 2.6. Tidal impoundment technologies

Tidal stream. This technique is based on kinetic energy and uses the energy from the currents occurring when the water levels are raising/ lowering. This type will be the main focus of this thesis.
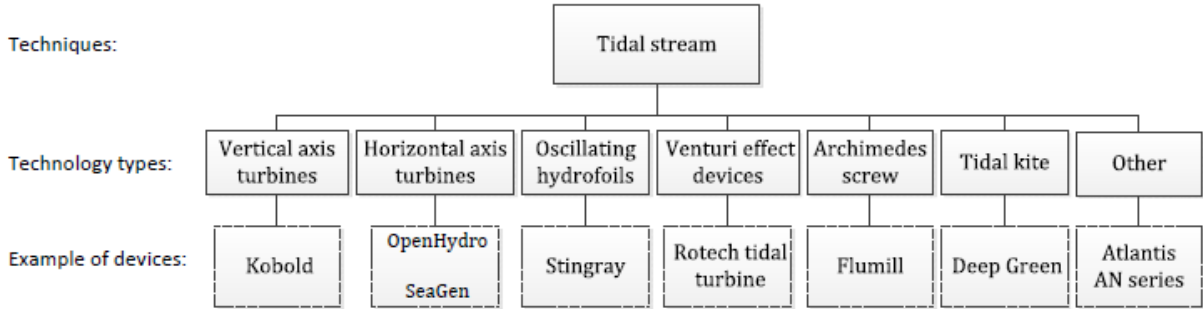
Figure 2.7. Tidal stream technologies

To get inspiration for further development of vertical axis technology the other devices will also be briefly studied. The different technologies and devices are organized in Figure 2.7.

2.2.1 Kobold

The Kobold tidal turbine is developed at INSEAN and Ponte di Archimede International S.p.A., both located in Italy. The device is a vertical axis turbine using the lift force to produce electricity. In 1995 Ponte di Archimede began to develop Kobold, the initial case was to develop a tidal turbine which especially had high efficiency but also a simple, reliable and economically preferable design. INSEAN was established in Rome 1927 as a model testing facility for navy ships (INSEAN, 2007). Nowadays the company possesses great experience in numerical modeling and testing of marine turbines and propellers which was the reason for the cooperation to begin.

The simulations was challenging because of the unsteady and non-uniform flow, unknown rotational speed, cavitation, viscous turbulent flow, stall and blade-to-blade effects. Two optimized test models were eventually produced and water tank testing of a three bladed and a four bladed version begun as seen in Figure 2.8. With the four bladed version wakes perturbation hydrodynamic negative interference was observed and the final device ended up having three blades. An significant improvement was then

observed when a free oscillation blade pitch of (0°, +10°) was used compared to the initial solution (-10°,+10°) that was expected to be optimal (INSEAN, 2007).
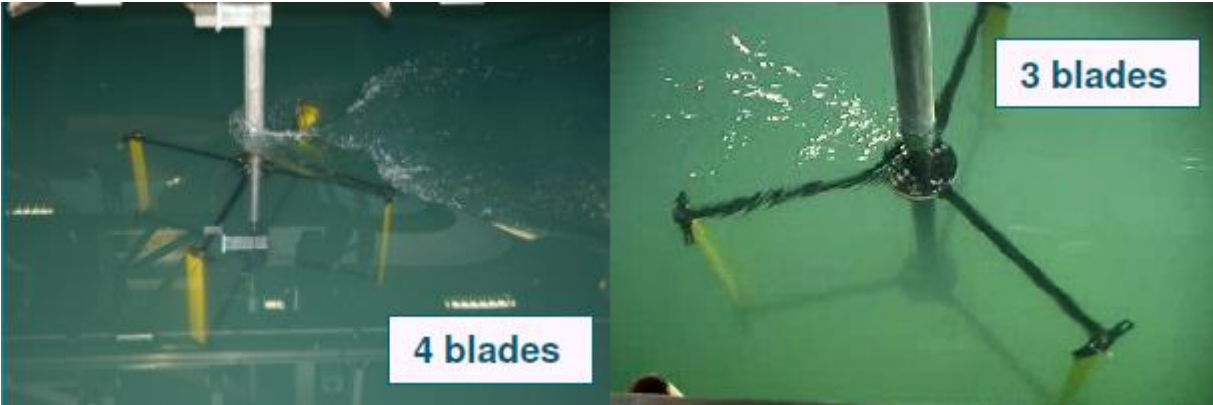
Figure 2.8. Three and four bladed model testing

In 2001 a pilot plant was installed 150 meters offshore near Messina. The tidal current at the site is between 1.5-2 m/s and at certain points in the area more than 3 m/s. The simulations resulted in the properties presented in Table 2.1 where the platform properties also can be read. The platform is designed to be big enough for all equipment but also to withstand the thrust of about 10 tonnes during standard working conditions. The platform is moored to displacements made out of concrete that is disposed 90° from one another at 18-35 meters depth (INSEAN, 2007).

Table 2.1. Kobolt specifics

Turbine		
Rotor diameter	6	meters
Blades height	5	meters
Chord	0.4	meters
Number of blades	3	
Blades material	Carbon fibre & epoxy resin	
Floating platform		
Diameter	10	meters
Depth	2.5	meters
Displacement (each)	35	tonnes
Mooring blocks	4	
Block material	Concrete	
Mooring line material	Textile rope and chains	

When deployed the turbine produces 25-30 kW at about 2 m/s and 18 rpm. The company presented the results of the turbine performance (in terms of electricity output) that can be seen in Figure 2.9 (INSEAN, 2007).
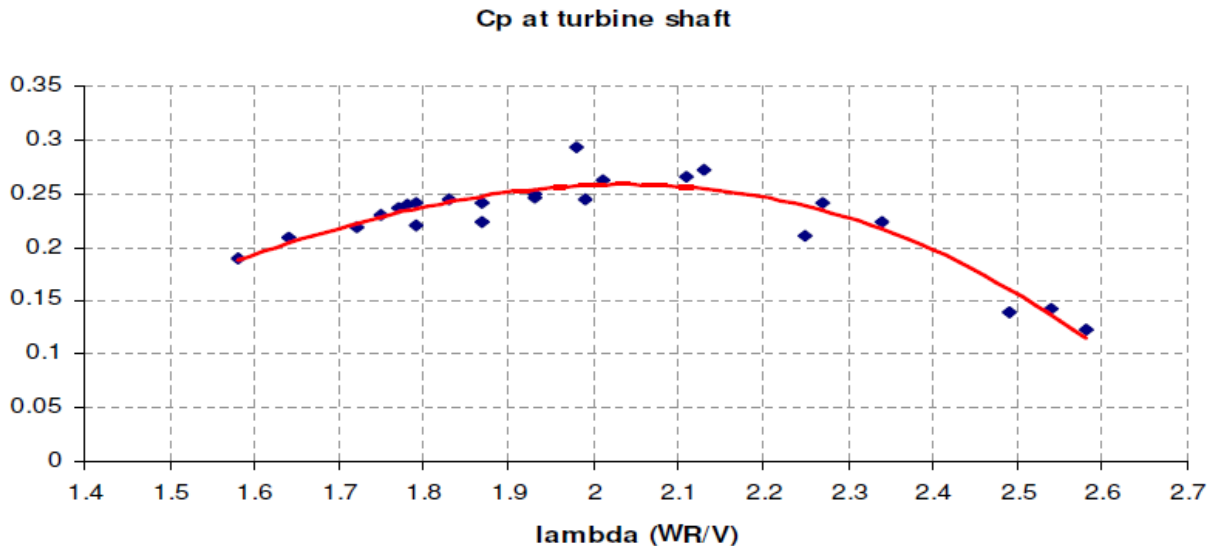
Figure 2.9. Performance of Kobolt versus tip speed ratio

In 2005 Kobold was connected to the electricity grid, all the electrical components were optimized in order to meet the grid requirements and a submarine cable was used to connect the turbine to the land based electrical grid. The resulting turbine can be seen in Figure 2.10 (INSEAN, 2007).

Figure 2.10. Kobolt

Kobold has been very reliable during its first 6 years at operation but a few problems have however occurred (INSEAN, 2007):

- The thrust bearing was made of Ertalon (a material that is usually used for propeller bearings) which gave two problems; stress weaknesses in the radial direction and water absorption. This led to a failure seen in Figure 2.11 and the bearing was then built out of Orkot.
- The rubber blocks that stop the blades when automatically pitched during the revolution also was a weak point.
- The carbon fibre blades have a very high electrolytic potential and generates strong galvanic currents in the steel structure. It is very important to correctly protect the structure against this in order to avoid corrosion problems.
- Scuba divers had to be sent down periodically to keep the turbine clean so that the efficiency will remain high.

Figure 2.11. Bearing failure

2.2.2 OpenHydro

OpenHydro is a slow-moving horizontal axis turbine with an open center as seen in Figure 2.12 and was the first tidal current energy company to connect to the UK national grid and commence electricity generation (Tidal energy update 2009, 2010). The development started in the United States during the early 1990s, now the company has its head office and assembly facility in Ireland.
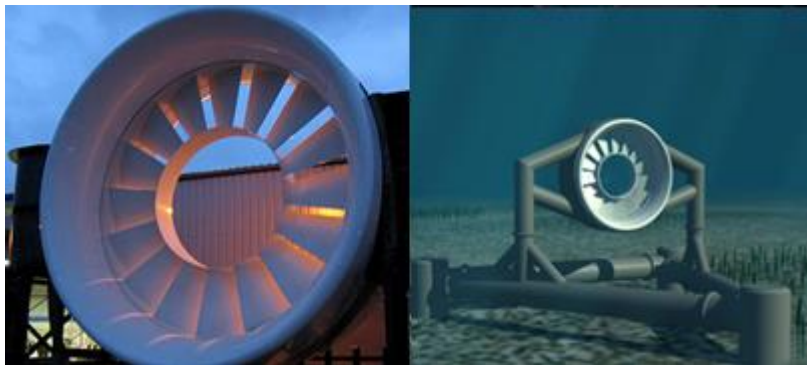
Figure 2.12. OpenHydro

The turbine is designed to be standing on the seabed (OpenHydro). It is 6m in diameter and has a rated power of 250kW (Tidal energy update 2009, 2010). It has a single piece rotor that is the only moving component in the turbine unit. Open-center and a shaped inlet duct improve turbine performance. The open-center solution also gets rid of the dangerous blade tips on conventional horizontal axis turbines and therefore decreases the risk of marine life to get injured. In the stator part there is a large efficient integrated permanent magnet generator making the slow moving concept work and minimizes the number of moving parts (OpenHydro). The cost for generating electricity with the OpenHydro solution is according to the company comparable with off-shore wind, but long term with a more large scale deployment it will trend towards on-shore wind costs (OpenHydro). The company has recently announced major projects in both Europe and North America.

2.2.3 SeaGen S

SeaGen S is a dual two bladed horizontal axis turbine with a more traditional horizontal axis wind turbine design, meaning that the rotors are connected to a gearbox to achieve a higher rotational speed on the shaft leading to the generator. The diameter of each rotor is 16 m and delivers a total rated power of 1.2 MW (Tidal energy update 2009, 2010). The rated power is achieved in currents faster than 2.4 m/s (MCT). The blades are also pitch controlled with a special 180 degree technique making the energy extraction

optimal and allow the device to operate in both ebb and flood (MCT). Another smart feature is that the rotors can be moved up and down vertically making it possible to operate at the highest third of the water column where the velocity is highest as seen in Figure 2.13. It also facilitates the maintenance since the rotors can be raised above the water surface. This function allows the SeaGen S system to achieve more than 48% efficiency over a broad range of current velocities (MCT).

Figure 2.13. SeaGen

SeaGen S is developed by Marine Current Turbines Ltd. and was installed in May 2008 after the successful smaller predecessor Seaflow with a rated power of 300kW (Tidal energy update 2009, 2010). No external electricity equipment is needed since all the electrical technique to produce grid compliant electricity is contained within the SeaGen S system itself. This makes it possible to daisy-chain the devices which reduces costs for cabling to the mainland (MCT). SeaGen S is capable of delivering 6000MWh per year which is comparable with a 2.4MW wind turbine (MCT). Marine Current Turbines Ltd. is now developing the next generation SeaGen U for deeper waters with a rated power of 3MW (MCT).

SeaGen was studied 3 years in an extensive environmental monitoring program that concluded that the device had no significant impact on the marine life at the site. The study included not only operation but also installation and other aspects (MCT).

2.2.4 Stingray

Stingray is an oscillating hydrofoil that changes the angle of attack towards the tidal current and can be viewed in Figure 2.14. This results in a lift force that makes the hydrofoil move in a periodic pumping motion. This nonlinear motion however, with a periodic loss of momentum, is resulting in a very large degree of mechanical complexity. 15% of the devices power rating is lost only to the hydraulic pressure accumulator to rapidly stop the hydrofoil, change the angle of attack and start the hydrofoil movement in the opposite direction (ESRU).
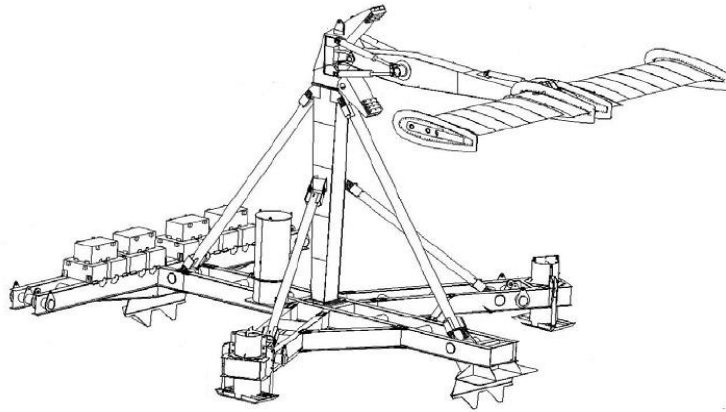
Figure 2.14. Stingray

2.2.5 Rotech tidal turbine (RTT)

Lunar Energy has developed the 1 MW RTT. As seen in Figure 2.15 below it is a horizontal axis bi-directional subsea turbine. The turbine is placed in the middle of a symmetrical venture duct. This solution accelerates the incompressible water past the turbine in order to maximize electricity production. It uses gravity foundation and can therefore be deployed easily on depths in excess of 40 meters (LEP). Another smart solution is that the turbine can be dismounted from the foundation as seen in Figure 2.15 so that only the turbine can be lifted to the surface.
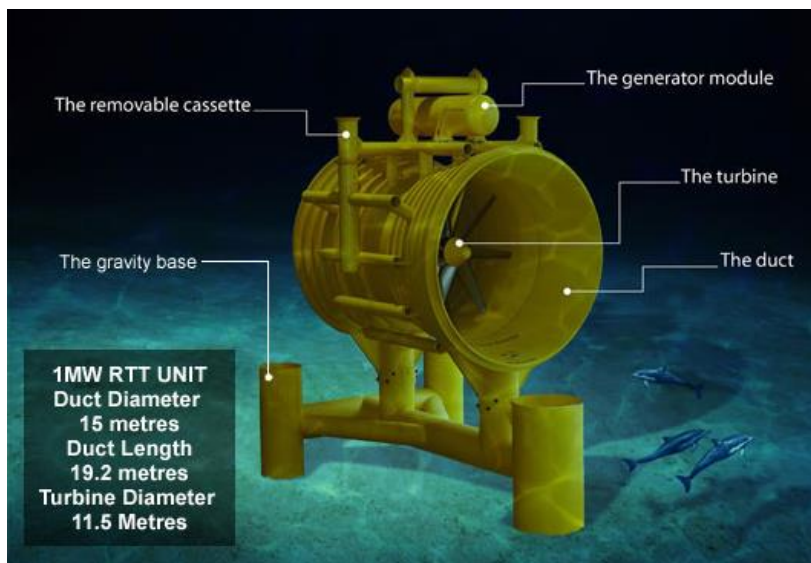
Figure 2.15. Rotech tidal turbine

2.2.6 Flumill

The Flumill solution is a Norwegian seabed located technology with a buoyant top that connects two turbines as seen in Figure 2.16. This solution makes it possible to easily tow the device and then submerge and install it which reduces the demand of large boats to lift the 40 meter high device and thereby lowers the installation cost. However the foundation has to be attached to the seabed before installing the Flumill system, this is done by the use of monopole or predrilled piles (Flumill).

Figure 2.16. Flumill

The device is self-regulating and is usually operating in angels between 25-50 degrees from its upright position making it possible to operate within a large span of tidal current velocities and minimizes the load on housing and the foundation (Flumill). When the water pass the helixes it changes direction thus forcing the helixes to turn along its own axis. The helixes are counter rotating and cause low turbulence and cavitation effects. They are built in composite materials due to durability, strength and relatively low costs while the rest of the device is made of steel. The housing is watertight and contains a generator from an original equipment manufacturer for standard subsea solutions.

After CFD simulations from two independent facilities with different software, towing, tank and pilot tests Flumill will now be built in a full scale for a pilot deployment in Rystraumen in northern Norway (Flumill).

2.2.7 Deep Green

Deep Green is a tidal kite technology developed by Minesto. The technology is very innovative within the tidal current field and works like a wind kite with a turbine mounted under the wing as seen in Figure 2.17. The technology is used to be able to utilize low velocity tidal currents to avoid the competition of the "hot spots" as the company call it, that is the locations with tidal currents exceeding velocities of 2.5 m/s which makes the number of suitable sites for the Deep Green huge (Minesto). Other advantages with Deep Green are that only attachment and detachment has to be done offshore which lowers the maintenance cost. Deep Green is also, in relation to many competitors, small and has a weight of 7 tonnes per 500kW unit (Minesto).
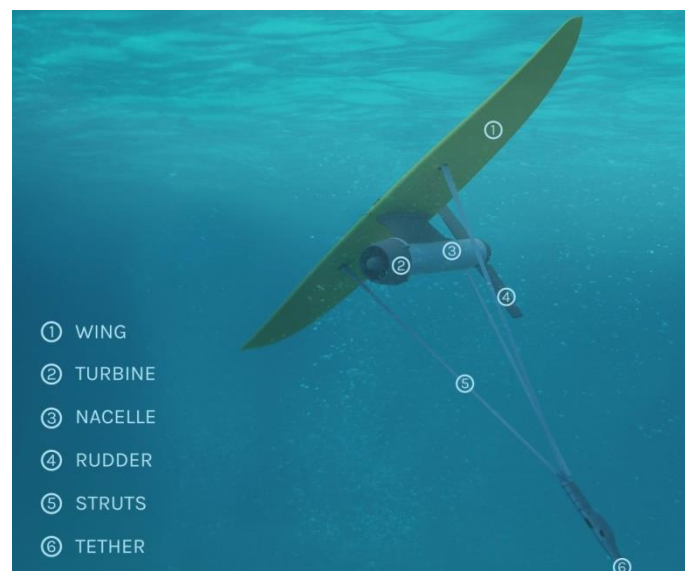
Figure 2.17. Deep Green

Minesto has previously performed different kind of tests including a smaller scale model ocean trial in 2011/2012. This has confirmed the functionality of the components, properties and that the technology operates safely and efficient in the ocean. Now optimization of fundamental parts are in progress and the next goal is to deploy a 3 MW array in 2015 and a 10 MW array in 2016 (Minesto).

2.2.8 Atlantis AN-400

The Atlantis AN series is developed for shallow waters. The AN-400 as seen in Figure 2.18 has been extensively tested with help of towing in 2008 and is connected to the electrical grid in Australia (ARC). Once again the lift is the driving force but this time with a high number of small blades mounted on a chain perpendicular to the flow. The turbine is designed not to break even when subjected to significant amounts of debris in the water. The device is also designed so that it is fully scalable for different locations and requests (ARC).

Figure 2.18. Atlantis AN-400

2.3 Power in the water

The operation of harvesting energy in free streaming water and currents is a field that is relatively poorly developed and explored when compared to other types of renewable energy. When utilizing the currents of the sea the procedure is much like wind energy conversion systems, which is a much more mature technology. When comparing the two, there are very little that separates the theory surrounding the energy within as well as the energy conversion of fluids in motion. It is therefore not surprising that many of the ideas employed in the wind energy sector are being reinvented in the marine current sector.

For a fluid in free stream the available kinetic energy (E_K) for any given cross section is given by Eq. 1.

$$E_K = \frac{1}{2}mu^2 \qquad\qquad 1$$

And the total power (P) can be expressed as Eq. 2.

$$P = \dot{E}_K = \frac{1}{2}\dot{m}u^2 = \frac{1}{2}\rho Au^3 \qquad\qquad 2$$

From Eq. 2 one can see the strength of applying similar technology in water. The density of water is roughly 833 times that of air which means that the same turbine could produce the same amount of power at considerably lower fluid velocities (almost at velocities a tenth of that of air). Another interpretation of this would be that since the fluid velocity is raised to the power of three, it is the single most important parameter when designing an energy conversion device utilizing free streaming fluids. For example, if the fluids velocity increases by 20% then the power in the fluid would increase by 72.8%.

In order to illustrate this, the parameters mentioned in section "1.2 Case" are used to get a sense of the power available in the current case.

Table 2.2. Schematic input values

Density [water at 5°C]	999.965	kg/m³
Radius	1	m
Height	4	m
Area	8	m²
Velocity	0.1-3	m/s

By using Eq. 2 and the figures in Table 2.2 the available power in the water can be calculated. The result is shown in Figure 2.19.
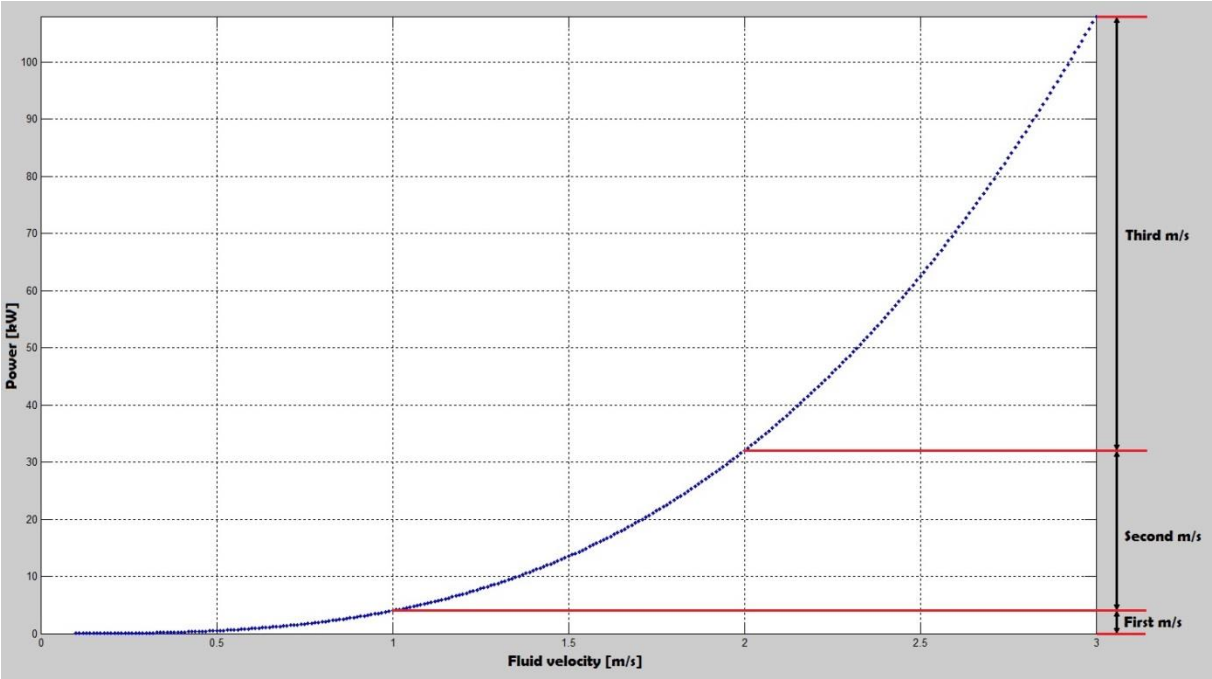
Figure 2.19. Total power available in the flowing water.

Figure 2.19 clearly visualizes the effect of the fact that the power is dependent on the velocity cubed creating a parabolic curve. At 1 m/s the power is 4 kW, at 2 m/s it is 32 kW and at 3 m/s it is 108 kW. This means that a good site selection will be very vital for the possible power extraction and therefore also for the economical aspect.

One fundamental aspect about energy is that it cannot be either created or destroyed, it is only possible to convert it. In this case it is the kinetic energy of the fluid that is converted in to kinetic energy of the rotor i.e. movement which makes the rotor turn along its axis. Through history there have been numerous

different ways of achieving this and these can be divided in two general groups, technology based on utilization of the drag force and technology utilizing the lift force.

2.4 Drag force fundamentals

When a physical body is immersed in a moving fluid the body is subjected to forces by the interaction between the body and the fluid. The forces are the result of pressure differences arising but also from the wall shear stress between the body and the fluid due to the viscous effects (B Munson, 2006). Depending on the shape of the body and the angle of which the moving fluid hits it (among other) the resulting force will be different. If the resulting force is not in the same direction as the upstream velocity the force is usually divided into a drag force and a lift force. The drag force is always present and is the part of the resulting force that acts in the same direction as the upstream velocity (B Munson, 2006). The lift force is the part acting perpendicular to the upstream velocity and will be described under the next headline.

In Figure 2.20 the pressure and shear forces that are acting on a small element of the surface of a body is visualized.
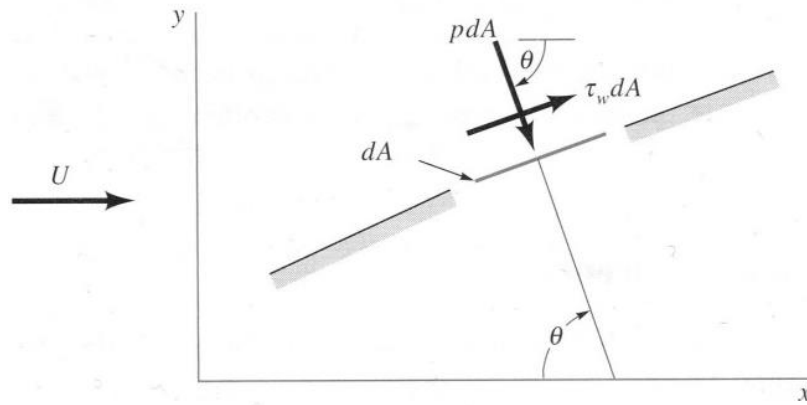
Figure 2.20. Pressure and shear forces on a small element of the surface of a body

If R would be the resulting force of the pressure and shear forces in Figure 2.20, then the drag force ($\mathfrak{D}$) would be R_x. By using Eq. 3 the drag force can be calculated.

$$\mathfrak{D} = \int R_x = \int p \cos(\theta)\, dA + \int \tau_w \sin(\theta)\, dA \qquad\qquad 3$$

Where θ is the angle to the upstream velocity in this specific case (B Munson, 2006). However, to obtain the shear stress and pressure distribution is very difficult and therefore dimensionless drag and lift coefficients for different body shapes has been developed. The drag coefficient is defined in Eq. 4.

$$C_D = \frac{\mathfrak{D}}{0.5\,\rho A u^2} \qquad\qquad 4$$

If a drag force coefficient is used from a table it is very important to know which characteristic area that is used. In Appendix 2 some drag coefficients for different shapes are presented together with the characteristic area (reference area).

If the drag coefficient is however used correctly it is very useful. By knowing C_d for a certain body shape the drag force caused by it in a moving fluid can easily be calculated by rearranging Eq. 4 to Eq. 5 below:

$$\mathfrak{D} = \frac{1}{2} C_D \rho A u^2 \qquad\qquad 5$$

If however a machine for energy extraction is built the periphery velocity (v) will be lower that the upstream velocity (u). Therefore this formula has to be modified if the possible energy extraction from the fluid is to be calculated. In Figure 2.21 a Persian wind wheel states a good example where the velocities of the free stream and of the blade have different speed.
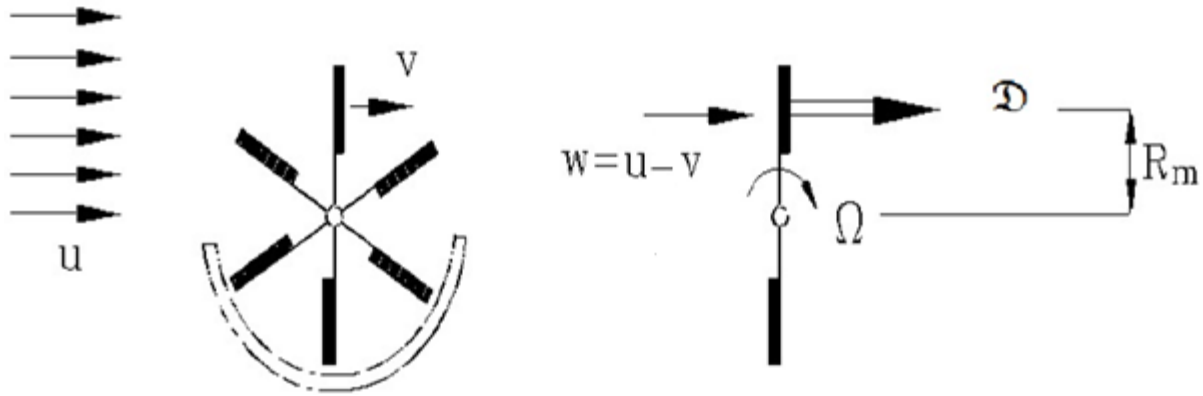
Figure 2.21. Persian wind wheel example

The modification then clearly has to be done to the velocity and if the characters in Figure 2.21 is used the result become Eq. 6.

$$\mathfrak{D} = \frac{1}{2} C_D \rho A w^2 = \frac{1}{2} C_D \rho A (u - v)^2 \qquad\qquad 6$$

2.4.1 Efficiency

As an example Savonius turbines are less efficient than vertical axis turbines using lift force technique and the Savonius wind turbines has an efficiency of about 15% as seen in Figure 2.22 (Belarusian web portal on renewable energy).

According to (Ackermann, 2011) a cup anemometer has an efficiency of up to 8% and an Persian wind wheel up to 16%. Since the principles of the fluid dynamics are the same in wind and water the only difference between tidal- and wind turbines are that tidal turbines are operating in a higher density fluid with lower velocities. Therefore the efficiencies of the different kind of devices should be the about the same as for wind turbines and Figure 2.22 can be used to determine which technique to use.
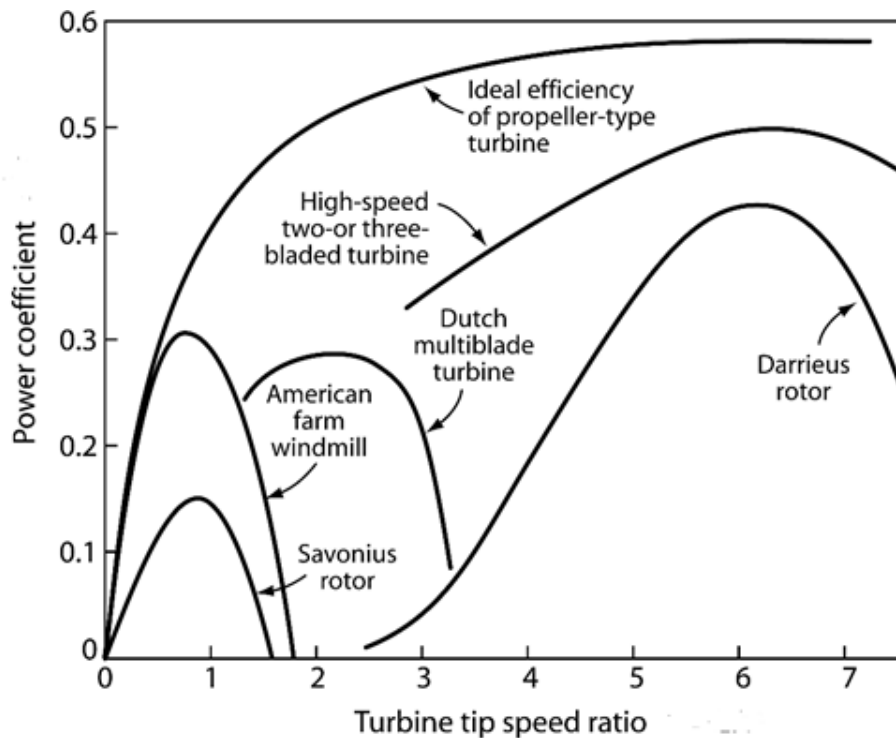
Figure 2.22. Comparison between different turbine design concepts

2.5 Lift force fundamentals

In a free stream the fluid flows in a parallel manner until it reaches an object (in this case a foil). The flow is commonly seen as a number of stream tubes which is parallel and has both constant mass (or mass flow) as well as constant energy. When the flow reaches an object the stream tube gets narrower as a result of the blockage and the flow is deflected from its original path and flows around the foil. As can be seen in Figure 2.23 the geometry of the foil forces a part of the flow to travel a longer distance on the upper side.
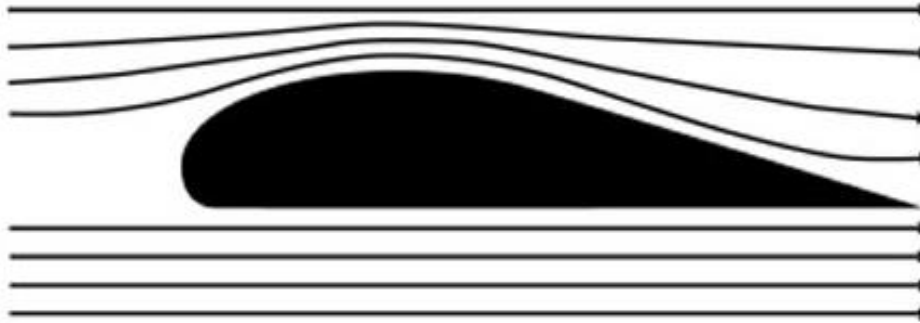
Figure 2.23. Deflected flow due to blockage

According to the conservation of mass (matter cannot be either created or destroyed) the flow on the upper side must (if incompressible fluid) obtain a higher velocity than that of the lower side in order to maintain constant mass flow rate which is illustrated in Figure 2.24.
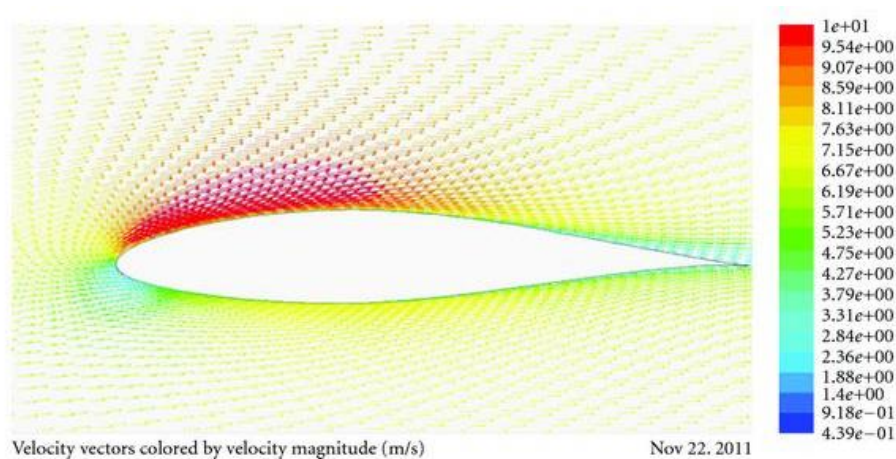
Figure 2.24. Velocity distribution over foil

In order to connect the stream tube velocities to the lift force the Bernoulli principle has to be applied. If the fluid flows with constant energy Bernoulli states that a difference in fluid velocity creates a difference in the local pressure of the fluid (assuming constant density) as can be seen in Figure 2.25.
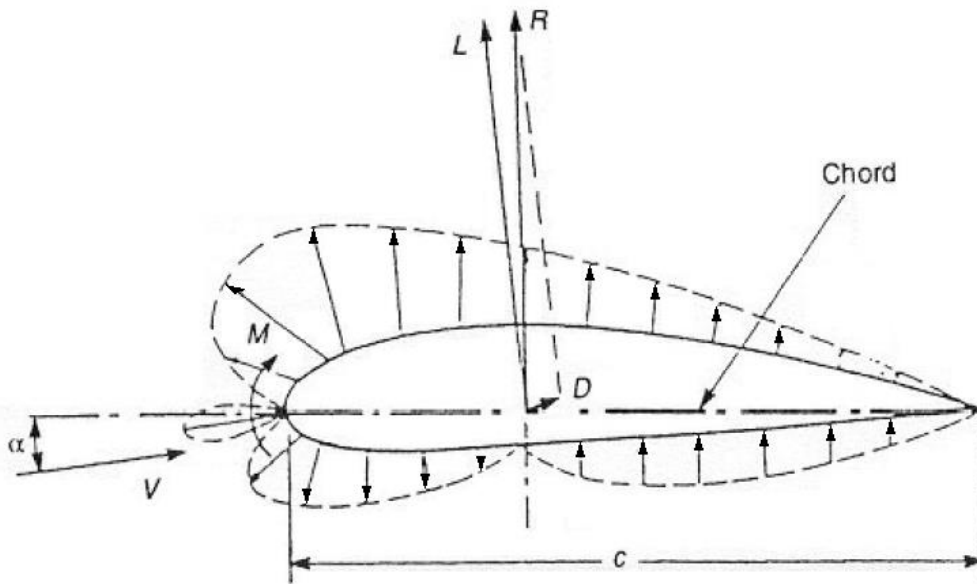
Figure 2.25. Pressure distribution and forces acting on the foil as it is placed in a moving fluid

The pressure difference between the upper and lower side creates a hydrodynamic force (R) acting on the foil. Figure 2.25 also illustrates the hydrodynamic force divided in to its components. The drag force (Ɗ) acting parallel to the flow direction and the lift force (L) acting perpendicular to the flow direction. Note that the flow in this case hits the foil at an angle called the angle of attack (α).

The design of the hydrofoil differs greatly depending on the application but even within the same field the design options can be innumerable. The hydrofoil can be either symmetric or asymmetric, where the symmetric foil demands an angle of attack to produce lift. Some of the design parameters can be seen in Figure 2.26.
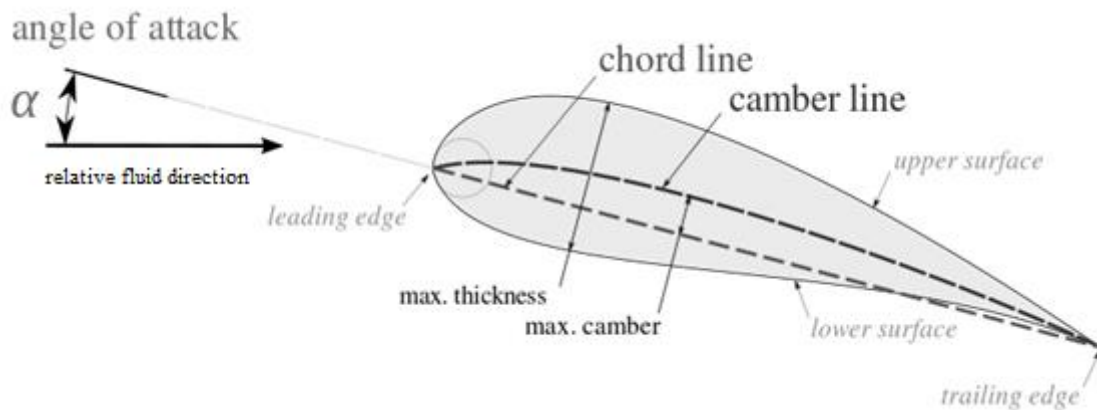
Figure 2.26. Hydrofoil parameters

The chord is a straight line drawn from the leading to the trailing edge. In a symmetric hydrofoil the chord line creates a perfectly mirrored image between the upper and lower half. The length of the chord line is directly proportional to the reactant force generated by the hydrofoil (A design methodology for cross flow water turbines, 2010).

If a line is drawn in the middle of the upper and lower surface the mean camber line is created. For symmetric hydrofoils this line will coincide with the chord line. For asymmetric hydrofoils these two will define the camber which is the maximum distance between the two aforementioned lines. The higher the camber the more curved the hydrofoil gets. When operating a cambered hydrofoil the geometry naturally creates a length difference between the upper and the lower side meaning that the asymmetrical hydrofoil

will generate lift at an angle of attack equal to zero. Generally the lift increases with an increasing camber but one has to be aware of that the drag will increase as well.

Every hydrofoil, regardless of type of cross section, experiences an increase in both lift- and drag coefficients (C_L and C_D respectively) as the angle of attack increases (assuming that Reynolds number remains constant). These dimensionless coefficients can be experimentally derived for any foil type and is a measure of how the foil will perform depending on the environment in which it is operating. However, the lift coefficient reaches a maximum after which the angle of attack becomes so great that the flow separates from the upper surface and the lift coefficient is decreased. This phenomenon is called stall and can be prevented or delayed by the use of different techniques like slots in the hydrofoil, vortex generators, pitching of blade etc.
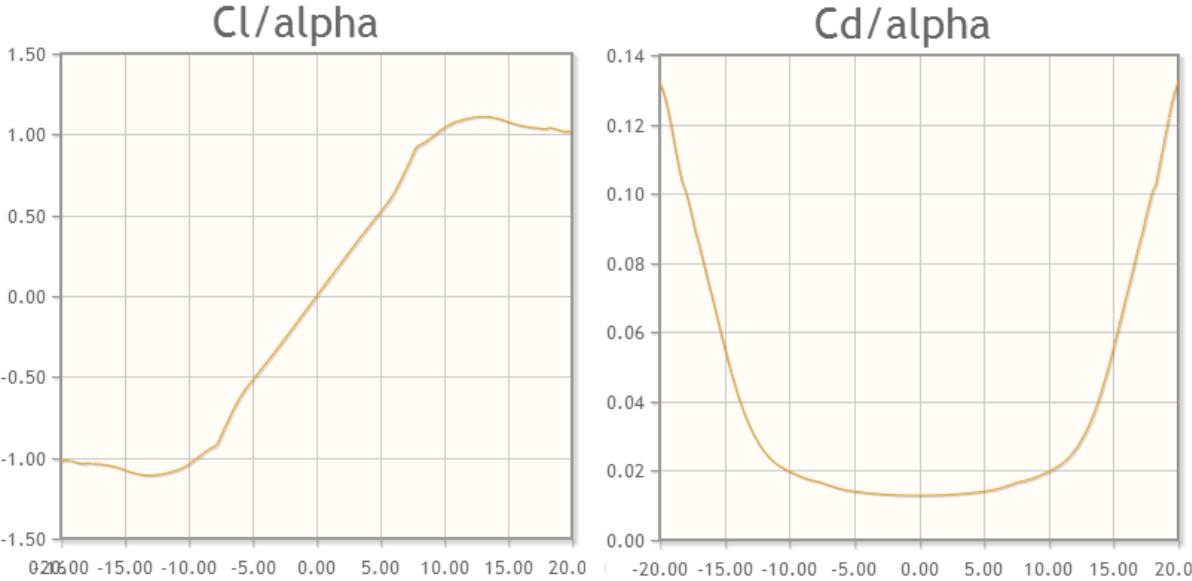
Figure 2.27. Example of Cl and Cd versus the angle of attack

The effect of an increasing thickness of the hydrofoil is a continuously increase of the drag experienced by the foil. But according to (Wainfan, 2010) a blunt leading edge is less sensitive to a turbulent incident flow. Since the blade of a VAWT is experiencing a path which allows the angle of attack to oscillate between a large variation of degrees and in addition allows the blade to follow in another blades turbulent wake the thickness of the leading edge could prove to be of great importance in order to prevent separation.

If the blade is viewed from the top its length is referred to as the span. The span of the blade is directly related to the total force generated by the blade. A longer blade generates higher forces (both lift and drag) but of course demands more of the structure in terms of stiffness, durability etc. This aspect will not be further examined and is not within the scope of this project. If the span is increased and the chord is kept constant the effect of tip vortices will decrease since these are considered constant regardless of blade length and the drag force per unit length will decrease.

2.6 Introduction to H-shaped Darrieus turbines

In the light of the literature study the decision was made that the project would focus on the optimization of an H-shaped Darrieus turbine (lift force utilization turbine) with the dimensions stated in section "1.2 Case".

The vertical axis turbines were first implemented in the wind turbine industry but have been largely outcompeted to the benefit of the horizontal axis turbines. However, the potential for vertical axis turbines for different water current applications are good.

The main disadvantages of the vertical axis turbine are (Performance investigation of H-rotor Darrieus turbine with new airfoil shapes, 2012):

- Comparable low efficiency.
- Little to no ability to self-start.
- Oscillating torque and power output which puts high demands on material and dimensioning.
- Large moment puts high demand on bearings and shafts.

The main advantages of the vertical axis turbine are (Performance investigation of H-rotor Darrieus turbine with new airfoil shapes, 2012):

- Compact design.
- Simple design with few moving parts
- No need for a yaw-control system
- Can be placed closer together when installing a whole park.

Of the energy available in the streaming fluid the theoretical maximum energy that can be converted by a turbine is 16/27 (C_{Pmax} = 59.26 %) and is called the Betz limit (Tong, 2010). However, Newman showed in (Multiple actuator-disc theory for wind turbines, 1986) that when a conventional vertical axis turbine is used the limit could be increased to 16/25 (C_{Pmax} = 64 %) due to the effect of having two halves operated in the same control volume.

2.7 Environmental aspects of tidal current energy extraction

The importance of using renewable energy sources has been widely accepted in the last decades. However renewable energy sources have their disadvantages and tides is an area with, so far, little experience. The advantages are easy to list with benefits such as reliable production, no visual pollution or CO_2-emissions etc., but what is the impact on the marine environment?

When SeaGen were to be tested an extensive 3-years multi-million dollar environmental monitoring program was conducted in order to obtain environmental permission for development and installation of the device (The impact of tidal stream turbines on large-scale sediment dynamics, 2009). The monitoring started by collecting data prior to the installation, during the installation and during operation. In general the results showed no major impacts on marine mammals or significant change to the ambient velocity or flow direction within the lough. However the results showed that some avoidance was monitored both under and above the surface. Below the water surface this avoidance is very positive since in the immediate surroundings of the turbine blades the risk for seals, porpoises etc. to come in contact with the moving rotors is reduced. Above the surface some fine scale displacement of birds was recorded but the overall numbers in the narrows remained stable. These results and more that can be read in (MCT, 2011). The conclusion was that the installation and operation of the SeaGen system, including the mitigation put in place, has not had any significant impact on marine life at the site.

A document from the Environmental Protection Agency in Sweden states that reduced velocities contributes to the accumulation of finer sediment such as sand that forms sandbanks etc. (Naturvårdsverket, 2011). This will naturally occur around the turbines too, the question is in how large scale.

A study of the Bristol Channel with a mean spring tide range of 12.2 meters and a mean neap tide range of 6 meters is performed with help of a one-dimensional numerical model. It concludes that "a small amount of energy extracted from a tidal system can lead to a significant impact on the sediment dynamics, depending on tidal asymmetry at the point of extraction." (The impact of tidal stream turbines on large-scale sediment dynamics, 2009). Tidal asymmetry refers to the interactions between quarter and semi-dual currents. This result can also affect far from the location where energy is extracted, in this rather extreme case up to 50 km away. This is however a very simplified model of the Bristol Channel which essentially describes the key features impact on each other and more research is certainly needed in this area.

2.8 Alternative evaluation methods

The aim of this project was to simulate and try to predict the interaction between the fluid and the turbine in order to do a preliminary design proposal for a small cross flow water turbine. Presently there are several different methods capable of achieving this goal, all with their own strengths and weaknesses. The appropriate method of evaluation is always a tradeoff between cost, time, capability and accuracy.

2.8.1 Computational Fluid Dynamics, CFD

The method is highly respected and is used in a broad spectrum of industries and applications. It provides solutions with high accuracy as well as the opportunity to create visual aids which provides a good understanding of how the fluid flows around the turbine.

Using CFD enables the user to choose between doing 2D and 3D simulations and the possibility of simulate how the flow is affected by the presence of the shaft, struts and foundation. It also provides a much more detailed simulation of the flow and important effects as for example dynamic stall and wake effects can be simulated.

The method is however very sensitive to user errors as the virtual reality that is created is of a very complex nature. This also indicates of another drawback of this method. As the accuracy is enhanced (by refining the mesh, shifting to 3D or adding shaft etc.) the complexity of the model increases. This increase creates high demands on the computational power available as well as an increase of the simulation time. For this reason the CFD approach could be more suitable for design details rather than for preliminary design optimization.

2.8.2 Scaled model

Building adjustable scaled models of the turbine is a convenient way of avoiding the need of a computer generated reality. Done correctly, the scaled model can be tested in nearly the exact conditions in which the turbine will operate and thus incorporating the impact of struts, shaft, vortices, dynamic stall and wake effects etc.

The accuracy of this method is highly dependent on the controlled environment in which the models are to be tested and therefore the quality of the test rig, measuring instruments, surface roughness of ingoing components and the preparatory work etc is of the essence. A big drawback of creating scaled models is that it is a relative expensive solution method. The manufacturing of the components, rig and testing environment are all costly and especially if a broad spectrum of different foils are to be tested.

Assuming that the financial demands can be met the creating of the right test conditions could prove the most challenging. The scaling can be performed in three different ways depending on the sought outcome. Geometric similarity implies that the ratios of prototype characteristic lengths to model lengths are equal (Chanson, 1999). The model will have the same shape (angles etc) as the full scale.

$$\frac{H_f}{H_M} = \frac{c_f}{c_M} = \frac{d_f}{d_M}$$

7

Kinematic similarity implies that the ratios of prototype characteristic velocities to
model velocities are the same (Chanson, 1999). Kinematic similarity ensures that the flow pattern is similar at different stages in the turbine.

$$\frac{u_f}{u_M} = \frac{c_{\infty,f}}{c_{\infty,M}} = \frac{d_{w,f}}{d_{w,M}}$$

8

Dynamic similarity implies that the ratios of prototype forces to model forces are equal (Chanson, 1999). Dynamic similarity also demands geometric similarity and if both dynamic and geometric demands are satisfied then kinematic similarity is achieved as well (NTNU).

$$\frac{F_f}{F_M} = \frac{l_f}{l_M} = \frac{D_f}{D_M} \qquad\qquad 9$$

For dynamic similarity several dimensional parameters (Fr, Eu, Re, We, Ma) has to be equal for the full scale and the model (Chanson, 1999). When using the same medium in both cases it is impossible to satisfy similarity for all these parameters and a tradeoff has to be made with regard to the predominant forces. In the present project the forces generated by the hydrofoils is strongly dependent on the Reynolds number and therefore Re must be as equal as possible to ensure a good correlation between the two cases.

$$Re_f = Re_m \qquad\qquad 10$$

$$\frac{\rho u_f c_f}{\mu} = \frac{\rho u_m c_m}{\mu} \qquad\qquad 11$$

$$\frac{u_f}{u_m} = \frac{c_m}{c_f} \qquad\qquad 12$$

Eq. 12 implies that if the turbine is scaled down by 1/5 (geometrically) then the velocity must be five times higher in the model than in full scale. This puts very high demands on the model tests and makes such tests both impractical and expensive in smaller projects.

3 Methodology

The blade element momentum model (BEM) has its origin in the blade element theory (BET) which was first developed by William Froude.

The model calculates the turbines performance by evaluating the momentum that is transferred from the fluid in the free stream on to the blades of the turbine as the fluid flows through it. By estimating how the turbine affects the fluid and how the fluid affects the turbine the theories can be combined thus creating a solution through an iterative process explained in this chapter.

The model used in the present work has evolved during the years as new theories have been implemented to increase its accuracy. The different theories will be described briefly as well as their contribution to the model used. The theories presented in (Numerical and Analytical Investigation of Vertical Axis Wind Turbine, 2013) will form the basis from which the simulations are made.

3.1.1 Single streamtube actuator disc

In the actuator disc theory the turbine is viewed as a disc with an infinite number of blades placed in the free stream (Figure 3.1). The part of the free stream that is affected by the presence of the disc is known as the streamtube and is defined both upstream and downstream of the disc. The fluid entering the streamtube is considered to flow within the control volume at all times until exiting without interaction with the surrounding fluid. This implies that the model only considers flows and velocities normal to the turbines axis of rotation in the streamwise direction.

According to (James F. Manwell, 2009) the assumptions made for the ideal actuator disc is:

- Homogenous, incompressible, steady state fluid flow
- No frictional drag
- An infinite number of blades
- Uniform thrust over the disc area
- A non-rotating wake
- The static pressure far upstream and far down stream of the rotor is equal to the undisturbed ambient static pressure
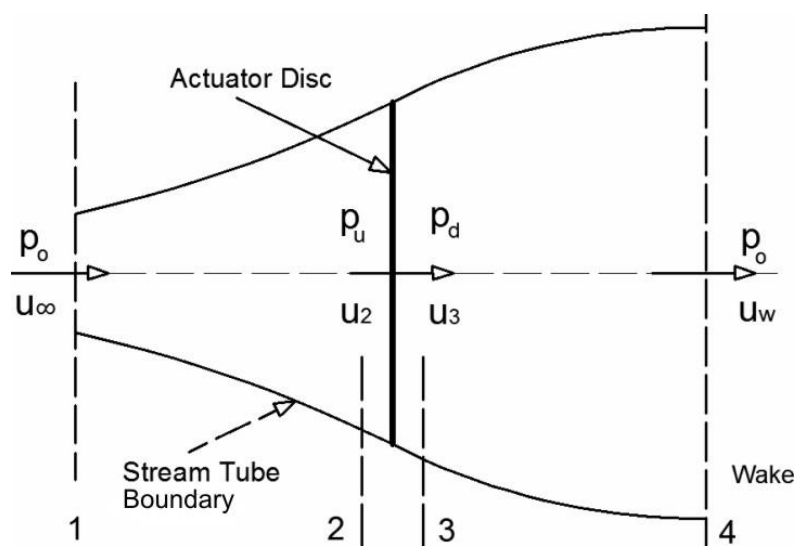- The fluid velocity is considered to remain the same across the rotor

Figure 3.1. Single actuator disc

The assumption is made that continuity of velocity through the disc exists. Therefore the velocities just before and just after become equal (Numerical and Analytical Investigation of Vertical Axis Wind Turbine, 2013).

$$u_2 = u_3 = u_R \qquad\qquad 13$$

As mentioned the total momentum within the system (streamtube) is considered constant. This imply that the force inflicted by the rotor on to the fluid is equal and in the opposite direction to the force caused by the fluid on the rotor, also known as thrust, T :

$$T = -\dot{m}(u_\infty - u_w) \qquad\qquad 14$$

Where ṁ is the mass flow rate of the fluid through the rotor and is defined by Eq. 15

$$\dot{m} = \rho A u_R \qquad\qquad 15$$

By the use of the Bernoulli equation and the fact that no work is performed on either side of the rotor the relationship between the pressures and velocities can be expressed for the upstream and downstream side of the rotor respectively.

$$p_0 + \frac{1}{2}\rho u_\infty{}^2 = p_u + \frac{1}{2}\rho u_R{}^2 \qquad\qquad 16$$

$$p_d + \frac{1}{2}\rho u_R{}^2 = p_0 + \frac{1}{2}\rho u_w{}^2 \qquad\qquad 17$$

It is now convenient to express the thrust acting on the rotor in terms of total pressure difference over the rotor.

$$T = A(p_u - p_d) \qquad\qquad 18$$

By combining equations 16 - 18 the thrust can now be expressed by:

$$T = \frac{1}{2}\rho A(u_\infty^2 - u_w^2) \qquad\qquad 19$$

One can now utilize the two expressions of the thrust and incorporating Eq. 15 in order to relate the velocities of the model to each other:

$$u_R = \frac{u_\infty + u_w}{2} \qquad\qquad 20$$

In order to get an understanding of how the turbine is interacting with the fluid and to predict the performance of the turbine the aim is to estimate the velocities at the rotor and downstream of it as the fluid exits the control volume. Since the turbine extracts kinetic energy from the fluid, and the fact that the model only considers in- and outflow in the streamwise direction, these velocities must be lower than the free stream velocity (u_∞). The fraction of which the velocities are decreased, known as the induction factor (a) can be introduced in the model and is defined in equation 21.

$$a = \frac{u_\infty - u_R}{u_\infty} \qquad\qquad 21$$

The induced velocity (u_R) and the downstream velocity (u_w) can now be expressed as a function of the free stream velocity and the induction factor

$$u_R = u_\infty(1 - a) \qquad\qquad 22$$

$$u_w = u_\infty(1 - 2a) \qquad\qquad 23$$

In accordance with (James F. Manwell, 2009) the power output from the turbine can be expressed as the thrust times the velocity at the rotor and by using Eq. 19 and simultaneously substituting the induced and the downstream velocity (Eq. 22 - 23) both the thrust and the power are expressed in terms of (a) and (u_∞).

$$T = 2\rho A a(1-a)u_\infty^2 \qquad\qquad 24$$

$$P = 2\rho A a(1-a)^2 u_\infty^3 \qquad\qquad 25$$

The dimensionless coefficients from which the performance is evaluated becomes:

$$C_T = \frac{T}{0.5\rho A u_\infty^2} = 4a(1-a) \qquad\qquad 26$$

$$C_P = \frac{P}{0.5\rho A u_\infty^3} = 4a(1-a)^2 \qquad\qquad 27$$

3.1.2 Hydrodynamics of the rotor

The second part in uncovering the interaction characteristics between the fluid and the turbine is to calculate the effects that the geometries and components of the turbine induce while operating in the moving fluid.

There are a few terms that are common for wind power applications or VAWT that play a significant role when designing and discussing the subject. The tip speed ratio (TSR) defines how fast the periphery of the turbine is spinning compared to the free stream velocity.

$$TSR = \frac{\omega r}{u_\infty} \qquad\qquad 28$$

The solidity of the turbine (σ) is a measure of how much of the total swept area that is occupied by the turbine in any given moment. The definition of the solidity varies and the following will be used throughout this project.

$$\sigma = \frac{Nc}{\pi D} \qquad\qquad 29$$

The flow field in which the VAWT is operating is relatively complex when compared to that of the HAWT. Since the axis of rotation is perpendicular to the streamwise direction the blades experience different conditions in every given azimuth location. The relative velocity (w) acting on the blade will vary as the blade alternates between moving toward and away from the free stream.

As does the angle of attack which is affected not only by the blades angle towards the streamwise direction but it is also greatly dependent on the fluctuations in the relative velocity. Unlike the HAWT the blades in the VAWT , due the aforementioned reasons, will experience large differences in the angle of attack which is oscillating between high values in both the positive and negative direction.
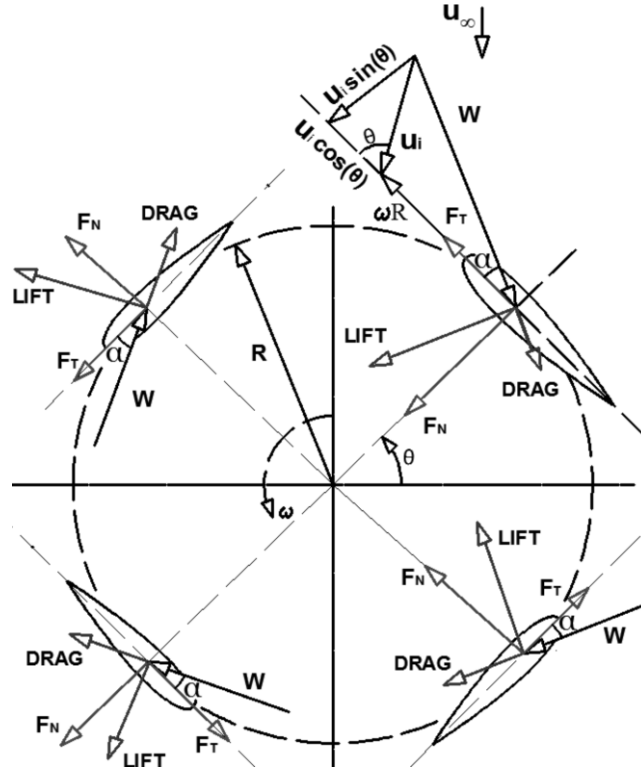
Figure 3.2. Top view of a vertical axis turbine

The relative velocity experienced by the individual blade is a combination of the free stream velocity and the rotational velocity of the turbine itself. Through basic geometric relationships it is possible to express it in terms of the velocities mentioned above as well as the azimuth location. This location is defined by the azimuth angle (θ) and can be seen in Figure 3.2.

$$w = \sqrt{(u_R \sin(\theta))^2 + (u_R \cos(\theta) + \omega r)^2} \qquad \text{30}$$

By applying equation 22 and 28 the relative velocity is rewritten as:

$$w = u_\infty \sqrt{((1-a)\sin(\theta))^2 + ((1-a)\cos(\theta) + TSR)^2} \qquad \text{31}$$

The angle of attack can be expressed in a similar fashion:

$$\alpha = \tan^{-1}\left(\frac{(1-a)\sin(\theta)}{(1-a)\cos(\theta) + TSR}\right) \qquad \text{32}$$

It is now possible to start evaluate the forces acting on the turbine and particularly the fraction acting in the tangential direction (driving the rotation) and the thrust which will be the solution to the iterating process.

As mentioned the forces generated by the fluid flow over the hydrofoil is dependent on the angle of attack as well as the non-dimensional Reynolds number (Re). Both the lift and drag coefficients are presented and can be seen in section 3.2.

$$Re = \frac{\rho w c}{\mu} \qquad \text{33}$$

The expressions for the tangential and normal force coefficients can be seen in equation 34 and 35.

$$C_t = C_L \sin(\alpha) - C_D \cos(\alpha) \qquad \text{34}$$

$$C_n = C_L \cos(\alpha) + C_D \sin(\alpha) \qquad \text{35}$$

These forces can then be calculated using:

$$F_t = \frac{1}{2}\rho w^2 H c C_t \qquad\qquad 36$$

$$F_n = \frac{1}{2}\rho w^2 H c C_n \qquad\qquad 37$$

The fraction of the force acting on one blade in the direction of the flow can be expressed for every azimuthal location. This force is known as the thrust (T) and in the presented model it is used to solve the iteration process. The instantaneous thrust is calculated in Eq. 38

$$T_i = F_t \cos\theta - F_n \sin\theta \qquad\qquad 38$$

By adding the thrust from each location the average thrust for the whole revolution can be calculated. By equating the momentum lost by the fluid and the momentum gained by the turbine the only unknown (the induction factor) can be calculated.

As the induction factor is known the velocity field and thus the forces acting throughout both the width and the depth turbine are known as well. The instantaneous torque from each individual blade and for every azimuthal location is given by:

$$Q_i = F_t r \qquad\qquad 39$$

The power as well as the dimensionless coefficients of performance of the turbine can now be evaluated as instructed below.

3.1.3 Multiple streamtube model

In the single streamtube model the induction factor is considered to be constant for the whole width of the turbine. In reality this is not the case since the blades interacts with the flow differently as it changes its azimuthal location, i.e. the flow velocity is decreased by different amount at different azimuthal locations.

Strickland first introduced the multiple streamtube model which allows the calculation of different induced velocities when solving the momentum equations for every streamtube separately (Figure 3.3).
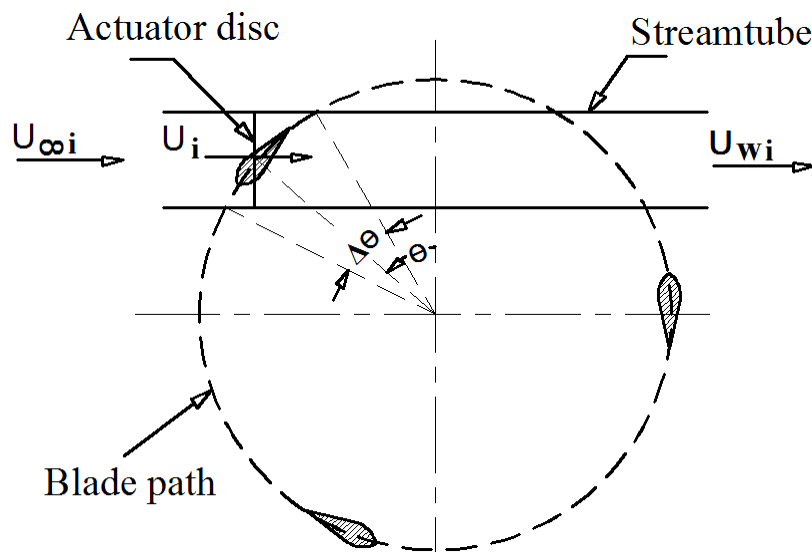

Figure 3.3. Multiple streamtube model

The swept frontal area of the turbine is divided into several smaller areas which will improve the accuracy of the model. The areas are separated by an equal share of the swept area which also determines the amount of streamtubes (N_θ) according to:

$$N_\theta = \frac{360^\circ}{\Delta\theta}$$
<div align="right">40</div>

Where $\Delta\theta$ denotes length along the periphery expressed in degrees.

The calculations are basically the same as for the single streamtube model but they are performed for each streamtube individually. To be able to make use of the improved model the average time that each blade spends in a given streamtube was used. (Gretton, 2009) describes it as time averaged chord length which (after slight modification to MST) is described by Eq. 41.

$$\check{c} = \frac{Ncd\theta}{\pi}$$
<div align="right">41</div>

(Gretton, 2009) states that the product Nc represents the total amount of blade-chord over one revolution while the fraction $d\theta/\pi$ is the proportion of the total circumference occupied by the streamtube. Therefore the following relationship between the time averaged force and the instantaneous force will be valid.

$$\frac{\check{c}}{c} = \frac{Nd\theta}{\pi} = \frac{T_{avg}}{T_i}$$
<div align="right">42</div>

By substituting T to T_{avg} and combining Eq. 26 and 41 the equation for solving the velocity field can be written as Eq. 43.

$$a = \frac{NT_i d\theta}{2\pi\rho A u_\infty^2} + a^2$$
<div align="right">43</div>

Note that A is the area of each streamtube and is defined by the following equation:

$$A = rH\sin(\theta)\,d\theta$$
<div align="right">44</div>

When combining the two the expression becomes:

$$a_{new} = \frac{NT_i}{2\pi\rho rH\sin(\theta)\,u_\infty^2} + a^2$$
<div align="right">45</div>

3.1.4 Double actuator disc

So far the velocity field is calculated once for the whole depth of the turbine. Since the blade of the VAWT passes the streamtube twice during one revolution it is reasonable to suspect that the velocity field is not linear throughout the depth turbine. In fact, since the fluid velocity is slowed down considerably from the first half to the second it is plausible that the interaction between the blade and the fluid is different as well as the available and supplied torque and power.

In the double actuator disc theory each passing of the blade is treated as an individual disc which ultimately means that two induction factors must be calculated, one for the upstream half (a) and one for the downstream half (á) (Figure 3.4).
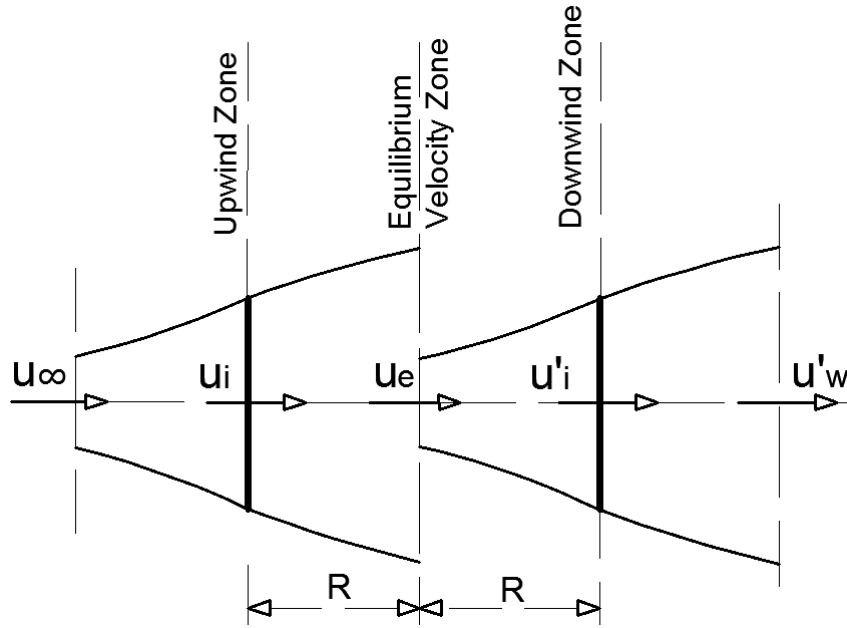
Figure 3.4. Double actuator disc

By introducing the second induction factor the velocities through the turbine is defined by Eq. 46-49.

$$u_i = u_\infty(1 - a) \tag{46}$$

$$u_e = u_\infty(1 - 2a) \tag{47}$$

$$\acute{u}_i = u_e(1 - \acute{a}) \tag{48}$$

$$u_w = u_e(1 - 2\acute{a}) \tag{49}$$

3.1.5 Glauert empirical formula

The Glauert empirical formula is a correction to the momentum theory which breaks down for large induction factors (Hansen, 2008). It describes how the thrust coefficient (C_T) and the induction factor (a) relates to each other. As the turbine decreases the velocity of the fluid (or the induction factor is increasing) the thrust will increase. This is a logical conclusion and the reason why the momentum theory (which reaches a maximum at a=0.5) has to be altered.

The following relations were used throughout the present project.

$$a \leq \frac{1}{3} \qquad\qquad C_T = 4a(1 - a) \tag{50}$$

$$a > \frac{1}{3} \qquad\qquad C_T = 4a(1 - \frac{1}{4}(5 - 3a)a) \tag{51}$$

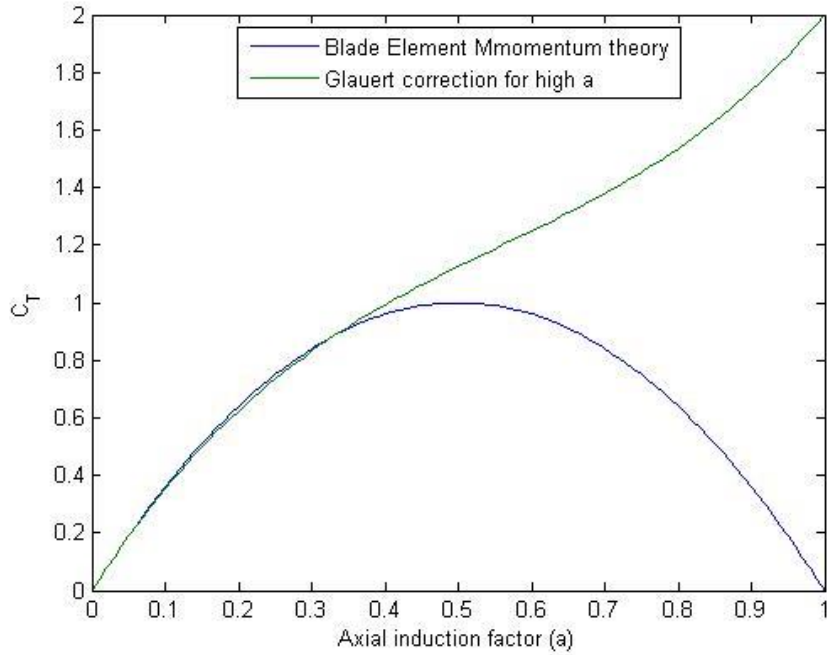The two different relations can be seen in Figure 3.5.

Figure 3.5. Thrust coefficient versus induction factor

3.1.6 Double multiple stremtube model

The combined method of the multiple streamtube and the double actuator disc theory is a much more accurate solution method. It allows velocity variations perpendicular to the flow direction as well as the ability to model parts of how the upstream half affects the downstream half of the turbine even though the two halves are assumed to be aerodynamically independent of each other (Aerodynamic analysis of the Darrieus rotor including secondary effects, 1983). The assumptions and limitations of the model are:

- The flow is assumed to be steady, isothermal, inviscid, incompressible and rotationless (Aerodynamic analysis of the Darrieus rotor including secondary effects, 1983)
- The static pressure far upstream and far down stream of the rotor is equal to the undisturbed ambient static pressure
- The model does not account for the presence of shafts or struts.
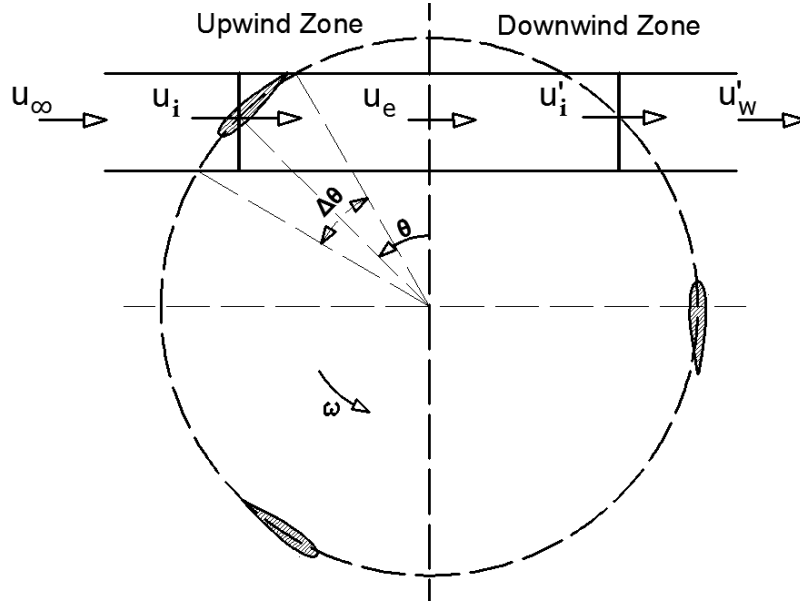- The model is unable to account for dynamic effects of dynamic stall and vortex shedding.

Figure 3.6. Double multiple streamtube model

The basics surrounding the final theory has already been shown although there are some mathematical differences to be made which are therefore presented in the following part. The equations leading to the solution of the iteration problem will also be presented both with and without the Glauert correction.

One distinct difference is the modifications made in Eq. 40. Since the blades flight path now is divided in two halves the blade only experiences a single streamtube once per revolution which ultimately means that fraction $d\theta/2\pi$ is now the proportion of the total circumference occupied by the streamtube. This leads to the fact that the relation between the time averaged force and the instantaneous force will be halved as the calculations will be doubled and more accurate.

$$\frac{Nd\theta}{2\pi} = \frac{T_{avg}}{T_i}$$

<div style="text-align: right">52</div>

For the upstream half:

$$w = \sqrt{(u_\infty(1-a)\sin(\theta))^2 + (u_\infty(1-a)\cos(\theta) + \omega r)^2}$$

<div style="text-align: right">53</div>

$$\alpha = \tan^{-1}\left(\frac{u_\infty(1-a)\sin(\theta)}{u_\infty(1-a)\cos(\theta) + \omega r}\right)$$

<div style="text-align: right">54</div>

$$a \leq \frac{1}{3} \qquad a_{new} = \frac{NT_i}{4\pi\rho rH\sin(\theta)\,u_\infty^2} + a^2$$

<div style="text-align: right">55</div>

$$a > \frac{1}{3} \qquad a_{new} = \frac{NT_i}{4\pi\rho rH\sin(\theta)\,u_\infty^2} + \frac{1}{4}(5-3a)a^2$$

<div style="text-align: right">56</div>

For the downstream half:

$$w = \sqrt{(u_e(1-\acute{a})\sin(\theta))^2 + (u_e(1-\acute{a})\cos(\theta) + \omega R)^2}$$

<div style="text-align: right">57</div>

$$\alpha = \tan^{-1}\left(\frac{u_e(1-\acute{a})\sin(\theta)}{u_e(1-\acute{a})\cos(\theta) + \omega R}\right)$$

<div style="text-align:right">58</div>

$$\acute{a} \leq \frac{1}{3} \qquad\qquad \acute{a} = \frac{NT_i}{4\pi\rho rH\sin(\theta)\,u_e^2} + \acute{a}^2$$

<div style="text-align:right">59</div>

$$\acute{a} > \frac{1}{3} \qquad\qquad \acute{a} = \frac{NT_i}{4\pi\rho rH\sin(\theta)\,u_e^2} + \frac{1}{4}(5 - 3\acute{a})\acute{a}^2$$

<div style="text-align:right">60</div>

As the velocity field is known the forces acting within the system is also known which ultimately means that the goal of calculating the momentum that is transferred from the fluid to the turbine is met. The sole remaining task is to calculate the performance of the turbine. The interesting values are those of average torque (Q_{avg}), power (P) and especially the dimensionless coefficients.

$$Q_{avg} = \sum F_t \frac{rNd\theta}{2\pi}$$

<div style="text-align:right">61</div>

$$P = Q_{avg}\omega$$

<div style="text-align:right">62</div>

The dimensionless coefficients for torque (C_Q) and power (C_P) can now be calculated and the performance of the turbine can be evaluated. It is by the use of these coefficients that the preferred design is going to be chosen.

$$C_Q = \frac{Q_{avg}}{0.5\rho u_\infty^2 2rHr}$$

<div style="text-align:right">63</div>

$$C_P = \frac{P}{0.5\rho u_\infty^3 2rH}$$

<div style="text-align:right">64</div>

3.2 C_L and C_D, data and approximations

The imported data used in the simulations are based on the data recovered from Airfoil Tools which is a web based airfoil database. The database contains data of over 1600 different profiles which are produced using the software Xfoil.

The data files are created using a 0.25° interval. The range of which the data is defined is dependent on both type of foil and Reynolds number as the range is dependent on when the individual foil stalls. The values for C_L are calculated for angles just beyond the stall angle.

Since the operation of a VAWT allows the angle of attack to vary beyond the stall angle (especially for low TSR applications) the post stall characteristics of the foil is of great interest. As the blade stalls its lift coefficient decreases dramatically but it is not equal to zero. The post stall approximations made are based on the resoning presented by (A low-Reynolds-number, high-angle-of-attack investigation of wind turbine aerofoils, 2011) For symmetrical foils the lift coefficient was approximated by a straight line from the last measured value to C_{Lmax} at the corresponding angle of $\alpha=45°$ and then linearly to $C_L=0$ at $\alpha=90°$ as can be seen in Figure 3.7. As the foil is symmetric the same procedure is made for the negative values of α.
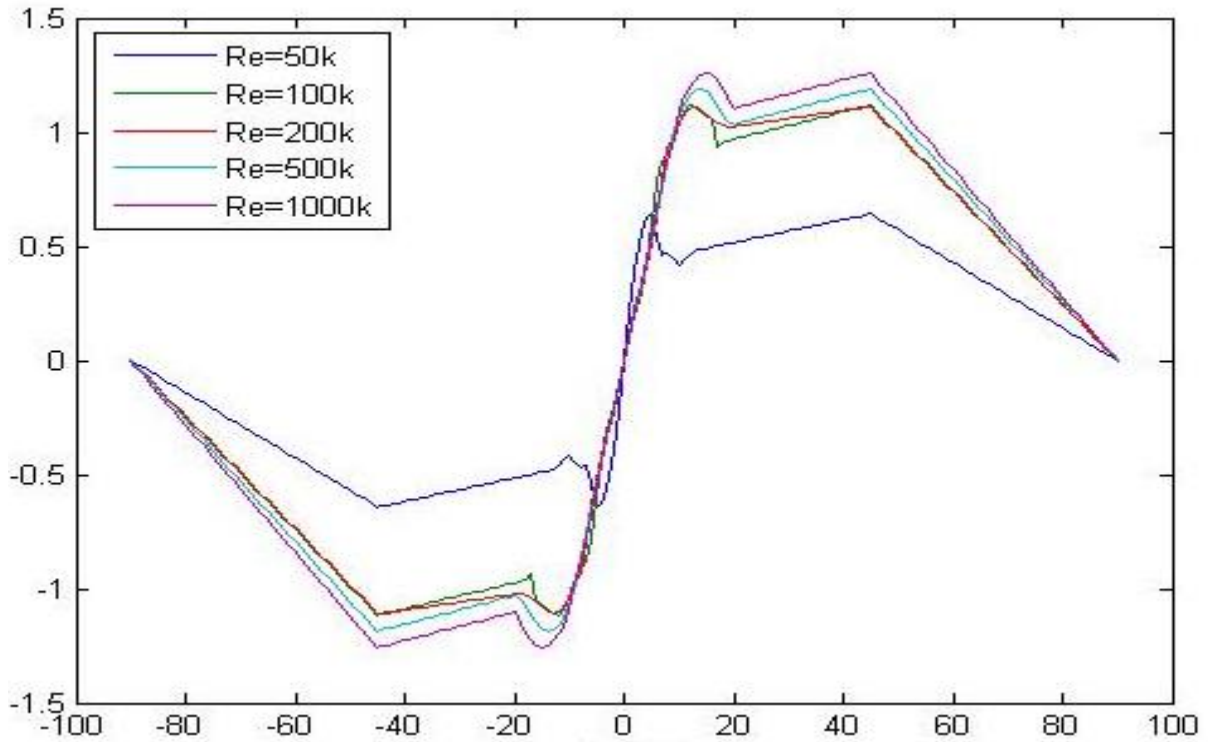
Figure 3.7. Approximations of the lift coefficient of a symetrical hydrofoil versus the angle of attack

For asymmetrical foils the last measured value is assumed to be constant for angles up to $\alpha=50°$ and then the lift coefficient is approximated much like the symmetrical one to $C_L=0$ at $\alpha=90°$. For negative angles of attack the lift coefficient is assumed to change linearly and passing two points (-60°, -0.7) and (-90°, 0) progressing backward from the first measured value. C_L plotted against α for asymmetrical foils can be seen in Figure 3.8.
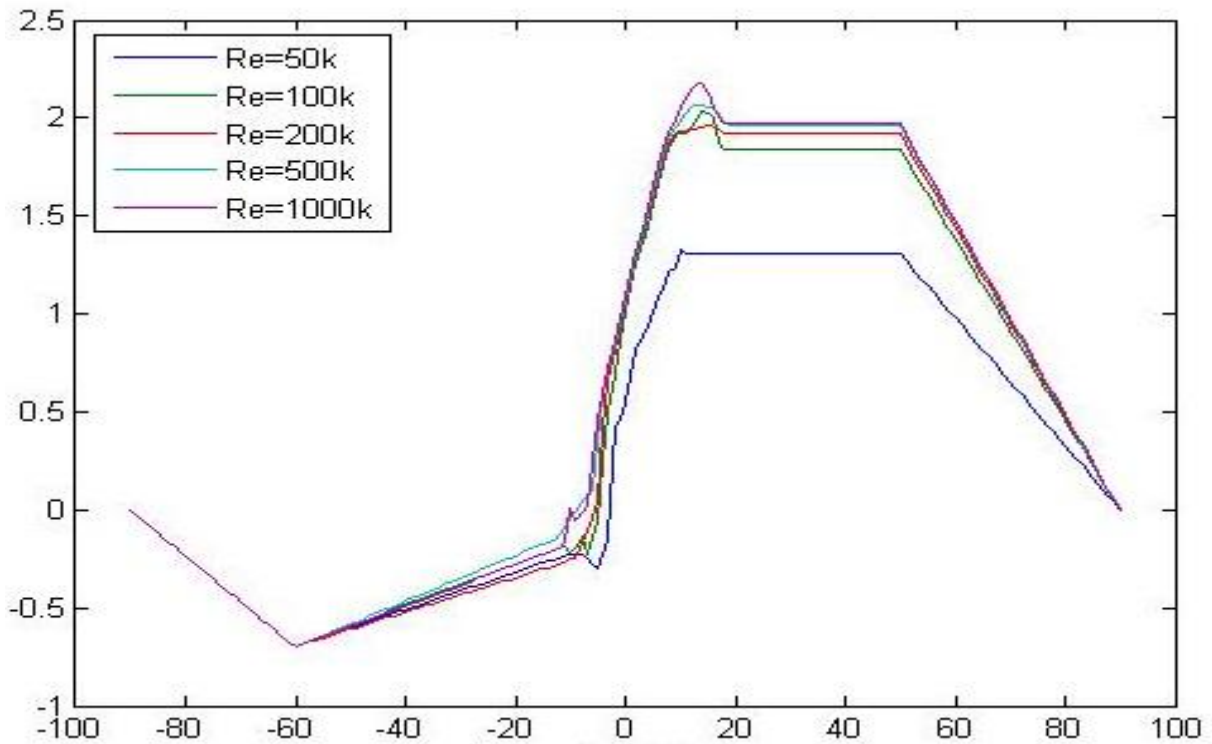
Figure 3.8. Approximations of the lift coefficient of a asymetrical hydrofoil versus the angle of attack

When approximating the drag coefficients the experimental data presented in (Robert E Sheldahl, 1981) was used as a template and the values of C_D were approximated from the first and last measured value to $C_D=1.8$ at $\alpha=-90°$ and $\alpha=90°$ respectively.
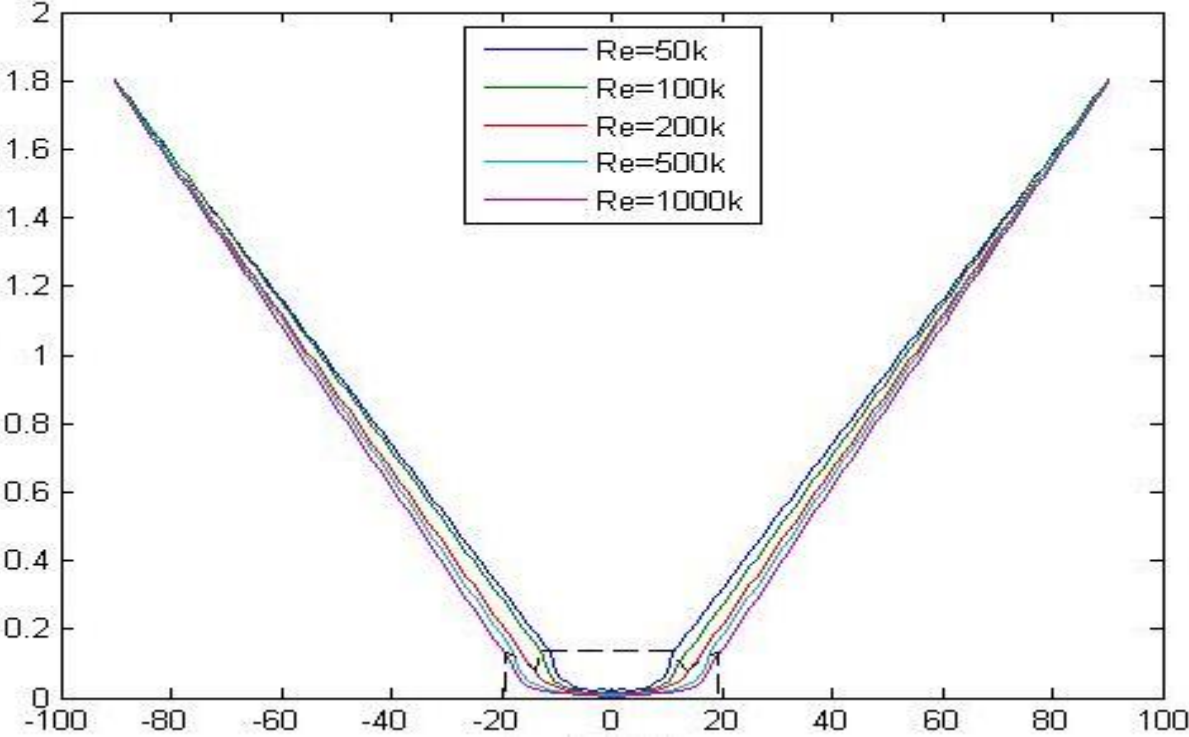

Figure 3.9. Approximations of the drag coefficient versus the angle of attack

3.3 Project specific choices

In this chapter the choices regarding accuracy, type of foil etc. is presented.

3.3.1 Selecting the number of streamtubes

When choosing the number of streamtubes used in the calculations there are several factors influencing the final decision. As the multiple streamtube model was implemented in order to increase the accuracy the logical interpretation would be to assume that the number of streamtubes should be chosen as large as possible. Looking at the iteration process and optimization code in Appendix 1 the need of keeping the number of calculations at a reasonable number becomes apparent, i.e. the simulation time has to be in relation to the level of accuracy needed.

In the calculations there is reason to avoid the definition of a streamtube at $\theta=0°$. This because of the fact that $\theta=0°$ makes $\sin(\theta)=0$ which ultimately means that no solution will be found as a will increase in to infinity as can be seen in Eq. 45

The azimuthal streamtube angles used starts at $\theta=5°$ and the step $\Delta\theta=10°$ meaning that the center of each streamtube are located in $5°, 15°, 25°…, 355°$.

3.3.2 Selecting the hydrofoils

When designing and especially when constructing a prototype for energy conversion purposes the choice of foil is an important and complex decision. There are numerous of variables affecting the foil of choice and every project and site could prove to demand their own design.

It is not within the scope of this project to decide the optimal foil type. Some of the reasons for this are the inability of the model to predict some 2D- but particularly 3D-effects. Even the fact that the medium in which the turbine will operate is water (density water exceeding 800 times that of air) ultimately puts high demands on the durability and structural strength of the foil which will not be evaluated here.

For this preliminary design four different foils have been chosen for further evaluation. The NACA 0012 is selected as a baseline or starting point. It is one of the most common profiles on the market and one of the most examined ones as well. It is a symmetrical foil with maximum thickness of 12% at 30% of the chord.
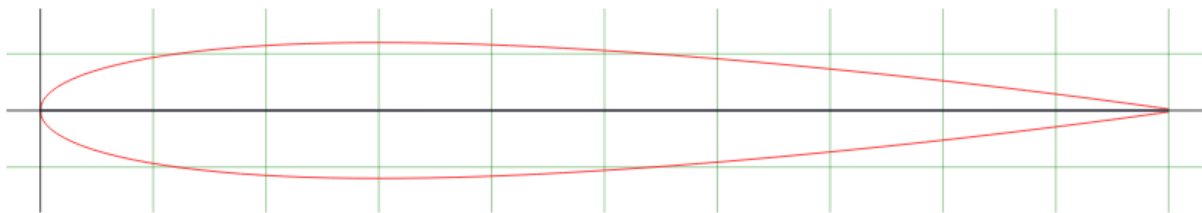

Figure 3.10. NACA 0012

The second one is the S-1046 which is also a symmetrical foil with much in common with the NACA 0018. The S-1046 has shown great potential for wind energy applications (Performance investigation of H-rotor Darrieus turbine with new airfoil shapes, 2012) and is an interesting symmetrical foil. The foil has a maximum thickness of 17% at 30.8% of the chord.
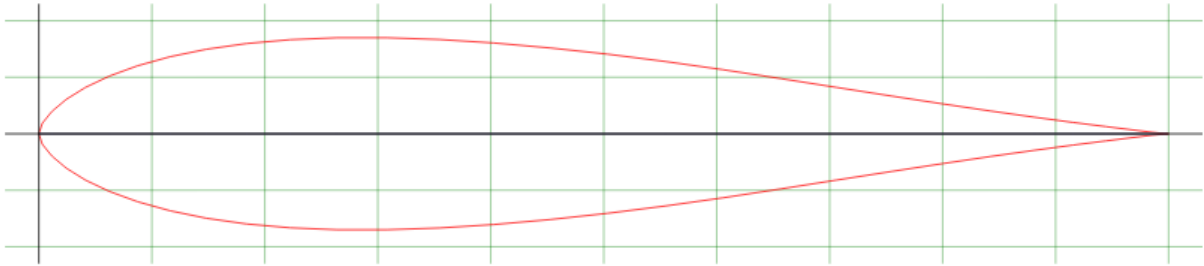
Figure 3.11. S-1046

The third one is the S-1210 which is an asymmetrical foil and produces high lift at relatively low Reynolds numbers. The S-1210 produces high drag at negative angles of attack when compared to the symmetrical ones. The foil has maximum thickness of 12% at 21.4% of the chord and maximum camber of 6.7% at 51.1% of the chord.
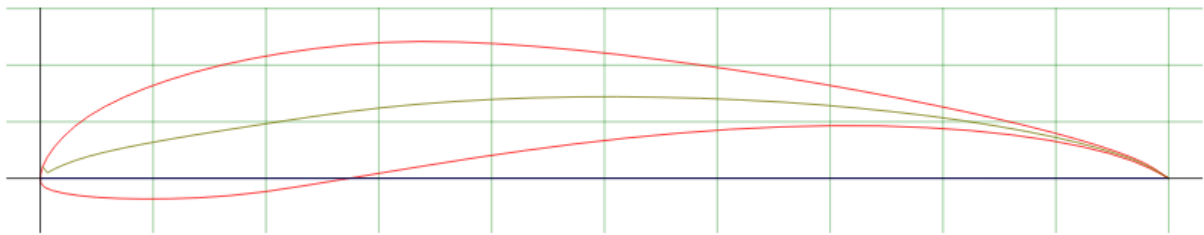

Figure 3.12. S-1210

The fourth foil to be examined is the Eppler E216. The asymmetrical foil is designed to perform well at low Reynolds numbers. Compared to the others the foil exhibits high stall angles at lower Re (around Re=50000). The foil has maximum thickness of 10.4% at 26.2% of the chord and maximum camber of 4.7% at 59% of the chord.
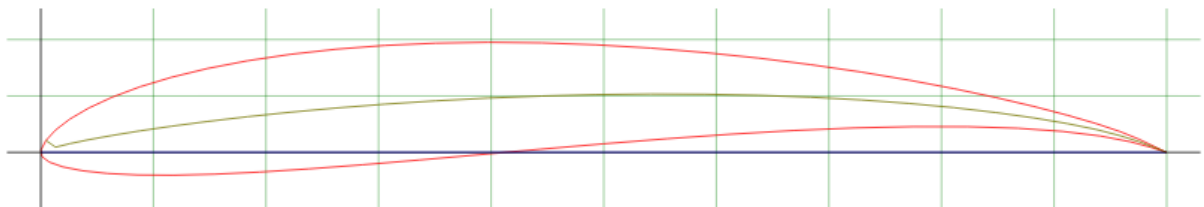

Figure 3.13. E216

4 Results

In this chapter the results from the optimization process will be presented for the design free stream velocity of 1.75 m/s. In addition to this the behavior and the performance associated with the final turbine design is also presented. Due to the models convergence problems (discussed in section 5) the results for the asymmetrical foils will not be presented in this section but instead in section 6.5.

The first step of the optimization process is presented in Figure 4.1-Figure 4.3 for S-1046. The plots show how the power coefficient varied with the tip speed ratio at different preset turbine configurations. The investigation were made for each setting of number of blades (N=2, 3, 4). Each line is represented by a constant solidity and they are all exhibiting an optimum at one specific TSR.
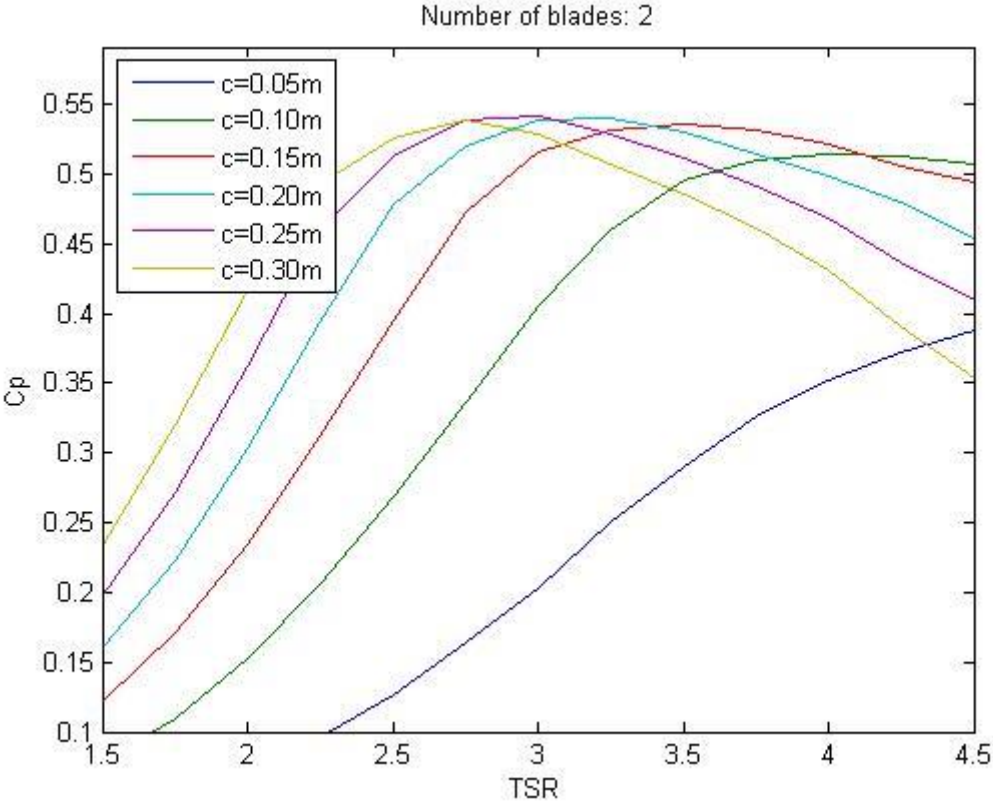

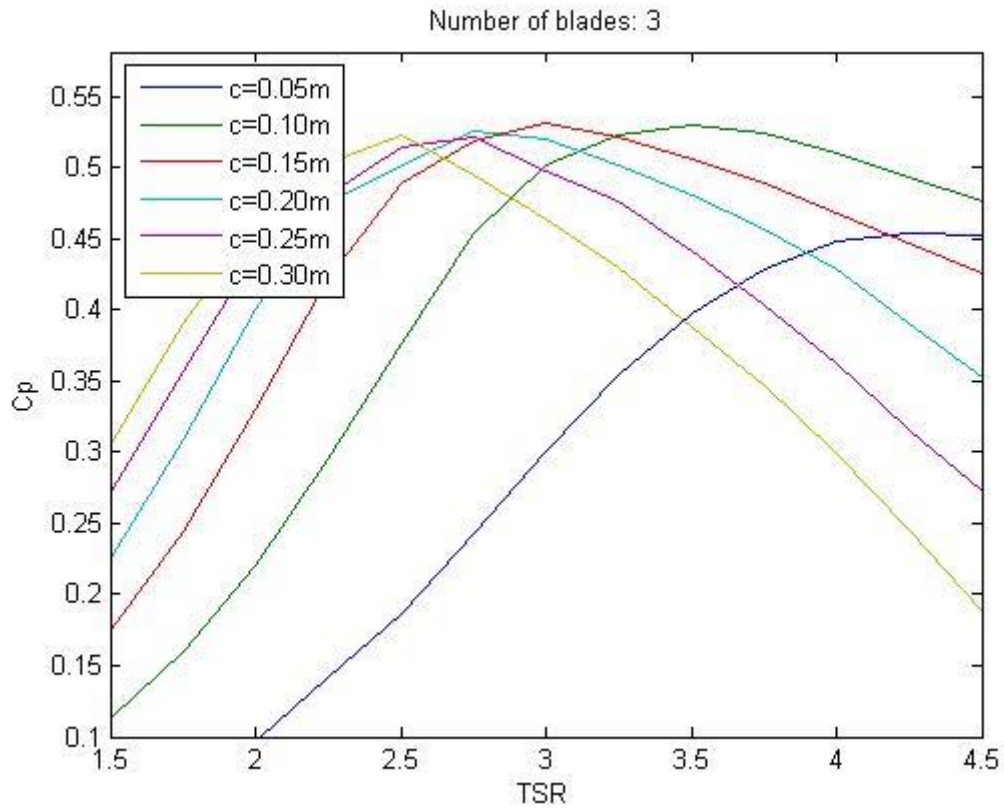**Figure 4.1. Power coefficient versus TSR (N=2)**

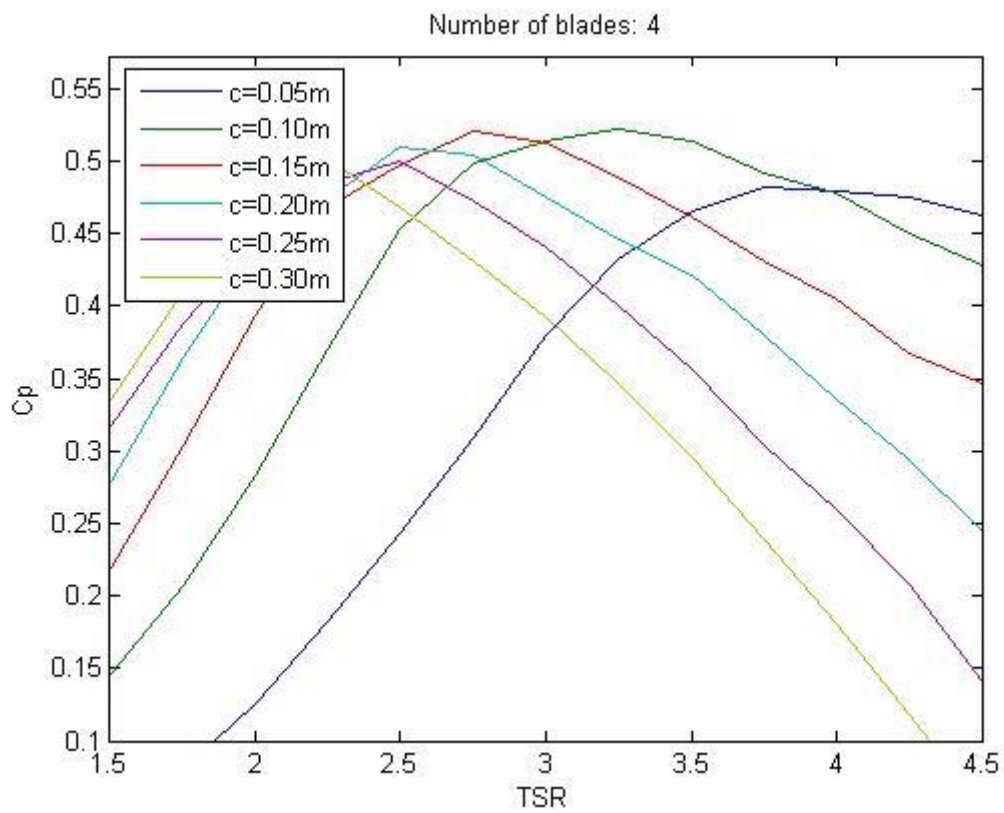**Figure 4.2. Power coefficient versus TSR (N=3)**

Figure 4.3. Power coefficient versus TSR (N=4)

In the case with two blades and the S-1046 hydrofoil the plot are shown for the range of chord lengths where the optimum is located. The plot was improved by a smaller calculations step for both the chord length and the tip speed ratio. Note that the optimum is defined for the coefficient of power only and the effects on the other coefficients of performance will be presented in Figure 4.4.
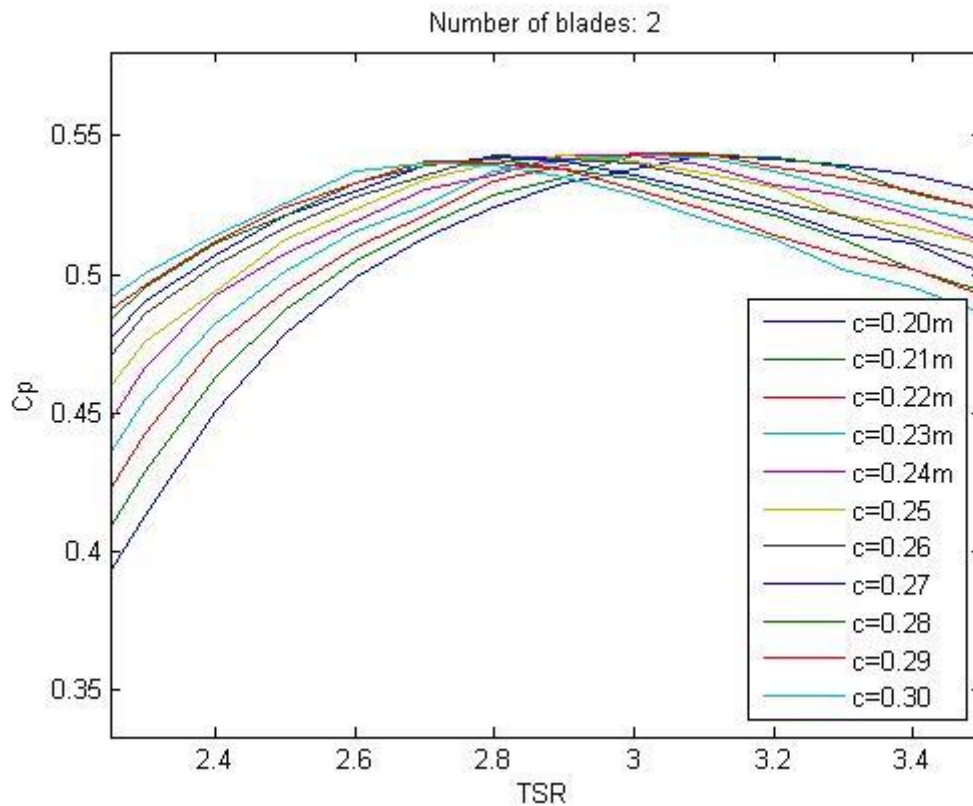

Figure 4.4. Power coefficient versus TSR (N=2)

A summary of the results for both of the symmetrical foil are presented in Table 4.1 for all the optimum turbine settings.

Table 4.1. Summary of the optimization process.

Hydrofoil	Number of blades	Max Cp	Chord at max Cp	TSR at max Cp	Solidity
NACA0012	2	0,5437	0,28	2,7	0,0892
	3	0,5289	0,12	3,2	0,0573
	4	0,5191	0,13	2,9	0,0828
S1046	2	0,5439	0,22	3,1	0,0701
	3	0,5347	0,13	3,2	0,0621
	4	0,5251	0,12	3	0,0764

The turbine corresponding to the highest power coefficient was with the S-1046 hydrofoil with two blades. The behavior of this turbine was further examined as well as its performance. The significance of this will be further discussed below, both to evaluate the turbine but also in order to validate the simulation method used.

As mentioned, the angle of attack varied quite a bit during the revolution and was dependent on both the angular position of its path but also on the relative velocity experienced by the blade. In Figure 4.5 the angle of attack is plotted for all azimuthal positions at a selection of different TSR's.
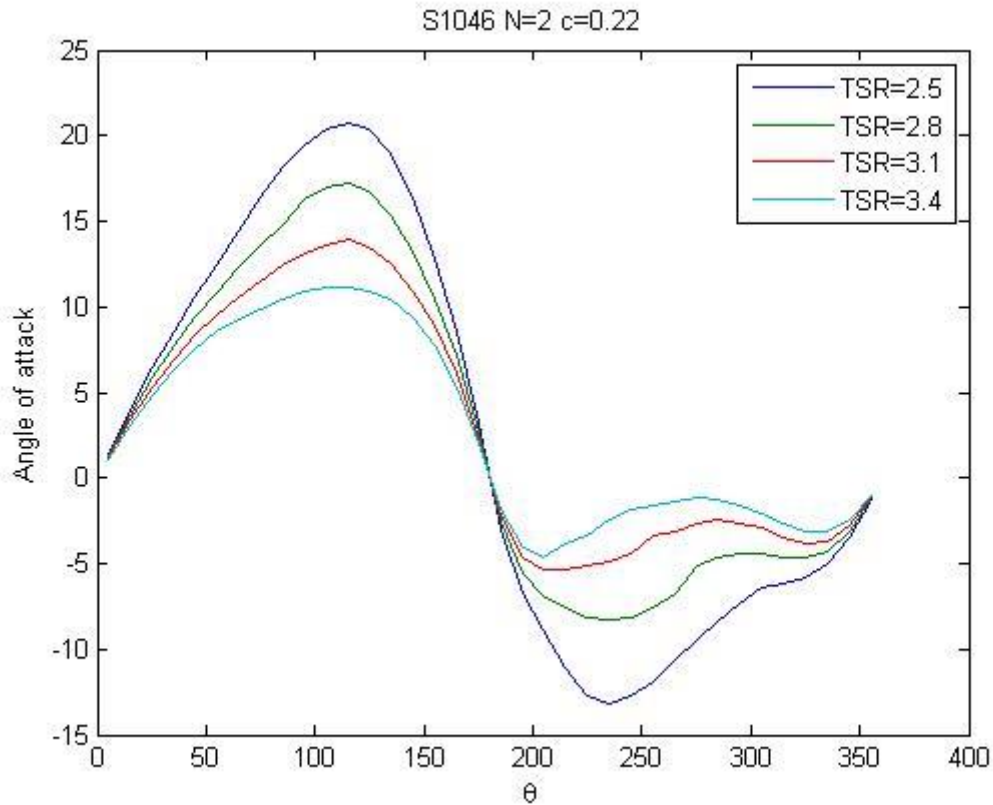
Figure 4.5. Angle of attack versus the azimuthal position

The effect of the increased TSR illustrates the dependency on the relative velocity well. For the downstream half (θ = 180-360°) the effect of the decreased velocity can be seen. As the induction factor is greater around θ = 90° and θ = 270° the constant tangential velocity will make the angle of attack to assume a value which tends to zero as TSR is increased.

In Figure 4.6 it is clear that the Reynolds number increased as it moved toward the free stream and vice versa. Of course, the maximum will coincide with θ = 0° and the minimum with θ = 180°. Again, the effect of the decreased velocities on the downstream half is apparent.
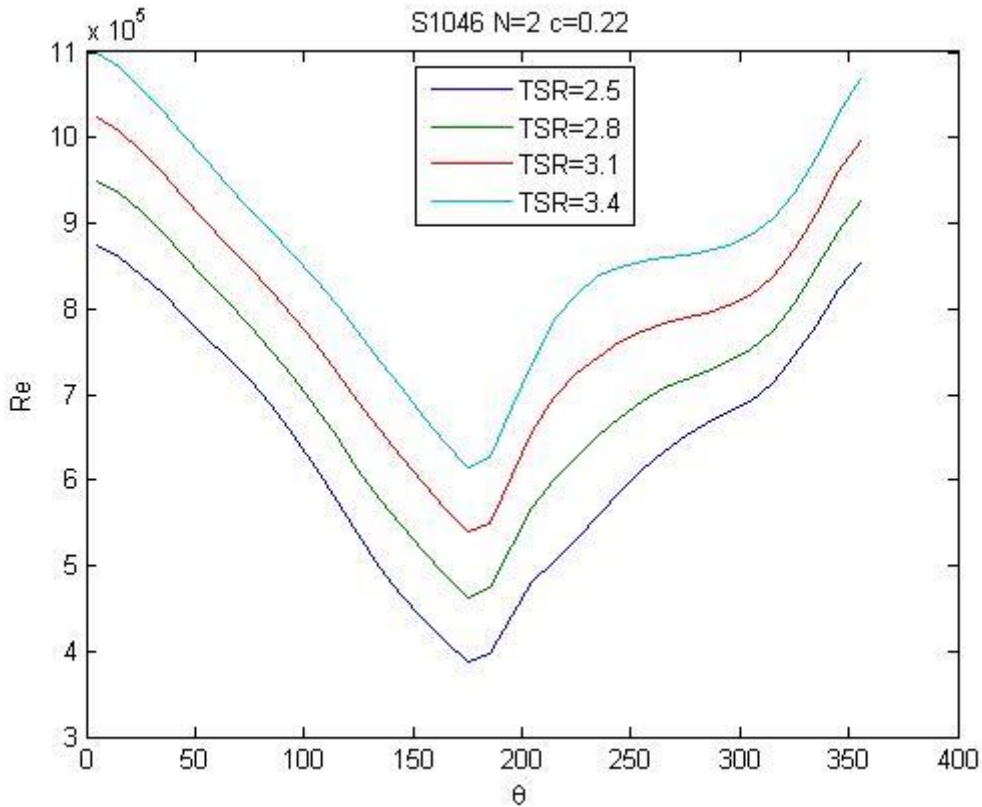
Figure 4.6. Reynolds number experienced by the blade versus the azimuthal position

The velocity field through the turbine can be seen in Figure 4.7. The induced velocity for each streamtube is plotted for the upstream half as well as the induced velocity of the subsequent streamtube on the downstream half.
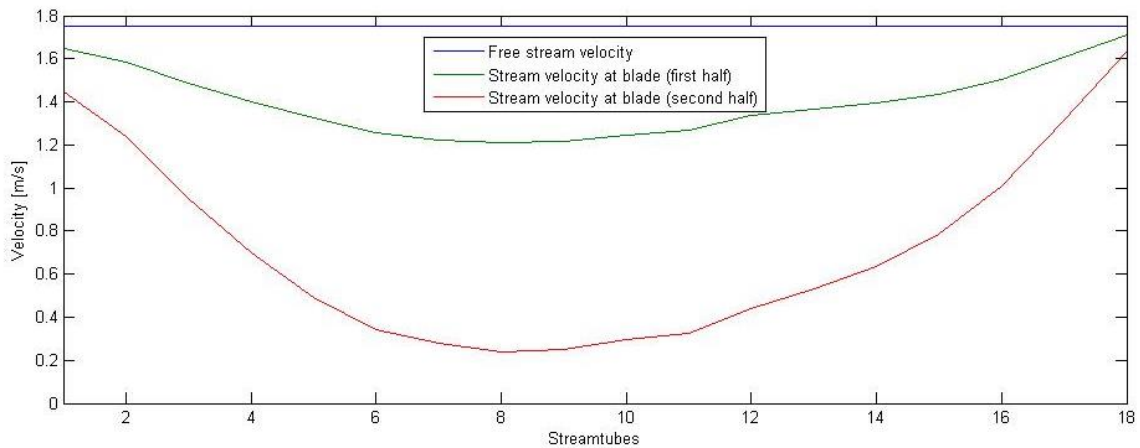

Figure 4.7. Velocity profile for S-1046. N=2

As predicted, the velocities experienced by the blades as they progressed on their downstream path were severely decreased. Note that the free stream velocity is not the velocity assumed to be experienced by the blade as it is progressing on the upstream half of the turbine.

In Figure 4.8 the induction factor for both the upstream and the downstream halves are illustrated. It can be seen that the flow in the streamwise direction was influenced more as the blade progresses towards the flow and that the flow was influenced more (in terms of percentage) on the downstream half where the velocity in the streamwise direction is decreased.

In the plot both the induction factor (a) and the iteration parameter named a_{new} is included. The plot shows a fully converged solution and the fact that the plot features two lines can only be seen around θ ≈ 260-280°.
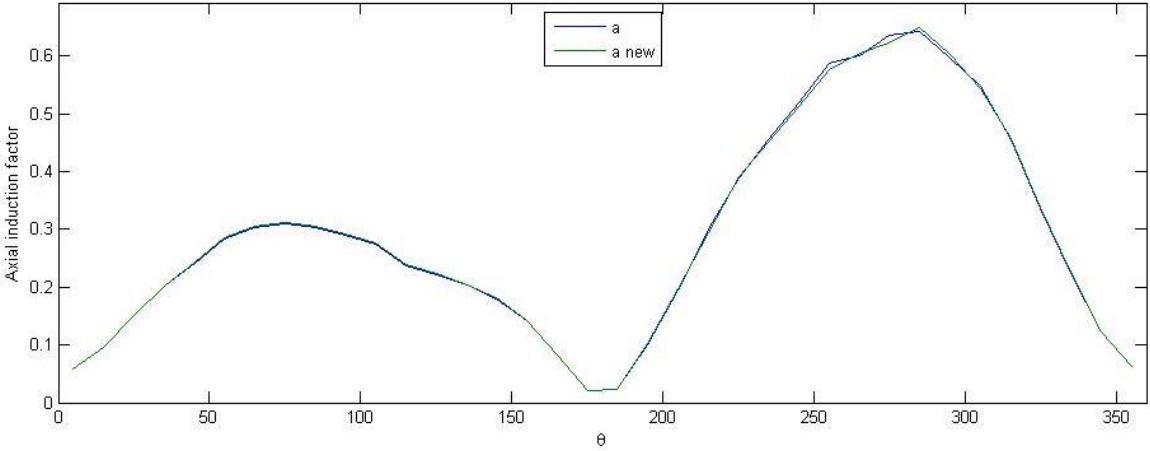

Figure 4.8. Induction factor versus the azimuthal position. S-1046 N=2

The torque produced by the turbine as it was operated in design settings is illustrated in Figure 4.9. The plot shows the torque (Nm) produced from each blade when it was at a specific azimuthal position as well as the total torque produced at these positions by the total number of blades (in this case two).
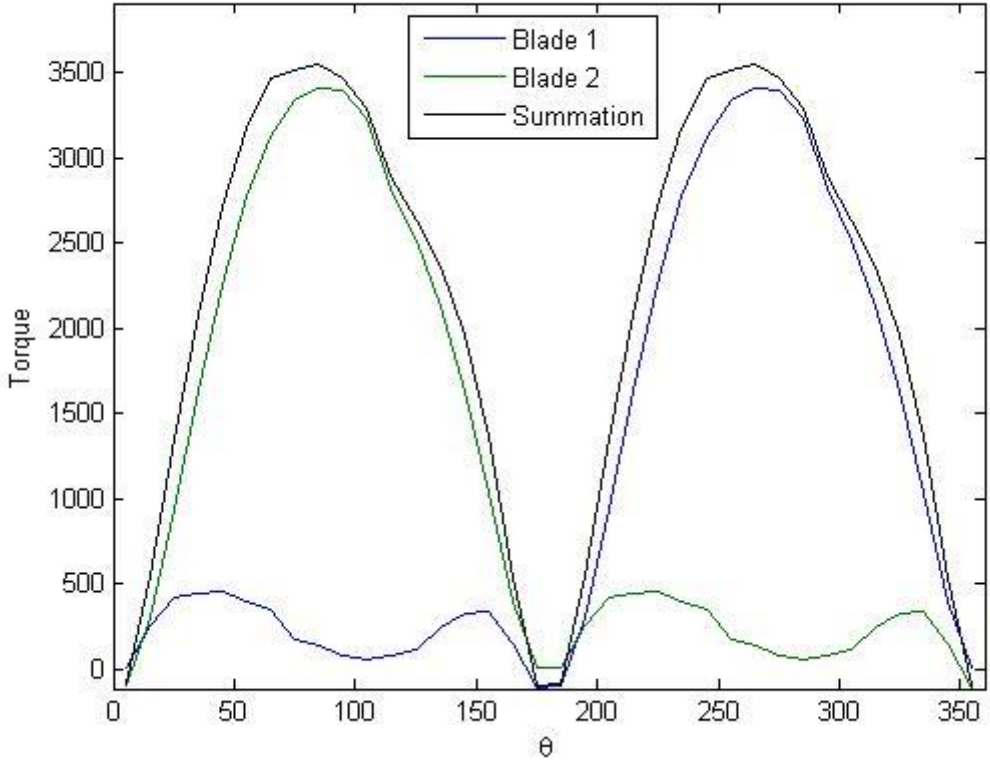

Figure 4.9. Instantaneous and total torque versus the azimuthal position. S-1046 N=2

In Figure 4.9 the drawback of designing a two bladed turbine becomes apparent. Since there were only two blades they will be offset by 180° from each other. As the first blade reached θ=180° the second reached θ=0°, two positions in where the blades produced little to no torque. According to the

summation the torque would oscillate between two values that differ greatly from each other. This is not ideal when operating the turbine and when the torque is illustrated for the three blade solution in Figure 4.10 the improvement is significant. The total torque over the revolution has become more consistent and the peaks now occur three times per revolution. This effect would be even stronger as the number of blades increased but as discussed in section 6.1 this is not always favorable.
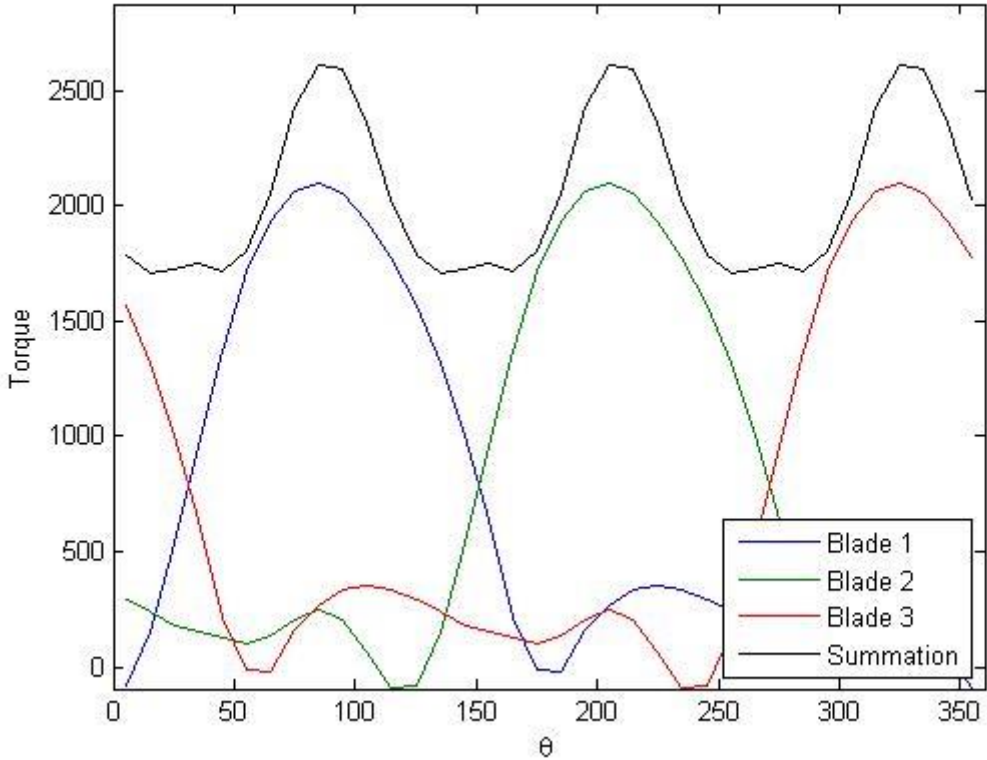

Figure 4.10. Instantaneous and total torque versus the azimuthal position. S-1046 N=2

The velocity field of the three bladed turbine (see Table 4.1) can be seen in Figure 4.11. Note that this turbine was predicted to influence the velocities in the streamwise direction less than the two bladed turbine which was featuring blades with longer chord.
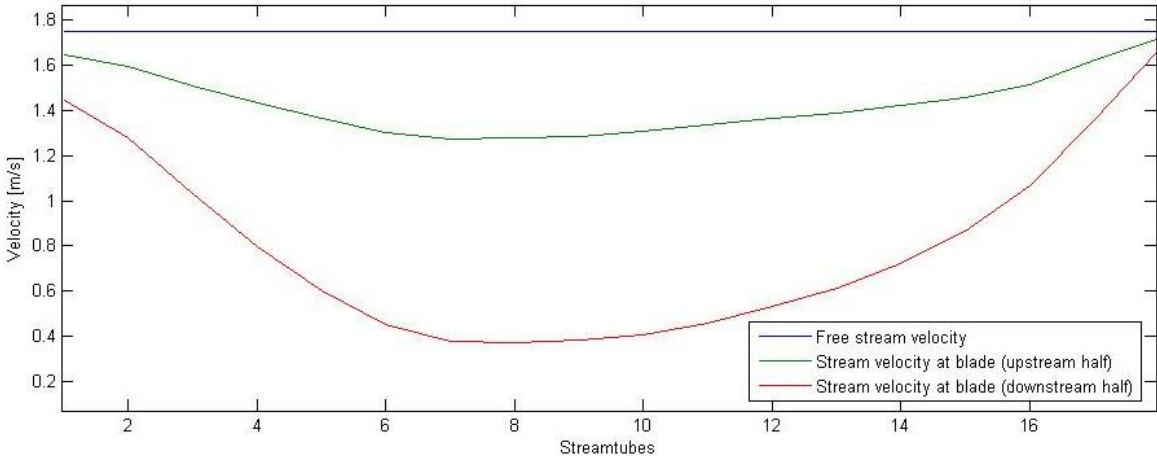

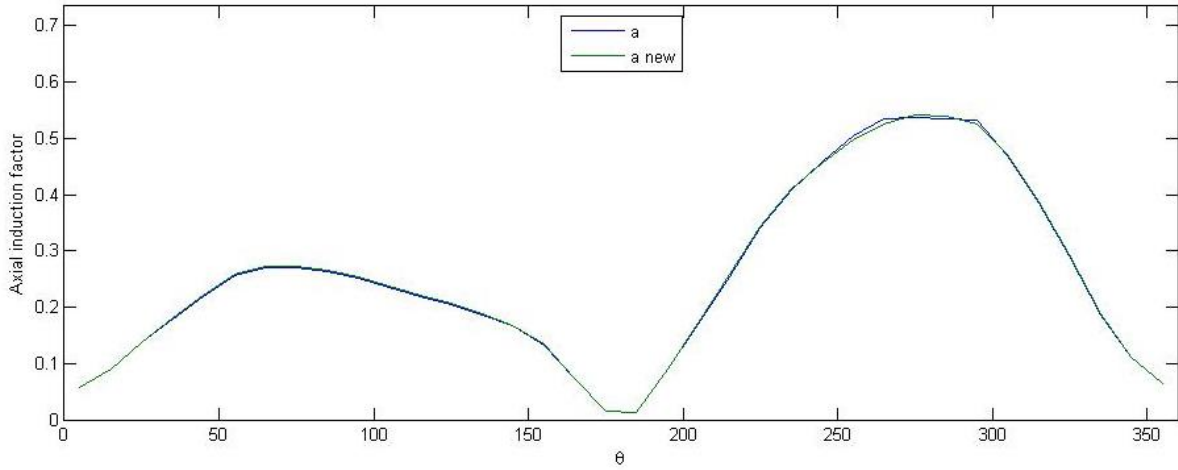**Figure 4.11. Velocity profile for S-1046. N=3**

-55-

Figure 4.12. Induction factor versus the azimuthal position. S-1046 N=2

If the blade was pitched by a fixed value the experienced angle of attack can be shifted along the revolution and thus altering the forces acting on the turbine in every specific azimuthal position. Depending on the operational settings this small alteration could prove to influence the performance of the turbine. Note that the desired pitch will change as the TSR is altered.
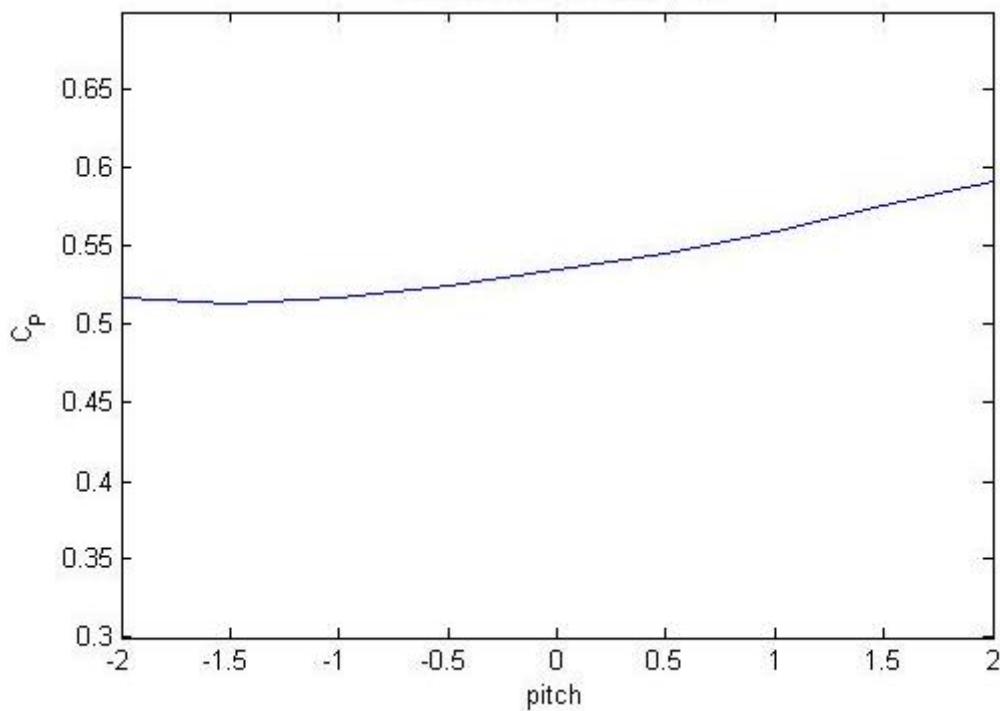

Figure 4.13. Power coefficient versus pitch angle. S-1046 N=3

Figure 4.14-Figure 4.15 illustrates turbines performance in the range of different conditions in which it will operate. In Figure 4.14 also shows the two different optimum values of TSR for both the torque and the power. This is an important optimization difference and the choosing of which to prefer depends on the final application.
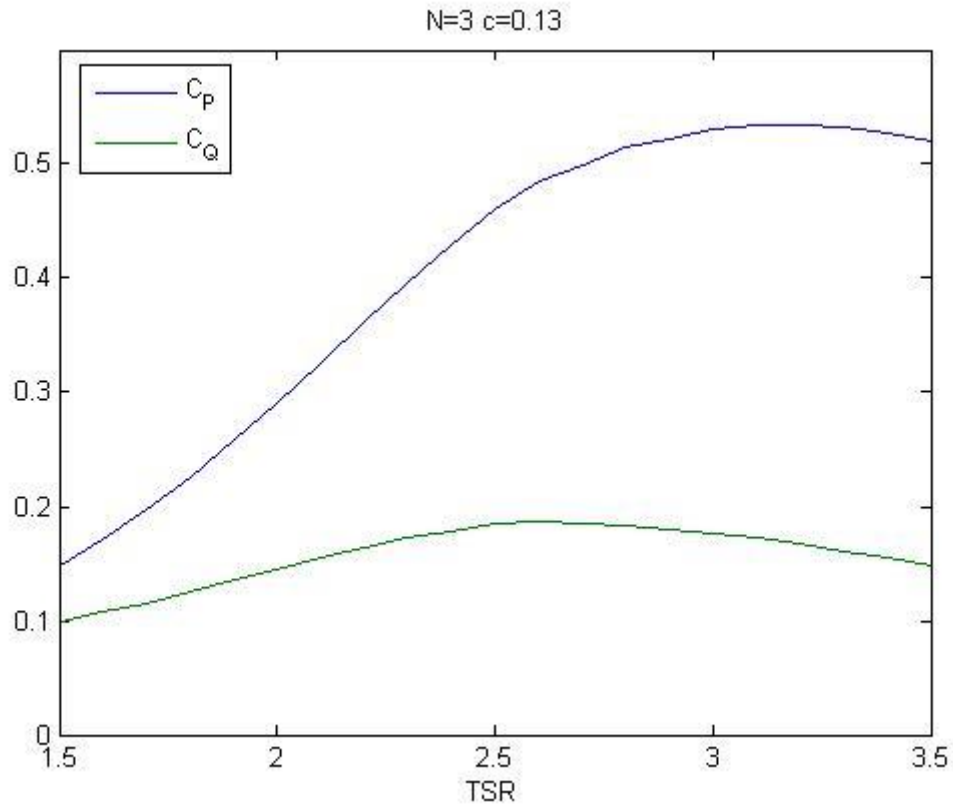
Figure 4.14. TSR range of power and torque coefficients. S-1046 N=3
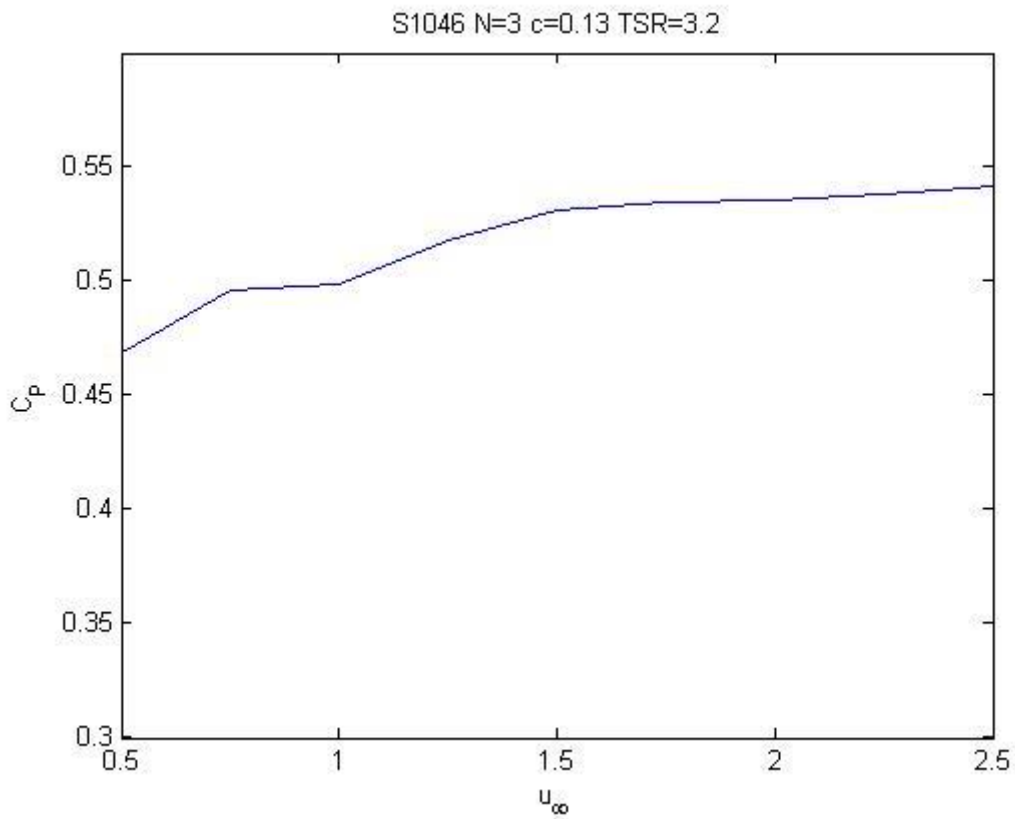

Figure 4.15. Free stream velocity range of power and torque coefficients. S-1046 N=3

5 Sensitivity analysis of the convergence problems for asymmetrical foils

When simulating how the turbine would interact with the fluid when fitted with asymmetrical foils the solution failed to converge as can be seen in Figure 5.1.
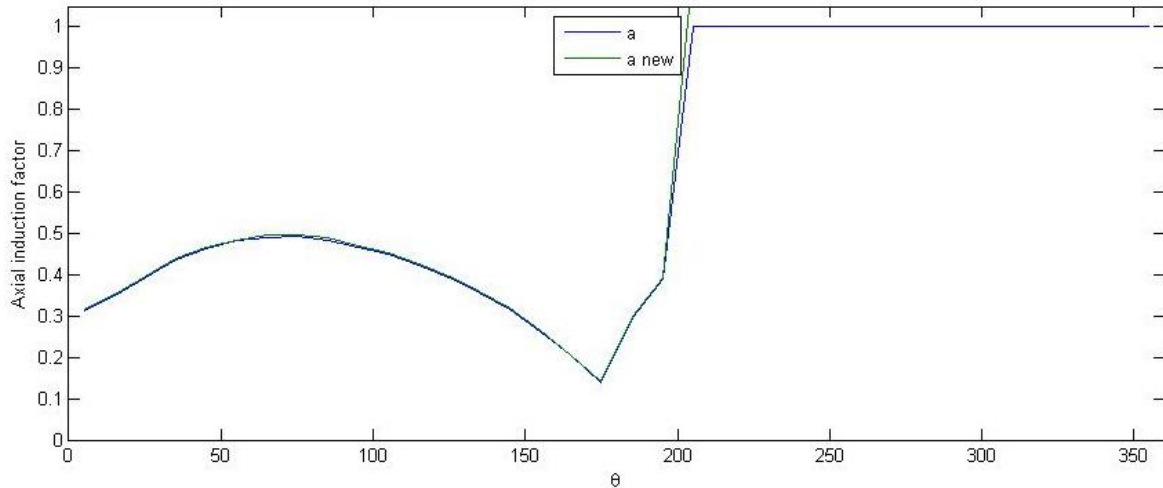

Figure 5.1. Solution have not converged and the induction factor increases beyond reasonable values

In order to evaluate how far from convergence that was achieved the required ratio a/a_{new} was given an increased flexibility. The solution did not converge well for reasonable values of a/a_{new}. Where reasonable values refers to a ratio where convergence is achieved while the accuracy of the solution could be maintained.

As the available airfoil data was recovered for Re = 50 000, 100 000, 200 000, 500 000, 1000 000 the convergence problems were suspected to origin from when the lift and drag data were collected from different Reynolds-lines as the induction factor increased. To test this, the range from where the data was collected was altered forcing the lift and drag to be collected at a single Reynolds-line. The convergence problems remained and this theory was discarded.

The number of streamtubes chosen was also suspected of having an impact on the convergence problem since the data points used could coincide with local mathematical problems (as was the case of $\theta=0°$. However the convergence problems remained and this theory was discarded.

Through the iteration process the induction factor was altered before each iteration by a constant step Δa. The step will of course influence the solution and if a solution is found or not. No alteration in Δa resulted in a difference in convergence and this theory was discarded.

Since the only difference in the code between the symmetrical and the asymmetrical blades were the input values of C_L and C_D the effect of these values had to be evaluated. The values could not be altered to improve the code but merely attempt to understand what happened. The values of C_L and C_D were kept constant one at the time and the theory of if either one of them assumed a value too small or too great for the code to handle were investigated. The convergence of the solution was found to be independent of any tried value of C_D. C_D was given constant values for the whole range (not only extreme points) but the outcome did not differ and no convergence was achieved. The solution converged for all constant values of C_L and this theory was therefore discarded.

The correlation between the induction factor and C_L is of a very complex nature and the reason for why the solution did not converge is hard to say.

The double multiple streamtube model do suffer from convergence problems for high values of the induction factors and the authors of this thesis believe that the problem (in this case) probably lies in an unfavorable combination between the induction factor and C_L. This reasoning is supported by the fact that the effect is isolated to the asymmetrical foils and that the sole thing altered between the simulations is the input of C_L and C_D.

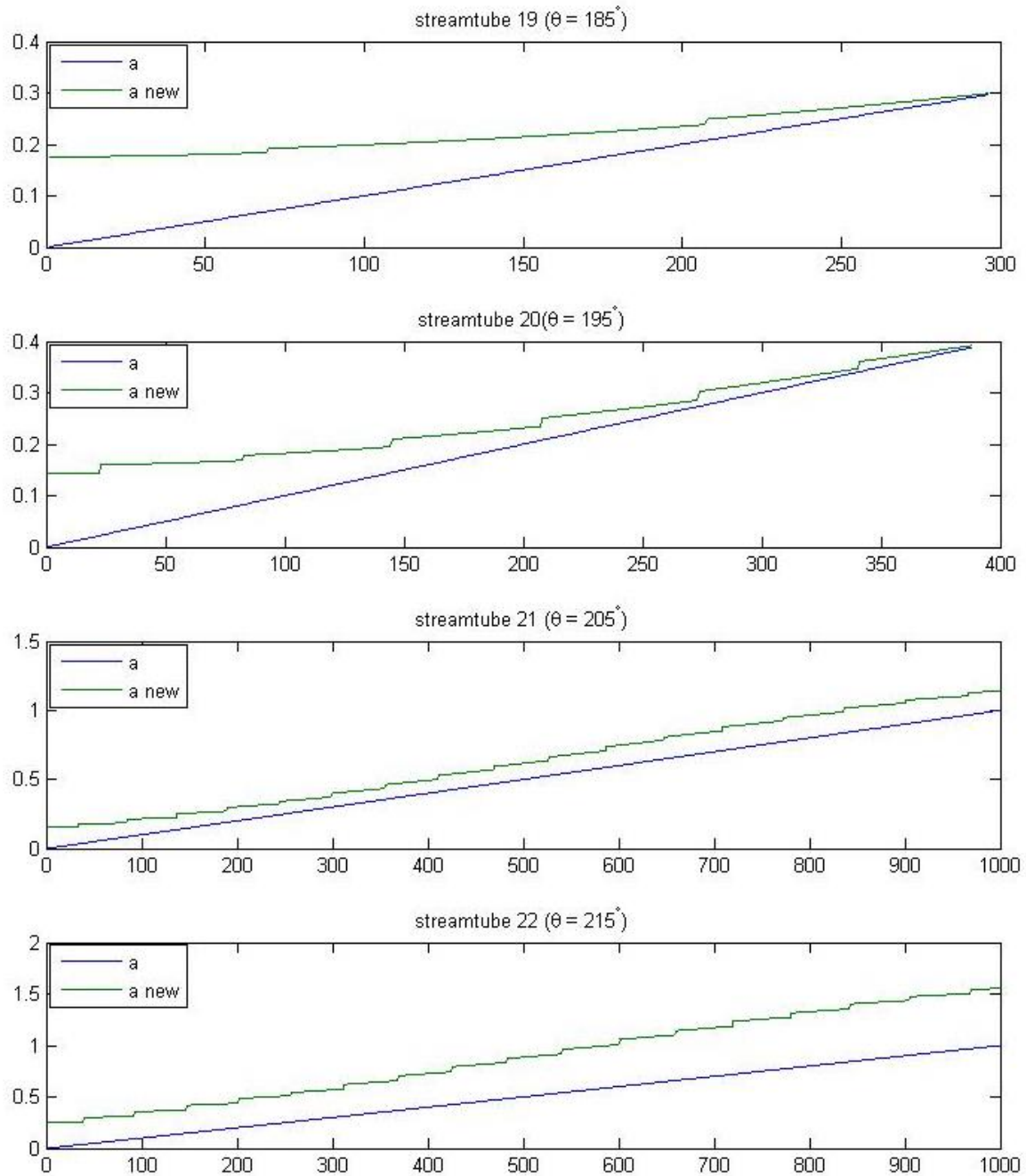
Figure 5.2. Convergence illustrated for streamtubes 19-22. 19-20 converges while 21-22 does not.

6 Discussion

The choices of both method and project specific choices will of course affect the outcome of the simulations. In this chapter the results will be discussed and interpreted and the method used will be evaluated. In addition to this the results regarding the asymmetrical foils will be presented and the impact of these on the outcome will be discussed.

The result and discussion section will together form the basis from which a conclusion will be made.

6.1 Number of blades

One of the most important design choices is the number of blades. The total torque generated by all the blades when the first blade reaches a specific azimuthal position is illustrated below. When operating a two bladed turbine the torque produced will oscillate between two values that differ greatly from each other as mentioned in section "4 Results". This effect combined with the higher maximum torque experienced will put higher demands on the design as well as the material used.

Looking at the three and four bladed turbine the torque becomes surprisingly similar with regard to the amplitude. The difference between the two lies in the number of periods carried out during the revolution making the torque more uniform. The choice depends on the final application and as seen in Figure 4.14 the maximum for the two coefficients do not coincide at the same turbine configurations. As a rule of thumb it can be said that few blades and low solidity offers good potential for power generation and many blades and high solidity is better for high torque purposes such as pumps.
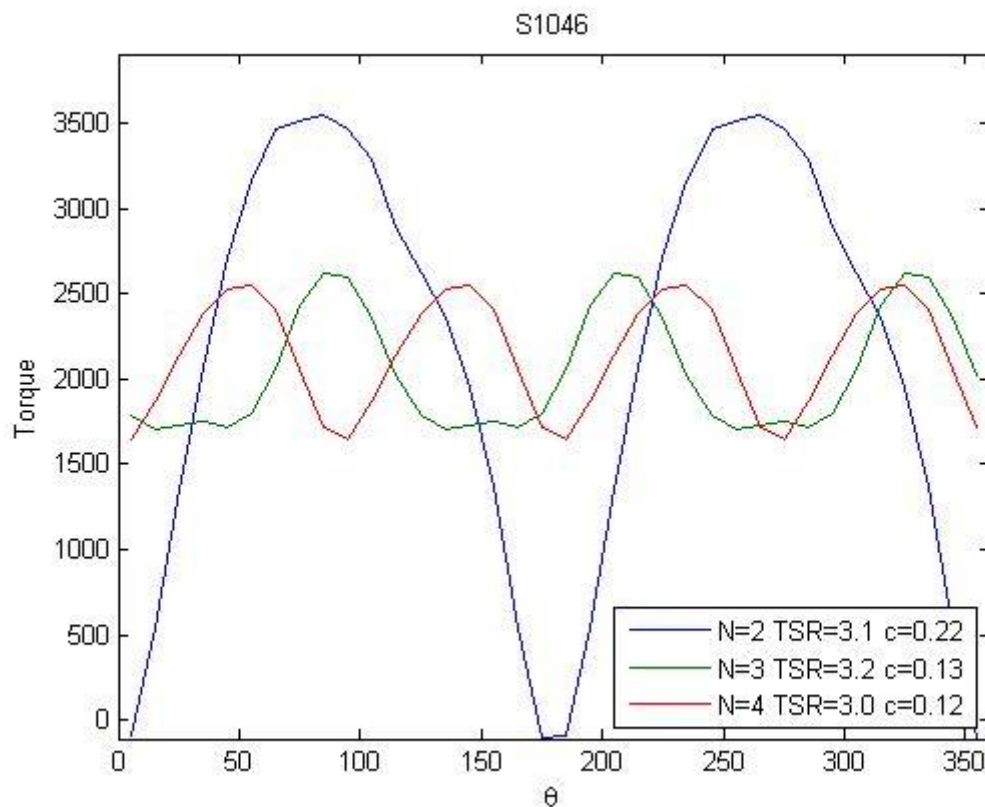

Figure 6.1. Total torque versus the azimuthal position.

It is well known by now that there are some effects that could not be implemented in the present study. Regarding the number of blades, the effect of that the blades operates in each other's wakes could affect the choice. A greater number of blades increases the number of blade to wake interactions making the

hydrodynamic performance of the blades to decrease and makes them hard to predict. In Figure 6.2 the wake to blade interaction is illustrated.
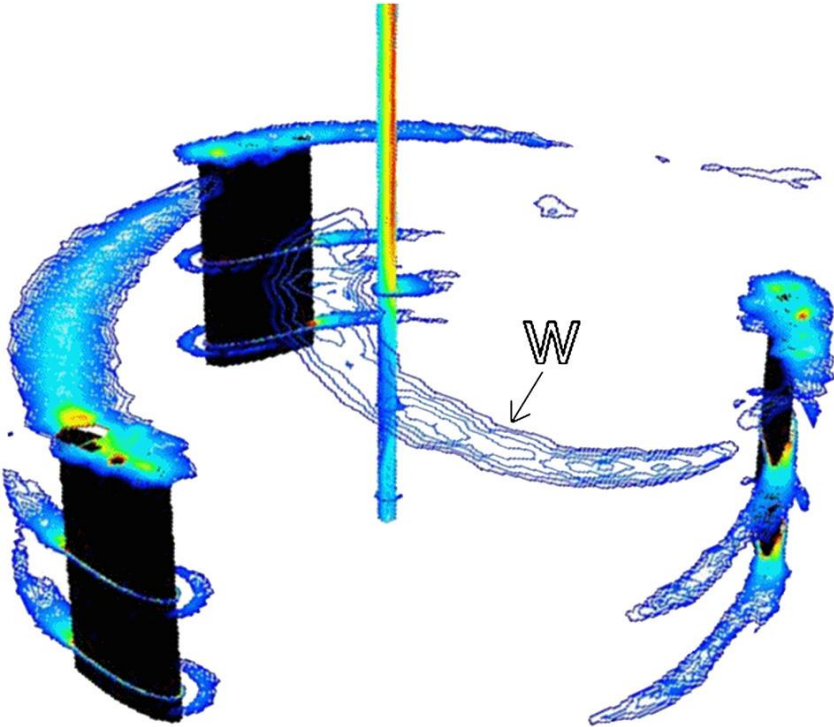

Figure 6.2. Wake (W) to blade interaction

6.2 Streamtube expansion

When a vertical axis turbine is in use the imaginary streamtubes will not be parallel but diverging. In the calculations the interpretation of this would be that the upstream area would be considered smaller than that of the downstream. The streamtube expansion have not been implemented in this model and the effect of this assumption (all streamtubes are parallel) is that the model overestimates the contribution of torque generated at the upstream half of the turbine and vice versa.

6.3 Input values of C_L and C_D

The modeled behaviors of the foils are governed by the lift and drag coefficients presented in section "3.2 C_L and C_D, data and approximations". These coefficients are directly related to the Reynolds number which is different for all azimuthal locations, velocities and chord lengths. The lift and drag coefficients used in the model were collected as shown in Table 6.1.

Table 6.1. Reynolds number range

Calculated Re	Re from which the input values are collected
Re < 75 000	50 000
75 000 ≤ Re < 150 000	100 000
150 000 ≤ Re < 350 000	200 000
350 000 ≤ Re < 750 000	500 000
750 000 ≤ Re	1000 000

Assuming the same behavior for a wide range of Reynolds numbers will of course affect the accuracy of the model. A combination of lack of available data and keeping reasonable simulation times will always govern the accuracy of this part when using the double multiple streamtube model.

The approximations made for the post stall behavior were made for generic foil shapes in both the symmetrical and asymmetrical case. The accuracy of these approximations can be debated but they are meant to serve as a qualified guess and it is the opinion of the authors that it is to be preferred over other solutions like equating C_L with zero for angels of attack beyond the range. Looking at Figure 4.5 these approximation are seldom used, especially for the optimized cases where the TSR is increased toward three.

All the input values used is evaluated for static conditions. In this case, as the angle of attack is changing in every instance, the effect of dynamic stall will be present. As the blade is rapidly "pitched" past the static stall angle a vortex forms at the leading edge and progresses downstream along the surface. This phenomenon causes increased lift due to the suction induced by the vortex but the lift rapidly plummets as the vortex reaches the trailing edge (Computational Prediction Of Airfoil Dynamic Stall, 1997). These vortices affect the lift and drag and the effects of this phenomenon are not modeled.

6.4 Pitch implementation

The effect of adding pitch to the blades is illustrated in Figure 4.13. Unfortunately the simulations resulted in non-logical behavior for high pitch angles. In the figure it can be seen that the power coefficient increases to relatively high values which are suspected to origin from the overestimation of the contribution from the upstream half. Never the less the pitching of the blades have an effect of the overall performance and seem to agree well with the theory of maximizing the performance on the upstream half.

6.5 Evaluation of the asymmetrical hydrofoils

The solutions corresponding to the asymmetrical hydrofoils did not converge well for the downstream half of the turbine (Figure 5.1). This is the reason why they are not included in the results section and also why they will be further examined within this chapter. Both of the asymmetrical foils experienced similar convergence patterns but for the S-1210 foil they were more severe and this foil will serve as a confirmation of the convergence problem for asymmetrical foils.

The performance of the turbine is of course a combination of the performance on the upstream and the downstream half meaning that the comparison between the four different foils was impossible to do. The reason why the asymmetrical foils were included in the study was that they were predicted to perform better than the symmetrical ones on the upstream half. This due to that they produce higher lift at positive angles of attack thus maximizing the efficiency where the velocity profile assumes its highest values. In order to estimate the effect of asymmetrical blades the simulations were carried out for the upstream half only.

The optimization process illustrated in Figure 4.1-Figure 4.4 could regrettably not be implemented when just calculating the contribution from the upstream half. The effect of finding the optimal configuration to perform well on the upstream half regardless of the effect it had on the downstream half was that C_P increased with increasing induction factor. This is not a logical outcome when both halves of the turbine are considered.

Therefore the comparison had to be made for specific turbine configurations in terms of chord, tip speed ratio and number of blades. In Figure 6.3 the configuration used was the same as for the optimized three bladed turbine presented in Table 4.1 and for a range of chord length between 0.1 and 0.14 m.
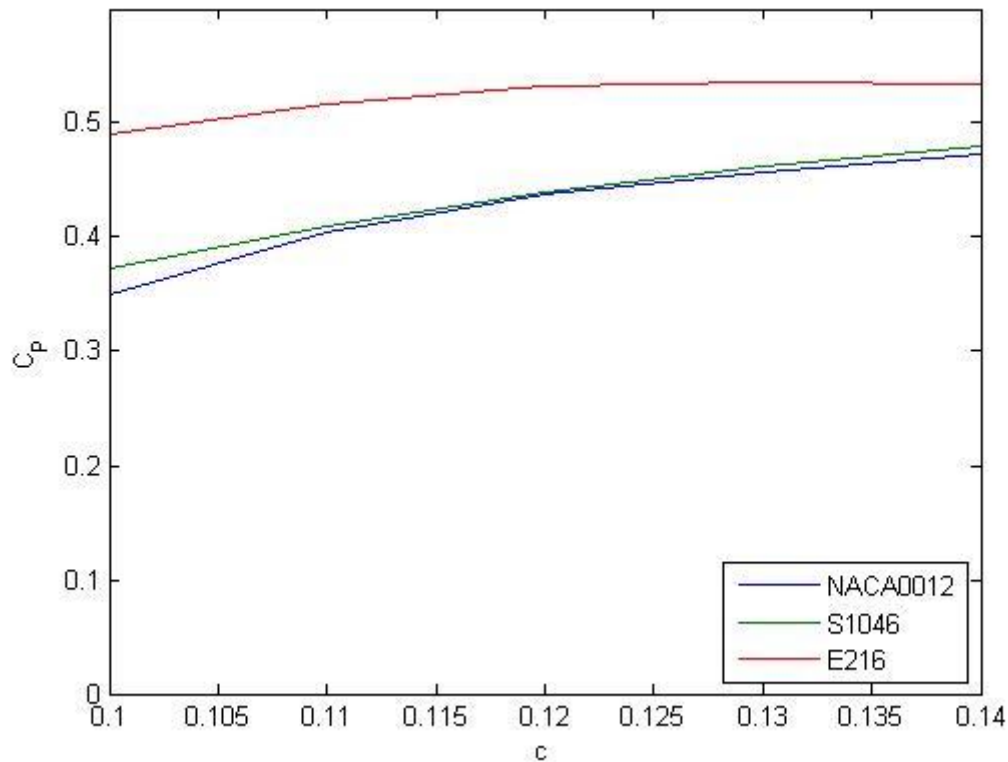
Figure 6.3. Power coefficient for three different foils at a chord range of 0.1-0.14 m

The power coefficient of the two symmetrical foils is very comparable but the asymmetrical shows higher performance potential when just looking at the upstream half. Note that the value of C_P in this case only is meant to act as a value of comparison between the foils and not as a value of performance of the turbine itself.

Despite that, the evaluation has some level of confidence as the upstream half is considered independent of the downstream and that convergence was achieved for the whole region of the upstream half. In addition to this the confidence level regarding the velocity field is higher at the upstream half (for all calculations within the project). This is because of that the assumptions made in the model would have had a greater influence as the fluid progresses through the turbine. In the downstream half the effects of wakes, struts, shaft etc. are apparent and this of course adds to the lowered confidence level at this half. As mentioned, the torque and consequently the power produced at the upstream half are to some degree overestimated. Therefore the C_P-lines in Figure 6.3 for the symmetrical and the asymmetrical foils should presumably be located closer together. In the light of this the use of asymmetrical foils for vertical axis turbines purposes still exhibit good potential.

6.6 Performance of the turbine

Using the double multiple streamtube model to simulate the performance of the turbine is an efficient way to perform the initial design steps. The model offers a good way to compare turbines with a wide range of parameters at reasonable simulation costs (in terms of computational power and simulation time). The model provides excellent understanding of the chain of events taking part in the turbine to fluid interaction. It also offers the opportunity to pinpoint specific parts of the blades path and makes it possible to further examine the processes taking place there. The model is considered to work well and the effects of the induced velocity field and blade characteristics can be seen throughout the simulations.

Having said this, the performance is overestimated in virtually every point and the reason for this (even if it is to be expected using this model) has to be clarified. Nearly all effects that could not be simulated are expected to have a negative impact on the turbines performance.

As discussed, the flow within the turbine is of an extremely complex nature and is not captured using a simplified 2D model. The complexity of the flow increases as the fluid progresses through the turbine. Wakes from the blades will have velocity components in all three dimensions and the velocity field can be very unfavorable for the blades passing at the downstream half.

The blade will, when subjected to the moving fluid, create vortices along its edges. The creation of vortices is demanding and is a source of losses. A good example of this is the tip vortices arising at the blades both tips and can be seen in Figure 6.4. The vortex is a result of that the foil having a high and a low pressure side thus making the fluid flow from one to the other. When this occurs the pressure difference will decrease and the lift force with it.
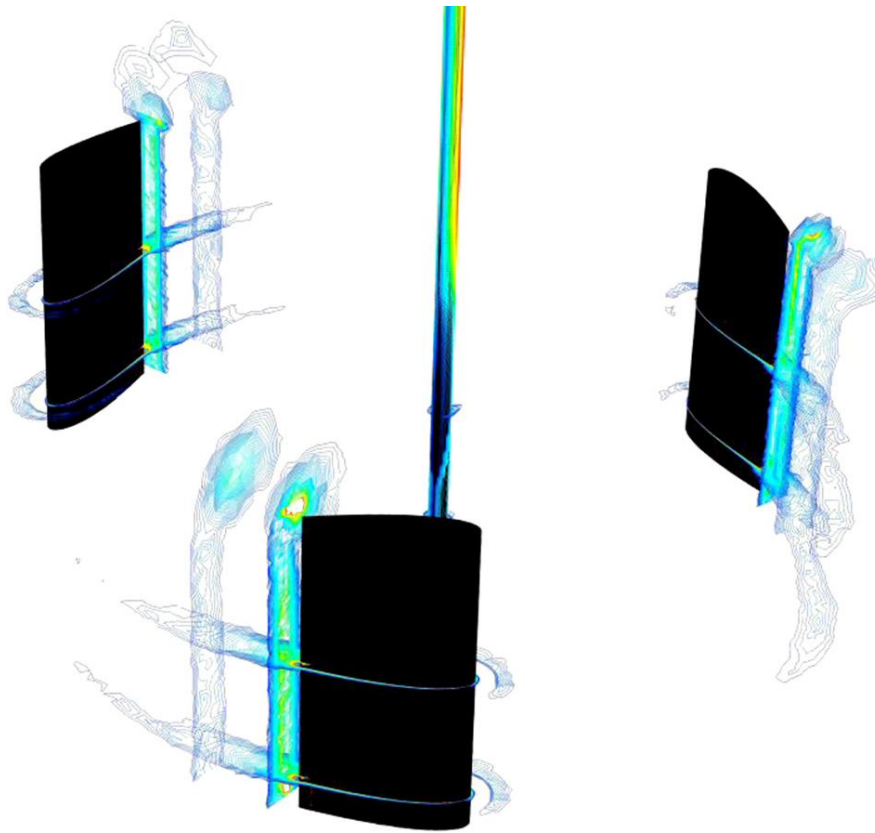
Figure 6.4. Tip vortices of a vertical axis turbine

Other examples of losses not included in the model are the drag induced by the rotating shaft, struts, nuts and bolts etc. This implies that the power coefficients calculated in this model are to be used as a comparison between the different turbine configurations and not as absolute values of performance.

7 Conclusion

An initial design study of a vertical axis turbine was to be performed and the first steps in the optimization process were to follow. From the literature study the case of a lift force driven turbine was determined and the performance as well as the effect of some key parameters was to be evaluated. The simulations were carried out by the use of the Double multiple stremtube model in MATLAB.

From the simulations the two bladed turbine fitted with the S-1046 hydrofoil showed the highest performance but was struggling with an unfavorable oscillating torque. In the light of this the three bladed turbine fitted with the S-1046 hydrofoil with a chord of 0.13 m and an optimal TSR of 3.2 was determined. From the simulations the power coefficient reached 53.47 % for this case. This configuration also showed good performance in a relatively wide range of both tip speed ratios and free stream velocities.

The simulations showed good potential for the use of asymmetrical foils in vertical axis turbines. The performance was evaluated for the upstream half of the turbine where the E216 foil exceeded the symmetrical foils in the range of ten percentage points.

8 Future work

When undertaking a project with a limited amount of time and resources the scope of the whole project will of course be limited. In this chapter a few of the collected thoughts and reflections that were not within the scope of this project are presented.

8.1 Simulation method

The double multiple streamtube model has shown great potential and when looking at the numerous different blades that could be of interest for this application the model has a lot to offer even in future work.

The obvious limitations of the model will however be in favor of other models. The major limitation being the inability to do 3D-simulations. The value of 3D-simulations does not only lie in getting a fair comparison between the foils but are vital in understanding how the turbine will perform when placed in its environment of operation. Well-designed 3D-simulations is also one of the few reliable ways of evaluate the final efficiency and also the power output of the final design.

8.2 Starting torque

As mentioned the vertical axis turbines often experience self-starting problems, especially at low free stream velocities. The problem can of course be solved by using the generator as a starting engine, something that is undesirable when designing a simple, robust and efficient turbine.

Since it is established that the part of the turbine facing the tidal current first extracts significantly more energy than the rear half it is the authors belief that a combination between a drag- and lift force turbine could be a good alternative. This is believed even though the flow will be affected in a way that impairs the extraction of energy from the hydrofoils on a significant part of the rear side.

When these ideas have been discussed there have quickly been established that the TSR relation between the two techniques is vital in order to get an efficient turbine. This is because one of them should not slow the other one down. According to our results the optimal TSR for lift force technique has been about 3. According to (Vertical axis resistance type wind turbines for use in buildings, 2009) the theoretical maximum TSR for energy extraction with a drag force wind turbine is around 0.3 as in Figure 8.1.
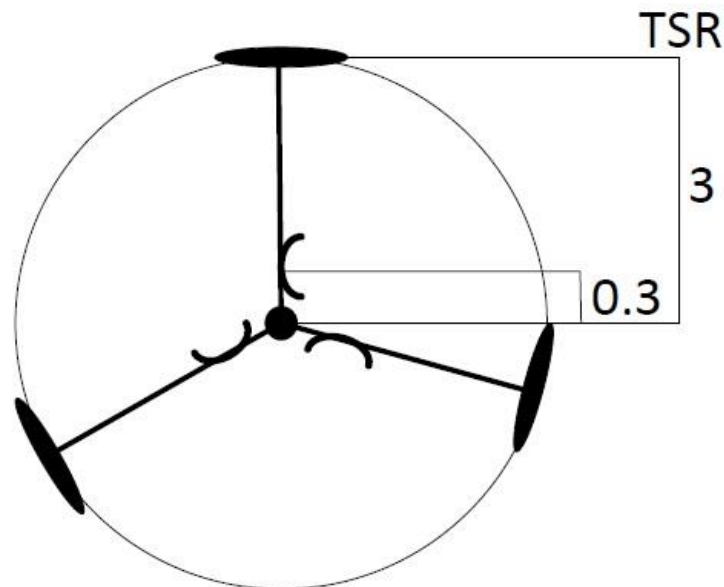

Figure 8.1. A first example of a combined turbine

An examination of this idea and how such a turbine would be optimized should be very interesting. This will probably lead to a choice of drag force turbine where a Savonius turbine might be of interest.

Another design alteration that could improve the starting torque is the implementation of helical blades. The design is called a Gorlov turbine and can be seen in Figure 8.2.

Figure 8.2. Example of Gorlov turbine

The twisted blades enables the turbine to start at considerably lower free stream velocities since parts of the blade always experience favorable conditions in terms of angle of attack. The blade helical shape also means that a stable torque will be produced during the whole revolution which will lower the risk of turbine damage as well as lower the structural demands on the material used.

A more expensive and technology demanding solution is the application of variable pitch. The solution requires that all blades can be controlled at any time and enable the blades to be pitched to their optimal angle towards the fluid in motion. This angle is highly dependent on azimuthal position (especially at low TSR's) and can not be compared with fixed pitch solutions.

Having the opportunity to pitch the blade at any position will of course not only improve the starting torque but improve the total performance of the turbine considerably. According to (Optimization of cycloidal water turbine and the performance improvement by individual blade control, 2009) the performance was improved by approximately 25 % after implementation of variable pitch.

8.3 Blade selection

As have been discussed there are a huge amount of different foils available and before they have been tested in the environment in which they will operate it is hard to narrow the search down to only one. In order to make the decision more difficult there are a few alterations that can be made to the foils that have shown the potential to be the future of vertical axis turbine blades. The lack of both data and the opportunity to perform 3D-simulations did regrettably means that the alterations could not be implemented in the project but the possible effects will be presented.

In the work (Flow control for VATT by fixed and oscillating flap, 2013) the effect of both adding a fixed flap (slotted blade) and an oscillating flap is presented. The investigation are made for a NACA 0018 profile as a baseline and the profile and the alterations are illustrated in Figure 8.3.
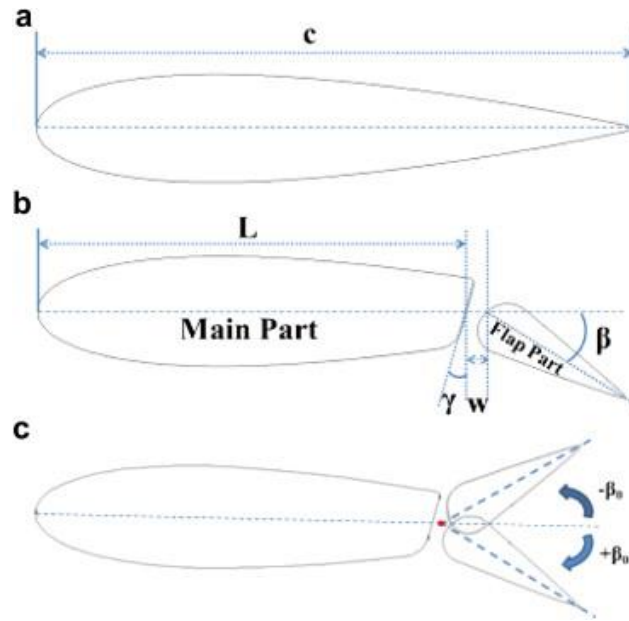
Figure 8.3. a) NACA 0018 b) fixed flap c) oscillating flap

According to (Flow control for VATT by fixed and oscillating flap, 2013) the improvement is related to an effective flow separation as well as vortex control which can be seen in Figure 8.4. The improvement of the power coefficient reached 28% under optimal flap and flow conditions.
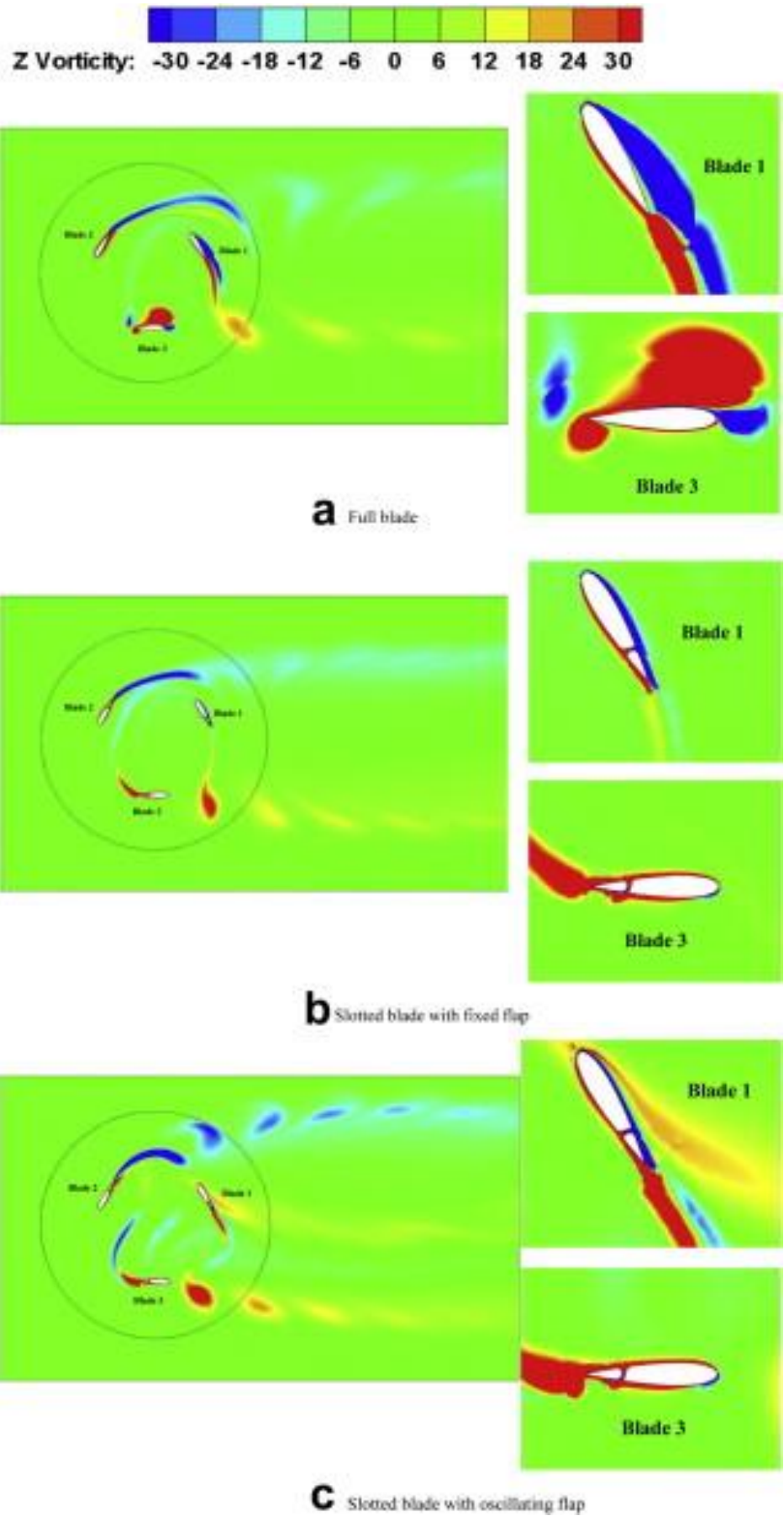
Z Vorticity: -30 -24 -18 -12 -6 0 6 12 18 24 30

a Full blade

b Slotted blade with fixed flap

c Slotted blade with oscillating flap

Figure 8.4. Effect of adding fixed and oscillating flap

9 Suggestions for improvement of the original turbine design

As promised to our partners at Subsea Technology Scandinavia AB (Subtech) and stated in the objectives of this report this section will contain tips for improvement of Subtech's original design. This design is called a 'Hunter turbine' since John Hunter has a patent (No.GB9524439.8) for this 6-bladed turbine concept illustrated in Figure 9.1. It is designed to extract energy from a river or ocean current (Fluid dynamic performance of a vertical axis turbine for tidal currents, 2011).
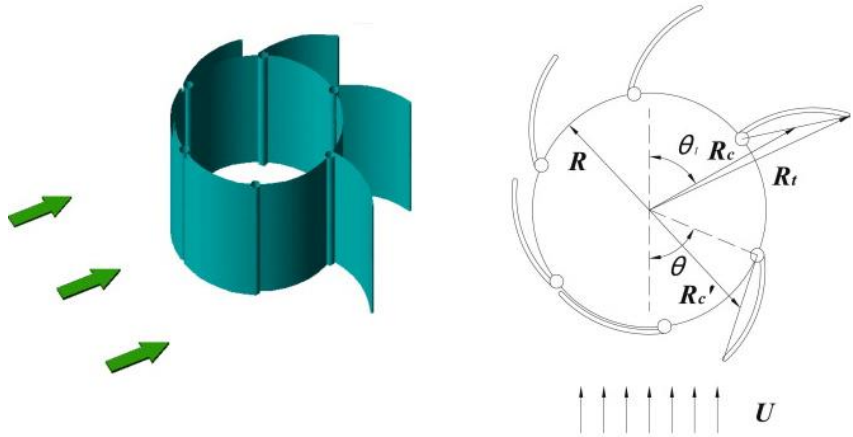
Figure 9.1. Hunter turbine setup

According to a 2-dimentional model this design has an optimal power coefficient of about 0.19 (Fluid dynamic performance of a vertical axis turbine for tidal currents, 2011) while a 3-dimensional model describes a number of reasons why this might be lower (Three-dimensional effects on the performance of a vertical axis tidal turbine, 2013). But with the suggested improvements in this chapter the authors of this work, without any careful calculations, believe that a power coefficient of about 0.2 can be obtained as visualized in Figure 9.2.
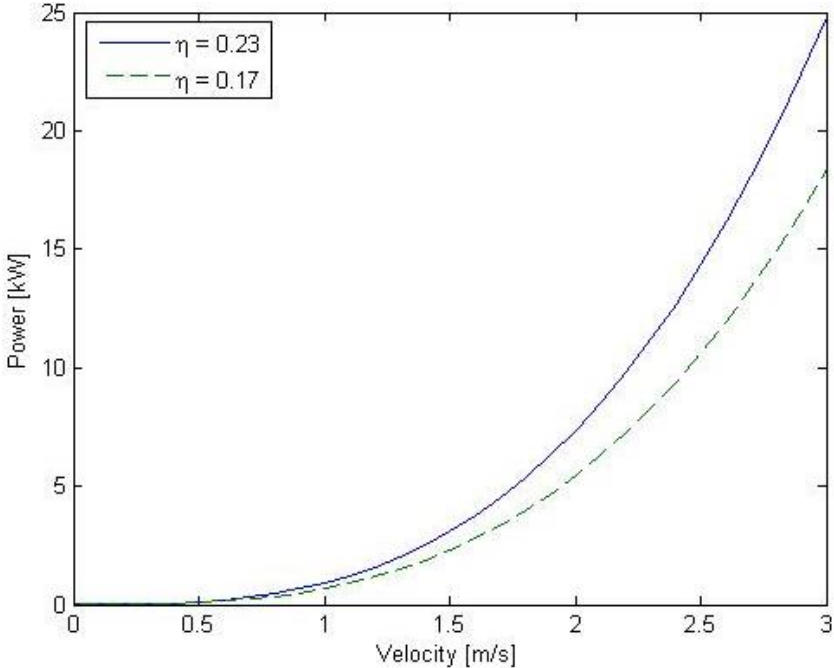

Figure 9.2. 23% and 17% curves of the power in the water

9.1 Opening and closing process

The opening and closing process was investigated in an experiment were it was concluded that the process was almost independent of the tip speed ratio, in other words the resistance to rotate. It was found that the opening process were started at about 90° and finished at 120° while the closing process lasted from 180° to 360° (Fluid dynamic performance of a vertical axis turbine for tidal currents, 2011). The possible impact of Reynolds number was not investigated.

The result of this study means that when the blade is in the optimal position 90° the opening process is only initiated. A solution that allowed the flow to get a hold of the blade earlier in order to start the opening process would probably lead to a greater efficiency.

9.2 Tip Speed Ratio

According to a 2-dimensional CFD simulation the optimal TSR (called flow coefficient in the report) is in the range of 0.44-0.47 resulting in a power coefficient of 0.19 based on the projected area transverse to the flow of the drum and one precipitated blade (Fluid dynamic performance of a vertical axis turbine for tidal currents, 2011).

With these results in mind it is preferable if the turbine has a good control system for the rotational speed, either by the generator resistance or through a gearbox in order to maximize the efficiency.

9.3 Three-dimensional effects

The three-dimensional effects have been investigated using a CFD model that shows that a rather large performance gap between 2-dimensional and 3-dimensional performance can occur depending on certain properties of both the turbine and the flow. This is due to the vortexes that are formed at the ends of the blades as shown if Figure 9.3 where the aspect ratio is defined by the height divided by the drum diameter.
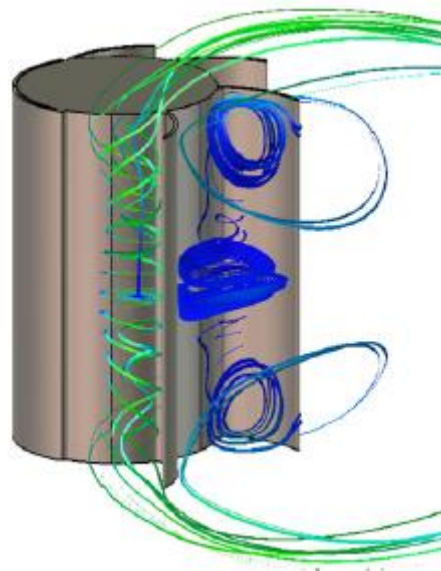

Figure 9.3. Visualization of blade ends vortexes at TSR=0.33 and aspect ratio=2

When looking at the pressures along the blade it is clear that the vortices at the blades ends lower the pressure on the blade as seen in Figure 9.4. These effects become much more significant at lower tip speed ratios and aspect ratios (Three-dimensional effects on the performance of a vertical axis tidal turbine, 2013).
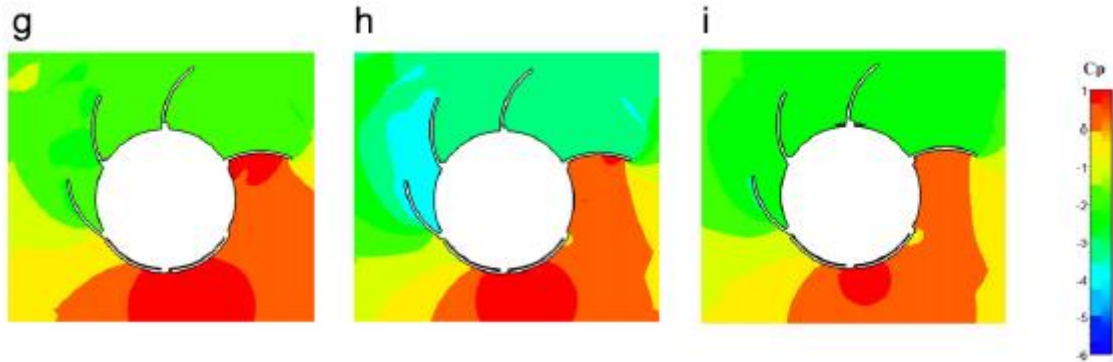
Figure 9.4. Pressure coefficients with TSR=0.44 and aspect ratio=2. (g) in the middle of the blade, (h) 40% from the middle, (i) 80% from the middle of the blade

To reduce these effects as much as possible a high aspect ratio should be pursued. To alter the design of the turbine a bit so that the blades get a covered edge (comparable to airplanes use of winglets) that prevents the tip vortexes would probably increase the efficiency even more as in Figure 9.5.

Figure 9.5. Proposed blade alteration

9.4 Other possible improvements

These are three other possible improvements that can be examined further in order to increase efficiency.

- Control the flow direction prior to the turbine in order to get better angels of attack and to initiate the opening process earlier.
- Use a funnel prior to the turbine to utilize a larger area of the tidal current. Both this and the solution mentioned above would however result in a greater weight which might be negative for the important kW/tonne ratio.
- Shape the outside of the blades in the same way as the surface of a golf ball in order to reduce the drag force on the surface that counteracts the rotation at the half of the turbine where the blades moves against the tidal current.

Figure references

Figure 2.1   (Evelyn Brown, 2005)

Figure 2.2   (Evelyn Brown, 2005)

Figure 2.3   (SEI)

Figure 2.4   (Tidal energy update 2009, 2010)

Figure 2.5   (NASA, 2009)

Figure 2.8   (INSEAN, 2007)

Figure 2.9   (INSEAN, 2007)

Figure 2.10   (INSEAN, 2007)

Figure 2.11   (INSEAN, 2007)

Figure 2.12   (OpenHydro)

Figure 2.13   (Seimens)

Figure 2.14   (ESRU)

Figure 2.15   (LEP)

Figure 2.16 left   (Forum, 2012)

Figure 2.16 right   (Flumill)

Figure 2.17   (Minesto)

Figure 2.18   (ARC)

Figure 2.20   (B Munson, 2006)

Figure 2.21   (Ackermann, 2011)

Figure 2.22   (Belarusian web portal on renewable energy)

Figure 2.23   (National air and space museum, 2011)

Figure 2.24   (Hindawi Publishing Corporation)

Figure 2.25   (Dept. of energy technology, 2011)

Figure 2.26   (Cleynen)

Figure 2.27   (Airfoil Tools)

Figure 3.1   (Numerical and Analytical Investigation of Vertical Axis Wind Turbine, 2013)

Figure 3.2   (Numerical and Analytical Investigation of Vertical Axis Wind Turbine, 2013)

Figure 3.3   (Numerical and Analytical Investigation of Vertical Axis Wind Turbine, 2013)

Figure 3.4   (Numerical and Analytical Investigation of Vertical Axis Wind Turbine, 2013)

Figure 3.6   (Numerical and Analytical Investigation of Vertical Axis Wind Turbine, 2013)

Figure 3.10   (Airfoil Tools)

Figure 3.11   (Airfoil Tools)

Figure 3.12   (Airfoil Tools)

Figure 3.13   (Airfoil Tools)

Bibliography

A design methodology for cross flow water turbines. **J. Zanette, D. Imbault, A. Tourabi. 2010.** 5, Grenoble, France : Elsevier Ltd, 2010, Vol. 35. 0960-1481.

A low-Reynolds-number, high-angle-of-attack investigation of wind turbine aerofoils. **S Worasinchai, G Ingram, R Dominy. 2011.** s.l. : Sage, 2011. 10.1177/0957650911405411.

Ackermann, Thomas. 2011. *Wind energy - Part 1.* KTH, Stockholm : Energynautics, 2011.

Aerodynamic analysis of the Darrieus rotor including secondary effects. **I. Paraschivoiu, F. Delclaux, P. Fraunie, and C. Beguier. 1983.** 5, 1983, Vol. 7. 10.2514/3.62672.

Airfoil Tools. *http://airfoiltools.com.* [Online] [Cited: July 19, 2013.] http://airfoiltools.com/airfoil/details?airfoil=s1046-il.

—. *http://airfoiltools.com.* [Online] [Cited: July 24, 2013.] http://airfoiltools.com/airfoil/details?airfoil=n0012-il.

—. *http://airfoiltools.com.* [Online] [Cited: July 24, 2013.] http://airfoiltools.com/airfoil/details?airfoil=s1046-il.

—. *http://airfoiltools.com.* [Online] [Cited: July 24, 2013.] http://airfoiltools.com/airfoil/details?airfoil=s1210-il.

—. *http://airfoiltools.com.* [Online] [Cited: July 24, 2013.] http://airfoiltools.com/airfoil/details?airfoil=e216-il.

ARC. [Online] Atlantis Resources Corporation . [Cited: July 22, 2013.] http://www.atlantisresourcescorporation.com/marine-power/atlantis-technologies/an-series.html.

B Munson, D Young, T Okiishi. 2006. *Fundamentals of fluid mechanics.* Ames, I, USA : John Wiley & Sons, 2006. 0-471-67582-2.

Belarusian web portal on renewable energy. *http://re.buildingefficiency.info/en/.* [Online] [Cited: July 23, 2013.] http://re.buildingefficiency.info/en/renewable-energy-technologies/wind/.

Chanson, Hubert. 1999. *The Hydraulics of Open Chanel Flow.* London, UK : Arnold, 1999.

Cleynen, Olivier. [Online] [Cited: July 01, 2013.] http://en.wikipedia.org/wiki/File:Wing_profile_nomenclature.svg.

Computational Prediction Of Airfoil Dynamic Stall. **John A Ekaterinaris, Max F Platzer. 1997.** Roskilde, Denmark : Elsevier Science Ltd., 1997, Vol. 33. 0376-0421/97.

COMPUTATIONAL PREDICTION OF AIRFOIL DYNAMIC STALL. **John A Ekaterinaris, Max F Platzer. 1997.** Roskilde, Denmark : Elsevier Science Ltd., 1997, Vol. 33. 0376-0421/97.

Belarusian web portal of renewable energy. *http://re.buildingefficiency.info/en/.* [Online] [Cited: July 23, 2013.] http://re.buildingefficiency.info/en/renewable-energy-technologies/wind/.

Dept. of energy technology. 2011. *Wind lecture - 2 - aerodynamics.* Stockholm : KTH, 2011.

EIA. [Online] U.S. Energy Information Administration. [Cited: July 22, 2013.] http://www.eia.gov/cfapps/ipdbproject/iedindex3.cfm?tid=2&pid=2&aid=12&cid=regions&syid=1980&eyid=2011&unit=BKWH.

ESRU. [Online] University of Strathclyde. [Cited: July 22, 2013.] http://www.esru.strath.ac.uk/EandE/Web_sites/05-06/marine_renewables/technology/oschydro.htm.

Evelyn Brown, Angela Colling, Dave Park, John Philips, Dave Rothery, John Wright. 2005. *Waves, Tides and Shallow-water processes.* Milton Keyenes, UK : Butterworth-Heinemann, 2005. 0-7506-4281-5.

Flow control for VATT by fixed and oscillating flap. **Qing Xiao, Wendi Liu, Atilla Incecik. 2013.** Glasgow, UK : Elsevier, 2013, Vol. 51. 0960-1481.

Fluid dynamic performance of a vertical axis turbine for tidal currents. **Bo Yang, Chris Lawn. 2011.** 12, s.l. : Elsevier, 2011, Vol. 36. 0960-1481.

Flumill. [Online] Flumill AS. [Cited: July 22, 2013.] http://www.flumill.com/.

Forum, VVS. 2012. *http://www.vvsforum.no.* [Online] April 02, 2012. [Cited: July 24, 2013.] http://www.vvsforum.no/artikkel/5805/rystraumen-tidevann-faar-konsesjon.html.

GRABCAD. *http://grabcad.com.* [Online] [Cited: July 24, 2013.] http://grabcad.com/contentfiles/209275.

Gretton, Gareth I. 2009. The hydrodynamic analysis of a vertical axis tidal current turbine. [Online] August 18, 2009. [Cited: July 22, 2013.] http://www.see.ed.ac.uk/~shs/Tidal%20Stream/Gretton2009.pdf.

Hansen, Martin O L. 2008. *Aerodynamics of Wind Turbines.* s.l. : Earthscan, 2008. 978-1-84407-438-9.

Hindawi Publishing Corporation. *http://www.hindawi.com.* [Online] [Cited: April 10, 2013.] http://www.hindawi.com/journals/ijce/2012/193021/fig6/.

INSEAN. 2007. *www.tidaltoday.com.* [Online] 2007. [Cited: July 22, 2013.] http://www.tidaltoday.com/tidal07/presentations/GuidoCalcagnoMoroso.pdf.

James F. Manwell, Jon G. McGowan, Anthony L. Rogers. 2009. *Wind Energy Explained: Theory, Design and Application.* Chichester, UK : John Wiley & Sons Ltd, 2009. 978-0-470-01500-1.

Kroo, Ilan. 2007. Applied Aerodynamics: A Digital Textbook. *www.desktop.aero.* [Online] Desktop Aeronautics Inc, 2007. [Cited: April 10, 2013.] http://www.desktop.aero/appliedaero/fundamentals/forces.html.

LEP. [Online] Lunar Energy Power Ltd. [Cited: July 22, 2013.] http://www.lunarenergy.co.uk/productOverview.htm.

MCT. [Online] Marine Current Turbines. [Cited: July 22, 2013.] http://www.marineturbines.com/Seagen-Technology.

—. 2011. *SeaGen Environmental Monitoring Programme.* Edinburgh, UK : s.n., 2011. 9S8562/R/303719/Edin.

Minesto. [Online] Minesto AB. [Cited: July 22, 2013.] http://www.minesto.com/.

Multiple actuator-disc theory for wind turbines. **Newman, B.G. 1986.** Montreal, Canada : Elsevier, 1986. 0167-6105.

NASA. 2009. *http://www.grc.nasa.gov.* [Online] NASA, April 09, 2009. [Cited: July 24, 2013.] http://www.grc.nasa.gov/WWW/k-12/airplane/boundlay.html.

National air and space museum. 2011. *http://blog.nasm.si.edu.* [Online] December 17, 2011. [Cited: April 10, 2013.] http://blog.nasm.si.edu/aviation/wings-from-the-wright-brothers-to-the-present/.

Naturvårdsverket. 2011. *Vägledning för 1130 Estuarier.* Stockholm : Naturvårdsverket, 2011. NV-04493-11.

NTNU. *http://www.ntnu.no/ivt.* [Online] TMR7 Experimental Methods in Marine Hydrodynamics. [Cited: 07 09, 2013.] ttp://www.ivt.ntnu.no/imt/courses/tmr7/lecture/Scaling_Laws.pdf.

Numerical and Analytical Investigation of Vertical Axis Wind Turbine. **Asress Mulugeta Biadgo, Aleksandar Simonovic, Dragan Komarov, Slobodan Stupar. 2013.** 1, Belgrad, Serbia : s.n., 2013, Vol. 41. FME Transactions (2013) 41, 49-58.

OpenHydro. [Online] DCNS. [Cited: July 22, 2013.] http://openhydro.com.

Optimization of cycloidal water turbine and the performance improvement by individual blade control. **In Seong Hwang, Yun Han Lee, Seung Jo Kim. 2009.** 9, Seoul, Republic of Korea : Elsevier, 2009, Vol. 86. 0306-2619.

Performance investigation of H-rotor Darrieus turbine with new airfoil shapes. **Mohamed, M.H. 2012.** 1, Cairo, Egypt : s.n., 2012, Vol. 47. 0360-5442.

Robert E Sheldahl, Paul C Klimas. 1981. *Aerodynamic Characteristics of Seven Symmetrical Airfoil Sections Through 180-Degree Angle of Attack for Use in Aerodynamic Analysis of Vertical Axis Wind Turbines.* Albuquerque, NM USA : National Technical Information Service, 1981. AND80-2114.

S Salon, A Crise, A J Van Loon. 2008. Dynamics of the Bottom Boundary Layer. [book auth.] A Camerlenghi M Rebesco. *Developments in Sedimentology.* Poznan, Poland : Elseiver, 2008, Vol. 60.

SEI. *Tidal & Current Energy Resources In Ireland.* s.l. : Sustainable Energy Ireland.

Seimens. *http://www.siemens.com.* [Online] [Cited: July 24, 2013.] http://www.siemens.com/innovation/en/news/2013/e_inno_1308_1.htm.

The impact of tidal stream turbines on large-scale sediment dynamics. **Simon P Neill, Emmer J Litt, Scott J Couch, Alan G Davies. 2009.** 12, s.l. : Elsevier, 2009, Vol. 34. 0960-1481.

Three-dimensional effects on the performance of a vertical axis tidal turbine. **Bo Yang, Chris Lawn. 2013.** s.l. : Elsevier, 2013, Vol. 58. 0029-8018.

Tidal energy update 2009. **Fergal O Rourke, Fergal Boyle, Anthony Reynolds. 2010.** 2, Dublin, Ireland : Elsvier Ltd., 2010, Vol. 87. 0306-2619.

Tong, Wei. 2010. *Wind Power Generation and Wind Turbine Design.* Ashurts, UK : WIT Press, 2010. 978-1-84564-205-1.

Unizar. *www.unizar.es.* [Online] Universidad de Zaragoza. [Cited: July 22, 2013.] http://www.unizar.es/dctmf/jblasco/mf/WHITE_SGChapt07.pdf.

Wainfan. 2010. *http://www.wainfan.com.* [Online] September 10, 2010. [Cited: July 23, 2013.] http://www.wainfan.com/wingdes.pdf.

Vertical axis resistance type wind turbines for use in buildings. **G Müller, M F Jentsch, E Stoddard. 2009.** 5, Southampton, UK : Elseiver, 2009, Vol. 34. 0960-1481.

Wind tunnel and numerical study of a small vertical axis wind turbine. **Robert Howell, Ning Qin, Jonathan Edwards, Naveed Durrani. 2010.** 2, Sheffield, UK : Elsevier, 2010, Vol. 35. 0960-1481.

Appendix 1 – MATLAB simulation code

```matlab
close all
clear all
clc
%-----data-----
TSR = 3.2;                              %Tip speed ratio [1], MUST BE 2/3/4
r   = 1;                                %Radious to the middle of the blade [m]
c   = 0.13;                             %Chord [m]
h   = 2*(2*r);                          %The height of the machine=2*diameter
[m]
N   = 3;                                %Number of blades
Pitch = 0;                              %Blades fixed pitch
disp('Progress: Importing excel data files')
indata50k           =     xlsread('C:\Users\dbrinck\Desktop\Modell    10juli
(EM)\Profiler\S1046\S1046Re50k.xlsx');
indata100k          =     xlsread('C:\Users\dbrinck\Desktop\Modell    10juli
(EM)\Profiler\S1046\S1046Re100k.xlsx');
indata200k          =     xlsread('C:\Users\dbrinck\Desktop\Modell    10juli
(EM)\Profiler\S1046\S1046Re200k.xlsx');
indata500k          =     xlsread('C:\Users\dbrinck\Desktop\Modell    10juli
(EM)\Profiler\S1046\S1046Re500k.xlsx');
indata1000k         =     xlsread('C:\Users\dbrinck\Desktop\Modell    10juli
(EM)\Profiler\S1046\S1046Re1000k.xlsx');
%Indata(:,1) = alpha
%Indata(:,2) = C_l
%Indata(:,3) = C_d
A   = 2*r*h;                            %Area in the stream
rho = 0.999965E3;                       %Density of water @ 5*C
my  = 1.519E-3;                         %Dynamic viscosity of water @ 5*C
d_theta = 10;                           %Streamtube step
theta = 5:d_theta:360;                  %Azimuth angles (streamtube positions)
v_max = 4;                              %Maximum fluid stream velocity [m/s]
speed=0;                                %Counter for the number of velocities
from 0.25 to v_max with the step 0.25
for y=1:v_max*4                         %Number of velocities (*4 becase if the
step size)
    speed=speed+0.25;
    for s=1:18                          %One velocity for each stream tube
        v_inf(s,y) = speed;            %Stream velocity matrix [m/s]
    end
end
%-----Initial values-----
vinkel_1=1;                                     %Streamtube  starting  value
(theta(vinkel_1))
vinkel_2=18;                            %Front side stream tube ending value
(theta(vinkel_2))
work = 0;
%-----calculations-----
for j=1:2                               %First the front half is calculated,
then the answers is used to the second half (180-360*)
    for i = 1:length(v_inf(1,:))        %Loop for every stream velocity
      z=0;
      if j==1
        WR(i)=v_inf(1,i)*TSR;           %Peripheral velocity
      end
    for k = vinkel_1:vinkel_2           %Loop  for  every  stream  tube  (inside
velocity loop!)
        z=z+1;                          %Counter
        a   = 0;                        %Induction factor [1] (initial value)
```

```matlab
        Konvergence = 0;                    %Resets convergence criteria for each
tube/velocity count
        while Konvergence<0.99         %Itterates a until konvergence is
between 0.99 and 1.01
            a = a + 0.001;              %Induction factor [1]
            if a>=1
                break
            end
            w(i,k)              =  sqrt(((v_inf(z,i)*(1-a)*sind(theta(k)))^2)  +
((v_inf(z,i)*(1-a)*cosd(theta(k))+WR(i))^2));        %Relative      velocity
(hydrofoil)
            alpha(i,k)                    =                    atand((v_inf(z,i)*(1-
a)*sind(theta(k)))/(v_inf(z,i)*(1-a)*cosd(theta(k))+WR(i)))+Pitch;    %Angle
of attack (blade)
            Re(i,k)    = rho*c*w(i,k)/my; %Reynolds number (hydrofoil)

            %Properties of the airfoil
          if Re(i,k)<75E3
              position = 51 + round(alpha(i,k)*4);
              if 12.5>=alpha(i,k) && alpha(i,k)>=-12.5
                  C_l = indata50k(position,2);
                  C_d = indata50k(position,3);
              else
                  if alpha(i,k)>0 && alpha(i,k)<=45
                      C_l = 0.005*alpha(i,k)+0.4161;
                  elseif alpha(i,k)<0 && alpha(i,k)>=-45
                      C_l = 0.0051*alpha(i,k)-0.4138;
                  elseif alpha(i,k)>0 && alpha(i,k)>45
                      C_l = -0.0143*alpha(i,k)+1.2856;
                  else
                      C_l = -0.0143*alpha(i,k)-1.285;
                  end
                  C_d = 0.0215*abs(alpha(i,k))-0.1305;
              end
          elseif 75E3<=Re(i,k) && Re(i,k)<150E3
              position = 71 + round(alpha(i,k)*4);
              if 17.5>=alpha(i,k) && alpha(i,k)>=-17.5
                  C_l = indata100k(position,2);
                  C_d = indata100k(position,3);
              else
                  if alpha(i,k)>0 && alpha(i,k)<=45
                      C_l = 0.006*alpha(i,k)+0.8479;
                  elseif alpha(i,k)<0 && alpha(i,k)>=-45
                      C_l = 0.0057*alpha(i,k)-0.8609;
                  elseif alpha(i,k)>0 && alpha(i,k)>45
                      C_l = -0.0248*alpha(i,k)+2.2326;
                  else
                      C_l = -0.0248*alpha(i,k)-2.232;
                  end
                  C_d = 0.0233*abs(alpha(i,k))-0.2979;
              end
          elseif 150E3<=Re(i,k) && Re(i,k)<350E3
              position = 81 + round(alpha(i,k)*4);
              if 20>=alpha(i,k) && alpha(i,k)>=-20
                  C_l = indata200k(position,2);
                  C_d = indata200k(position,3);
              else
                  if alpha(i,k)>0 && alpha(i,k)<=45
                      C_l = 0.0035*alpha(i,k)+0.9536;
                  elseif alpha(i,k)<0 && alpha(i,k)>=-45
                      C_l = 0.0035*alpha(i,k)-0.9538;
```

```matlab
            elseif alpha(i,k)>0 && alpha(i,k)>45
                C_l = -0.0247*alpha(i,k)+2.2204;
            else
                C_l = -0.0247*alpha(i,k)-2.2186;
            end
            C_d = 0.0238*abs(alpha(i,k))-0.3443;
        end
    elseif 350E3<=Re(i,k) && Re(i,k)<750E3
        position = 81 + round(alpha(i,k)*4);
        if 20>=alpha(i,k) && alpha(i,k)>=-20
            C_l = indata500k(position,2);
            C_d = indata500k(position,3);
        else
            if alpha(i,k)>0 && alpha(i,k)<=45
                C_l = 0.0063*alpha(i,k)+0.9069;
            elseif alpha(i,k)<0 && alpha(i,k)>=-45
                C_l = 0.0063*alpha(i,k)-0.9043;
            elseif alpha(i,k)>0 && alpha(i,k)>45
                C_l = -0.0264*alpha(i,k)+2.3772;
            else
                C_l = -0.0264*alpha(i,k)-2.3748;
            end
            C_d = 0.0238*abs(alpha(i,k))-0.3435;
        end
    elseif 750E3<=Re(i,k)
        position = 81 + round(alpha(i,k)*4);
        if 20>=alpha(i,k) && alpha(i,k)>=-20
            C_l = indata1000k(position,2);
            C_d = indata1000k(position,3);
        else
            if alpha(i,k)>0 && alpha(i,k)<=45
                C_l = 0.0063*alpha(i,k)+0.9766;
            elseif alpha(i,k)<0 && alpha(i,k)>=-45
                C_l = 0.0062*alpha(i,k)-0.9793;
            elseif alpha(i,k)>0 && alpha(i,k)>45
                C_l = -0.028*alpha(i,k)+2.5176;
            else
                C_l = -0.0279*alpha(i,k)-2.5148;
            end
            C_d = 0.024*abs(alpha(i,k))-0.3596;
        end
    end
    Save_Cl(i,k) = C_l;
    Save_Cd(i,k) = C_d;

    C_n(i,k)   =   C_l*cosd(alpha(i,k))   +   C_d*sind(alpha(i,k));
%Normal force coefficient
    C_t(i,k)   =   C_l*sind(alpha(i,k))   -   C_d*cosd(alpha(i,k));
%Tangential force coefficient
    F_N(i,k)            =            0.5*rho*(w(i,k)^2)*h*c*C_n(i,k);
%Normal force
    F_T(i,k)            =            0.5*rho*(w(i,k)^2)*h*c*C_t(i,k);
%Tangential force
    T_i(i,k)   =   F_T(i,k)*cosd(theta(k))   -   F_N(i,k)*sind(theta(k));
%Instantaneous thrust

    if                                                            a<=0.33
%Momentum equation breaks down
        a_new                                                           =
(N*abs(T_i(i,k)))/(4*pi*rho*r*h*abs(sind(theta(k)))*v_inf(z,i)^2)+(a^2);
    else
```

```matlab
        a_new                                          =
(N*abs(T_i(i,k)))/(4*pi*rho*r*h*abs(sind(theta(k)))*v_inf(z,i)^2)+(a^2)*(5-
3*a)*0.25;
        end
      Konvergence = a/a_new;                 %Compare the solution methods,
if they are about the same the itteration stops
      end
      Save_a(i,k)      = a;                           %Saving a for controll
purposes
      Save_a_new(i,k) = a_new;                   %Saving a_new for controll
purposes
      Save_konv(i,k)   = Konvergence;           %Saving Konvergence for
controll purposes
      v_history(i,k)  = v_inf(z,i);            %Saves the freestream velocity
and the "free stream" velocities that enters the second half/exits the
first half
      v_inf(z,i)        = v_inf(z,i)*(1-2*a); %After the program run this
matrix will have the output velocities after the machine

    end
    clc
    work = work+1;                              %Counts loops (32 in total,
16velocities*up- and downstream)
    Progress = work/32*100;                     %Progress in % calculated to
inform user of calculation speed
    disp(['Progress: ' num2str(round(Progress)) '%']) %Displays Progress
    end
 v_inf=flipud(v_inf);
 vinkel_1 = 19;                                 %Back side stream tube starting
value
 vinkel_2 = 36;                                 %Back side stream tube ending
value
end
for l=1:length(F_T(:,1))
    Q_avg(l) = sum(F_T(l,:))*r*(N*d_theta/360);
    C_Q(l)   = Q_avg(l)/(0.5*rho*(v_history(l,1)^2)*2*r*h*r);
    C_P(l)   = C_Q(l)*TSR;
end
clc
disp('Progress: Plotting...')
figure(1)
subplot(2,1,1)
plot(1:18,v_history(7,1:18),1:18,(v_history(7,36:-
1:19)+1.75)/2,1:18,(v_history(7,36:-1:19)+v_inf(:,7)')/2)
ylabel('Velocity [m/s]')
xlabel('Streamtubes')
axis([1 18 0 1.8])
legend('Free stream velocity', 'Stream velocity at blade (upstream half)',
'Stream velocity at blade (downstream half)', 'Location', 'North' )
subplot(2,1,2)
plot(theta, Save_a(7,:), theta,Save_a_new(7,:))
legend('a', 'a new', 'Location', 'North' )
ylabel('Axial induction factor')
xlabel('\theta')
axis([0 360 0 (max(max(Save_a)+0.05))])

figure(2)
plot(theta, Re(7,:))
ylabel('Reynolds')
xlabel('\theta')
grid on
```

```matlab
figure(3)
plot(theta, alpha(7,:))
ylabel('Angle of attack')
xlabel('\theta')
grid on
figure(4)
plot(v_history(:,1),C_P(:))
axis([0.5 2.5 0.3 0.6])
xlabel('u_\infty')
ylabel('C_P')
title('S1046 N=3 c=0.13 TSR=3.2')

%MOMENTPLOTTAR HÅRDKODADE
for w=1:length(theta)
    Q_i_blade(w) = F_T(7,w)*r;
end
figure(5)
if N==2
    Q_i_2blade = [Q_i_blade(19:36) Q_i_blade(1:18)];
    summering=Q_i_blade+Q_i_2blade;
    plot(theta,Q_i_2blade,theta, Q_i_blade, theta, summering,'k')
    legend('Blade 1','Blade 2','Summation')
elseif N==3
    Q_i_2blade = [Q_i_blade(25:36) Q_i_blade(1:24)];
    Q_i_3blade = [Q_i_blade(13:36) Q_i_blade(1:12)];
    summering  = Q_i_blade+Q_i_2blade+Q_i_3blade;
    plot(theta, Q_i_blade, theta, Q_i_2blade, theta, Q_i_3blade, theta,
summering,'k')
    legend('Blade    1','Blade    2','Blade    3','Summation','Location',
'SouthEast')
else
    Q_i_2blade = [Q_i_blade(28:36) Q_i_blade(1:27)];
    Q_i_3blade = [Q_i_blade(19:36) Q_i_blade(1:18)];
    Q_i_4blade = [Q_i_blade(10:36) Q_i_blade(1:9)];
    summering  = Q_i_blade+Q_i_2blade+Q_i_3blade+Q_i_4blade;
    plot(theta, Q_i_blade, theta, Q_i_2blade, theta, Q_i_3blade, theta,
Q_i_4blade, theta, summering,'k')
    legend('Blade 1','Blade 2','Blade 3','Blade 4','Summation','Location',
'SouthEast')
end
    axis([0 360 min(Q_i_blade)*1.1 max(summering)*1.1])
    xlabel('\theta')
    ylabel('Torque')
clc
disp('Progress: Ready!')
if max(max(abs(alpha)))>90
    disp('WARNING: At some point the angle of attack is larger than +/-90
degrees. The airfoil indata is not defined outside this interval which may
led to errors in the results!')
end
```

Appendix 2 – Drag force coefficients
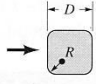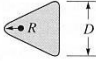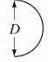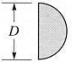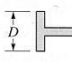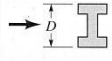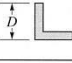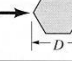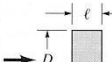
Shape	Reference area A (b = length)	Drag coefficient $C_D = \dfrac{\mathcal{D}}{\frac{1}{2}\rho U^2 A}$	Reynolds number $Re = \rho UD/\mu$
Square rod with rounded corners	$A = bD$	$\begin{array}{c\|c} R/D & C_D \\ \hline 0 & 2.2 \\ 0.02 & 2.0 \\ 0.17 & 1.2 \\ 0.33 & 1.0 \end{array}$	$Re = 10^5$
Rounded equilateral triangle	$A = bD$	$\begin{array}{c\|cc} R/D & \rightarrow & \leftarrow \\ \hline 0 & 1.4 & 2.1 \\ 0.02 & 1.2 & 2.0 \\ 0.08 & 1.3 & 1.9 \\ 0.25 & 1.1 & 1.3 \end{array}$	$Re = 10^5$
Semicircular shell	$A = bD$	$\rightarrow$ 2.3 $\leftarrow$ 1.1	$Re = 2 \times 10^4$
Semicircular cylinder	$A = bD$	$\rightarrow$ 2.15 $\leftarrow$ 1.15	$Re > 10^4$
T-beam	$A = bD$	$\rightarrow$ 1.80 $\leftarrow$ 1.65	$Re > 10^4$
I-beam	$A = bD$	2.05	$Re > 10^4$
Angle	$A = bD$	$\rightarrow$ 1.98 $\leftarrow$ 1.82	$Re > 10^4$
Hexagon	$A = bD$	1.0	$Re > 10^4$
Rectangle	$A = bD$	$\begin{array}{c\|c} \ell/D & C_D \\ \hline \leq 0.1 & 1.9 \\ 0.5 & 2.5 \\ 0.65 & 2.9 \\ 1.0 & 2.2 \\ 2.0 & 1.6 \\ 3.0 & 1.3 \end{array}$	$Re = 10^5$

Figure 0.1. Typical drag coefficients for regular two-dimensional objects
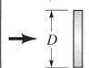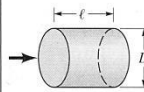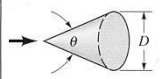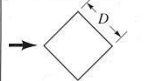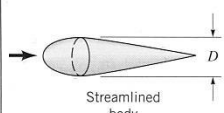
Shape	Reference area A	Drag coefficient C_D	Reynolds number $Re = \rho U D/\mu$
Solid hemisphere	$A = \frac{\pi}{4}D^2$	→ 1.17 ← 0.42	$Re > 10^4$
Hollow hemisphere	$A = \frac{\pi}{4}D^2$	→ 1.42 ← 0.38	$Re > 10^4$
Thin disk	$A = \frac{\pi}{4}D^2$	1.1	$Re > 10^3$
Circular rod parallel to flow	$A = \frac{\pi}{4}D^2$	ℓ/D : C_D 0.5 : 1.1 1.0 : 0.93 2.0 : 0.83 4.0 : 0.85	$Re > 10^5$
Cone	$A = \frac{\pi}{4}D^2$	θ, degrees : C_D 10 : 0.30 30 : 0.55 60 : 0.80 90 : 1.15	$Re > 10^4$
Cube	$A = D^2$	1.05	$Re > 10^4$
Cube	$A = D^2$	0.80	$Re > 10^4$
Streamlined body	$A = \frac{\pi}{4}D^2$	0.04	$Re > 10^5$

Figure 0.2. Typical drag coefficients for regular three-dimensional objects